

**A PROGNOSTIC HEALTH MANAGEMENT BASED FRAME-
WORK FOR FAULT-TOLERANT CONTROL**

A Ph.D Dissertation
Presented to
The Academic Faculty

by

Douglas W. Brown

In Partial Fulfillment
of the Requirements for the Degree
Doctor of Philosophy in the
School of Electrical and Computer Engineering

Georgia Institute of Technology
August 2011

Copyright © 2011 by Douglas W. Brown

A PROGNOSTIC HEALTH MANAGEMENT BASED FRAME- WORK FOR FAULT-TOLERANT CONTROL

Approved by:

Dr. George Vachtsevanos, Advisor
School of Electrical and Computer
Engineering
Georgia Institute of Technology

Dr. Linda Wills
School of Electrical and Computer
Engineering
Georgia Institute of Technology

Dr. David Taylor
School of Electrical and Computer
Engineering
Georgia Institute of Technology

Dr. Michael Roemer
School of Mechanical Engineering
Rochester Institute of Technology

Dr. Jennifer Michaels
School of Electrical and Computer
Engineering
Georgia Institute of Technology

Date Approved: Pending Approval

To my family...

ACKNOWLEDGEMENTS

This work was supported through a cohesive effort coordinated between multiple government organizations, private industry, educational institutions and other non-profit organizations. More specifically, the author would like to acknowledge the Georgia Institute of Technology (GA Tech), specifically the department of electrical and computer engineering (ECE), for initial support through the GA Tech graduate research / teaching assistantship (GTA/GRA) Fellowship program and the Schlumberger Fellowship; Dr. George Vachtsevanos and everyone from the intelligent controls systems laboratory (ICSL) whose collaboration, guidance and support was essential in the success of all the programs related / relevant to this body of work; and the American Society for Engineering Education (ASEE) for sponsorship through the National Defense Science and Engineering Graduate (NDSEG) fellowship

TABLE OF CONTENTS

ACKNOWLEDGEMENTS	iv
LIST OF TABLES	x
LIST OF FIGURES	xi
NOMENCLATURE	xiv
SUMMARY	xxiii
CHAPTER I: INTRODUCTION	1
1.1 The Origin and History of the Problem	1
1.1.1 Relevance	1
1.1.2 Current Initiatives	2
1.2 State of the Art	4
1.3 Organization of Dissertation	5
CHAPTER II: LITERATURE REVIEW	6
2.1 Conceptual Overview	6
2.1.1 Electro-Mechanical Actuator (EMA) Example	6
2.1.2 Physical Constraints	8
2.2 Fault Detection and Diagnosis (FDD)	9
2.2.1 Preliminary Definitions	9
2.2.2 Previous Work	10
2.2.3 Particle Filtering Based Diagnosis	10
2.3 Failure Prognosis & Long-Term Prediction	12
2.3.1 Preliminary Definitions	12
2.3.2 Data-Driven Prognostics	15
2.3.3 Model-Based Prognostics	16
2.3.4 Hybrid-Based Prognostics	16

2.3.5	Particle Filtering Based Prognostics	16
2.4	Fault-Tolerant Control (FTC) Strategies	17
2.4.1	Passive Fault-Tolerant Control Systems (PFTCS)	18
2.4.2	Active Fault-Tolerant Control Systems (AFTCS)	18
CHAPTER III:	RESEARCH AIMS	28
3.1	Aim #1 – Define a Control Architecture.....	29
3.2	Aim #2 – Prove Stability and Boundedness.....	29
3.3	Aim #3 – Derive and Benchmark the MPC Algorithm.....	30
3.4	Aim #4 – Demonstrate Feasibility with an Example	30
CHAPTER IV:	CONTROL ARCHITECTURE.....	31
4.1	Introduction	31
4.1.1	Qualitative Example	32
4.2	Hierarchical PHM Control Architecture.....	34
4.2.1	Low-Level Control Reconfiguration	34
4.2.2	Mid-Level Control Redistribution	36
4.2.3	High-Level Mission Adaptation.....	36
4.3	Reconfigurable Control Architecture	37
4.3.1	Plant (Nominal System)	37
4.3.2	Reconfigurable Controller	42
4.3.3	PHM Module	45
CHAPTER V:	STABILITY AND UNCERTAINTY ANALYSIS	47
5.1	Reference Model	47
5.2	Composite System	49
5.2.1	Plant.....	49
5.2.2	MPC Controller.....	49

5.3	Error Analysis.....	51
5.3.1	Tracking Error	51
5.3.2	Modeling Error	52
5.4	State-Variable Adjustment Analysis.....	57
5.4.1	Ideal (Matched) Case.....	57
5.4.2	Non-Ideal (Unmatched) Case	58
5.5	RUL Analysis	59
5.5.1	Boundary Conditions.....	59
5.5.2	Metrics	60
CHAPTER VI: MPC ALGORITHM		62
6.1	Reference / Prediction Model.....	62
6.2	Description	64
6.3	Optimizer.....	65
6.3.1	Objective Function	65
6.3.2	Medium-Scale Quadratic Programming	66
6.3.3	Aliasing.....	67
CHAPTER VII: EXAMPLE APPLICATION.....		69
7.1	General Design Criteria	69
7.1.1	System Model and Evaluation	71
7.1.2	Constraints and Operating Conditions.....	71
7.1.3	RUL Feasibility	71
7.2	Electro-Mechanical Actuator (EMA) Design Criteria	73
7.2.1	System Model and Evaluation	73
7.2.2	Constraints and Operating Conditions.....	74
7.2.3	RUL Feasibility	75

7.3	Determining MPC Weights	79
7.4	Selecting an Adaptation Function	81
7.5	Model Uncertainty	85
7.6	Long-Term State Predictions with Uncertainty	87
7.7	RUL Estimation & Uncertainty	89
7.7.1	Sinusoidal Signals with Fixed Amplitude and Frequency	89
7.7.2	Aperiodic Signal	91
7.8	Load Disturbances	94
CHAPTER VIII: CONCLUSIONS		99
APPENDIX A: NOTATION		100
A.1	Functional Notation	100
A.1.1	Continuous-Time Functions	100
A.1.2	Discrete-Time Functions	100
A.1.3	Zero-Order Hold (ZOH) Discretization	100
A.2	Symbolic Notation	102
A.2.1	Variable Types	102
A.2.2	Common Constants	102
A.2.3	Vector Operations	103
APPENDIX B: DEFINITIONS & THEOREMS		105
B.1	Function Definitions	105
B.1.1	Dirac-delta Function	105
B.1.2	Norm Function	105
B.1.3	System Properties	106

APPENDIX C: MPC DERIVATIONS	107
C.1 State Predictor Constants	107
C.2 Weight Matrices	109
C.3 Inequality Constraints	110
C.3.1 Box Constraints.....	110
C.3.2 Rate of Set-Point Adjustment	110
C.3.3 Constraint Concatenation.....	111
C.4 Kuhn Tucker Conditions	112
APPENDIX D: LINEAR ACTUATOR MODEL	114
D.1 Linear State Space Model	114
D.2 Modeling Parameters	117
APPENDIX E: ACTUATOR / PROGNOSTIC MODEL	118
E.1 Failure Modes and Effects.....	118
E.2 Physics Based Model	119
E.3 Fault Growth Model.....	120
E.4 Prognostic Model	122
REFERENCES.....	124
VITA	131

LIST OF TABLES

Tables 7.1:	Actuator constraints applied to system reconfiguration.....	74
Tables 7.2:	Adaptation function parameters.....	82
Tables 7.3:	Computed values for RUL and RLI for different externally applied load disturbances	97
Tables D.1:	List of actuator modeling parameters with values and corresponding uncertainty.	117
Tables E.1:	List of prognosis modeling parameters.	123

LIST OF FIGURES

Figure 2.1:	Block diagram of the plant comparing the original production controller and physical process against two different reconfiguration strategies	7
Figure 2.2:	Block diagram of three-phase actuator.....	8
Figure 2.3:	Predicted fault growth curves, hazard zone and corresponding projection on the time-axis	15
Figure 2.4:	Procedure to estimate the lifetime adjustment parameter.....	25
Figure 2.5:	Plot showing the adjusted set-points and predicted output of the MPC over a prediction horizon.....	26
Figure 2.6:	Block diagram of MPC with plant and signals	26
Figure 4.1:	Conceptual plots illustrating the fault dimension, probability of failure and tracking error for three different reconfiguration scenarios	33
Figure 4.2:	Reconfigurable control architecture 3-tier hierarchical strategy highlighting the low-level reconfiguration, mid-level redistribution and high-level mission adaptation.....	35
Figure 4.3:	Reconfigurable controller illustrating the internal MPC controller and supervisor elements in addition to the external PHM module and connected plant.	38
Figure 4.4:	Illustrative example for a given set of incremental set-point adjustments and the corresponding set-point adjustment.	42
Figure 4.5:	Flowchart of the low-level supervisor	44
Figure 5.1:	Block diagram of the composite system showing the inner-connections between the state observer, reference model and optimizer within the MPC.....	50
Figure 5.2:	Predicted fault-growth curves, hazard zone and corresponding projection on the time axis for the best-case and worst-case reconfiguration boundaries.....	61
Figure 6.1:	MPC showing common elements.	64
Figure 6.2:	Pseudo-code for the active set algorithm.	66

Figure 6.3:	Average floating point operation count for different size prediction horizons.	68
Figure 7.1:	Flowchart used to determine feasibility criteria for the reconfigurable control design.	70
Figure 7.2:	Photo of the X-38 crew re-entry vehicle and its corresponding rudder actuator.....	73
Figure 7.3:	Simulated plots of motor current versus time for a set of ramp inputs with a constant slope.....	76
Figure 7.4:	Simulated plots of motor current versus time for a set of sinusoidal reference inputs.....	77
Figure 7.5:	Simulated plots of actuator position and motor current before and after applying the MPC controller.....	78
Figure 7.6:	Simulated plots of the reconfiguration efficiency versus the adaptation parameter for different sinusoidal inputs.....	80
Figure 7.7:	Plots of the adaptation parameter applied set-point adjustment versus time after applying the MPC controller with parameter adaptation.....	83
Figure 7.8:	Plots of the actuator position and motor current vs time both before and after applying the MPC controller with parameter adaptation.....	84
Figure 7.9:	Plots for the maximum percent change versus frequency and corresponding histogram.....	86
Figure 7.10:	Plots of the actuator position, applied set-point adjustment and corresponding motor current with ninety-five percent uncertainty boundaries.....	88
Figure 7.11:	Plot of life consumed versus prognostic horizon before and after reconfiguration for a sinusoidal reference input with a fixed amplitude and frequency.....	90
Figure 7.12:	Plots of the actuator position signal, applied set-point adjustment and motor current before and after applying the MPC controller.....	92
Figure 7.13:	Plot of life consumed versus prognostic horizon before and after reconfiguration for a reference input using Figure 7.12 as a repeated sequence.....	93

Figure 7.14:	Plots of actuator position and motor current before and after applying the MPC controller with no external load and a fixed external load condition.....	95
Figure 7.15:	Plot of the maximum reconfiguration efficiency versus the externally applied actuator load.....	96
Figure 7.16:	Plots of the lower RUL boundary, change in RUL and RLI vs. actuator load over a range of externally applied loads.....	98
Figure D.1:	Block diagram of the fifth-order actuator model.	116
Figure E.1:	Schematic of the first-order thermal model.	119
Figure E.2:	Block diagram equivalent fault-growth state-space model.	121

NOMENCLATURE

Abbreviations

AAD	Aircraft Aging and Durability
AFRL	Air Force Research Laboratory
AFTCS	FTC Systems
AI	Artificial Intelligence
ARE	Algebraic Riccati Equation
ASP	Aviation Safety Program
CL	Confidence Level
DRE	Differential Riccati Equation
DTC	Direct Torque Control
EMA	Electro-Mechanical Actuator
ESMD	Exploration Systems Mission Directorate
FA	Fundamental Aeronautics
FDD	Fault Detection and Diagnosis
FHOC	Finite Horizon Optimal Control
FMECA	Failure Modes, Effects and Criticality Analysis
FSFCC	F/A-18 Fleet Support Flight Control Computer
FTC	Fault-Tolerant Control
IHOC	Infinite Horizon Optimal Control
IIFD	Integrated Intelligent Flight Deck
IRAC	The Integrated Resilient Aircraft Control
IVHM	Integrated Vehicle Health Management
JANNAF	Joint Army Navy NASA Air Force
JSF	Joint Strike Fighter
LMI	Linear Matrix Inequality
LQR	Linear Quadratic Regulator

LTI	Linear Time Invariant
MPC	Model Predictive Control
PCoE	Prognostics Center of Excellence
pdf	Probability Density Function
PFTCS	Passive Fault Tolerant Control Systems
PHM	Prognostic Health Management
PUI	Prediction Uncertainty Increase
RLI	Remaining Life Increase
RUL	Remaining Useful Life
SISO	Single-Input Single-Output
SVM	Space Vector Modulation
UAV	Unmanned Aerial Vehicle

Symbols

α	False alarm rate (or type I error)
$\bar{\omega}_\ell$	Load speed equilibrium
$\bar{\omega}_m$	Motor speed equilibrium
$\bar{\theta}_\ell$	Load position equilibrium
$\bar{\theta}_m$	Motor position equilibrium
\bar{i}_m	Motor current equilibrium
β	Type II error
Δ_o	Observation offset matrix
Δ_p	Prediction offset matrix
δ_{\max}	Maximum incremental set-point
δ_{\min}	Minimum incremental set-point
δ_u	Incremental set-point
λ_p	LaGrange multiplier vector
λ_p^*	MPC LaGrange multiplier vector
$\Delta t_{\text{RUL}(lb)}$	Change in lower RUL boundary
δ	Dirac-delta function
$\Delta \hat{\mathbf{x}}$	Estimated state vector offset
$\Delta \mathbf{A}_m$	Transition matrix modeling offset
$\Delta \mathbf{B}_{m,r}$	Input matrix modeling offset
$\Delta \mathbf{B}_{m,v}$	Disturbance input matrix modeling offset
$\Delta \mathbf{C}_m$	Observation matrix modeling offset
$\Delta \mathbf{u}$	Set-point adjustment
$\Delta \mathbf{u}^d$	Predicted set-point adjustments (discrete)
$\Delta \mathbf{u}_p$	MPC set-point adjustment
$\Delta \mathbf{u}_{\max}$	Maximum set-point adjustment
$\Delta \mathbf{u}_{\min}$	Minimum set-point adjustment

$\Delta \mathbf{u}_p^*$	Optimal MPC set-point adjustment
$\Delta \mathbf{x}$	State vector offset
$\Delta \mathbf{x}_{lb}$	State vector offset lower-bound
$\Delta \mathbf{x}_{ub}$	State vector offset upper-bound
ϵ_{RUL}	RUL confidence interval
ϵ_{RUL}^*	Reconfigured RUL confidence interval
η	Reconfiguration efficiency
Γ	Adaptation function
γ_{ϵ_η}	Adaptation threshold
γ_ρ	Adaptation gain
\hat{i}_m	Estimated motor current
$\bar{\mathbf{e}}_o$	Observation error equilibrium
$\bar{\mathbf{e}}_p$	Prediction error equilibrium
$\bar{\mathbf{u}}$	Control input equilibrium
$\bar{\mathbf{v}}$	Measured disturbance equilibrium
$\bar{\mathbf{x}}$	State equilibrium
$\bar{\mathbf{x}}_m$	Modeled state equilibrium
$\bar{\mathbf{y}}$	Deterministic plant output
$\tilde{\mathbf{e}}_o$	Equilibrium shifted observation error
\mathbf{A}_e	Tracking error transition matrix
\mathbf{A}_m	Transition matrix model
\mathbf{A}_m^d	Discrete transition matrix model
$\mathbf{A}_{\delta u}$	MPC set-bound adjustment constraint matrix
\mathbf{b}_0	MPC quadratic cost vector
$\mathbf{b}_{\delta u(lb)}$	MPC set-point adjustment constraint lower-boundary vector
$\mathbf{b}_{\delta u(ub)}$	MPC set-point adjustment constraint upper-boundary vector
$\mathbf{B}_{m,r}$	Control input matrix model

$\mathbf{B}_{m,r}^d$	Discrete control input matrix model
$\mathbf{B}_{m,v}$	Disturbance input matrix model
$\mathbf{B}_{m,v}^d$	Discrete disturbance input matrix model
\mathbf{c}	MPC inequality constraint upper-boundary vector
\mathbf{C}_m	Observation matrix model
$\mathbf{D}_{m,v}$	Disturbance matrix model
\mathbf{e}	Tracking error
\mathbf{e}^+	Extended tracking error
\mathbf{e}_m	Modeling error
\mathbf{e}_o	Observation error
\mathbf{e}_p	Prediction error
\mathbf{e}_{\max}	Maximum tracking error
\mathbf{e}_{\max}^+	Maximum extended tracking error
\mathbf{e}_{\min}	Minimum tracking error
\mathbf{e}_{\min}^+	Minimum extended tracking error
\mathbf{f}	Feature vector
\mathbf{g}	Equality functional mapping
\mathbf{h}	Inequality functional mapping
\mathbf{H}_0	MPC quadratic cost matrix
\mathbf{K}	Riccati gain matrix
\mathbf{k}	Riccati gain vector
\mathbf{k}_x	MPC state estimation vector
\mathbf{L}	Observer gain
\mathbf{M}	MPC inequality constraint matrix
\mathbf{n}_1	Process noise
\mathbf{n}_2	Observation noise
\mathbf{Q}	State weight matrix

\mathbf{Q}_p	MPC state weight matrix
\mathbf{R}	Control weight matrix
\mathbf{r}	Input reference
\mathbf{r}^d	Future references (discrete)
\mathbf{R}_p	MPC control weight matrix
\mathbf{r}_p	MPC future reference input
\mathbf{S}	Terminal boundary condition
\mathbf{S}_u	MPC control input matrix
\mathbf{S}_x	MPC state transition matrix
\mathbf{S}_{vx}	MPC input disturbance matrix
\mathbf{u}_f	Prognostic control input
\mathbf{u}_{\max}	Maximum control input
\mathbf{u}_{\min}	Minimum control input
\mathbf{v}	Measured disturbance
\mathbf{v}_p	MPC future measured disturbances
\mathbf{x}_{m0}^d	Initial MPC state
\mathbf{x}^+	Reconfigured state
\mathbf{x}^*	Desired state-space vector
\mathbf{x}_0	Initial state
\mathbf{x}_m	Modeled state estimate
\mathbf{x}_p	MPC predicted state vector
\mathbf{x}_p^*	MPC desired state-space vector
\mathbf{x}_{lb}	State vector lower-bound
\mathbf{x}_{m0}	Modeled initial state
\mathbf{x}_{ub}	State vector upper-bound
\mathbf{y}_m	Modeled output
\mathcal{L}	Lagrangian (or cost operator)

\mathcal{T}_{RUL}	RUL space
\mathcal{U}	Control space
\mathcal{U}_δ	Set-point adjustment space
\mathcal{X}	State space
ω_m	Motor speed
ω_ℓ	Actuator speed
Φ	End-point (or terminal) cost
Ψ	Final damage cost
ψ_{nl}	Non-linear mapping
ρ	Adaptation parameter
ρ^*	Optimal adaptation parameter
ρ_{max}	Maximum adaptation parameter
θ_m	Motor position
θ_ℓ	Actuator position
ϖ	Random Gaussian variable
b_m	Motor damping
b_ℓ	Load damping [in · lbf / (rad/s)]
c_0	Constant of proportionality
C_{wa}	Thermal capacitance
e	Tracking error
E_a	Activation energy
e_{max}	Maximum tracking error
e_{max}^+	Maximum extended tracking error
e_{min}	Minimum tracking error
e_{min}^+	Minimum extended tracking error
f_0	MPC quadratic cost scalar
f_m	Process model

f_p	Fault growth mapping
f_{ub}	Frequency range upper-bound
h_m	Observation model
h_p	Feature mapping
H_λ	Hamiltonian mapping
H_{lb}	Hazzard zone lower-bound
H_{ub}	Hazzard zone upper-bound
i_m	Motor current
$i_{m,\max}$	Maximum motor current
$i_{m,\min}$	Minimum motor current
J	Cost functional
J_m	Motor inertia
J_x	Cost functional of the states
$J_{\Delta u}$	Cost functional of the set-point adjustments
J_ℓ	Load inertia
k_1	Controller gain 1
k_2	Controller gain 2
k_3	Controller gain 3
k_4	Controller gain 4
k_5	Controller gain 5
k_e	Back-emf coefficient
k_T	Boltzmann's constant
k_t	Motor torque coefficient
k_ℓ	Load stiffness
k_{cs}	Coupling stiffness
L	Fault dimension
L_0	Initial fault dimension

L_{tt}	Turn-to-turn inductance
m	Control horizon
n_r	Reference dimension
n_v	Disturbance dimension
n_x	State dimension
N_{cl}	Load coupling
N_{cm}	Motor coupling
p	Prediction horizon
r	Number of constraints
R_0	Winding resistance
R_{tt}	Turn-to-turn resistance
R_{wa}	Thermal resistance
T	Finite time horizon
t	Time
t_0	Initial time
T_a	Ambient temperature
t_f	Final time
T_s	Sampling period
T_w	Winding temperature
$t_{\text{RUL}(lb)}$	Lower RUL boundary
$t_{\text{RUL}(lb)}^*$	Reconfigured lower RUL boundary
$t_{\text{RUL}(ub)}$	Upper RUL boundary
$t_{\text{RUL}(ub)}^*$	Reconfigured upper RUL estimate
t_{RUL}	Remaining Useful Life
t_{detect}	Initial fault detection time
t_{mission}	Mission time
$t_{\text{prognosis}}$	Initial failure prediction time
T_{wa}	Winding-to-ambient temperature
\mathbf{x}_d^*	Desired model states (discrete)

SUMMARY

The emergence of complex and autonomous systems, such as modern aircraft, unmanned aerial vehicles (UAVs) and automated industrial processes is driving the development and implementation of new control technologies aimed at accommodating incipient failures to maintain system operation during an emergency. The motivation for this research began in the area of avionics and flight control systems for the purpose to improve aircraft safety. A prognostics health management (PHM) based fault-tolerant control architecture can increase safety and reliability by detecting and accommodating impending failures thereby minimizing the occurrence of unexpected, costly and possibly life-threatening mission failures; reduce unnecessary maintenance actions; and extend system availability / reliability.

Recent developments in failure prognosis and fault tolerant control (FTC) provide a basis for a prognosis based reconfigurable control framework. Key work in this area considers: (1) long-term lifetime predictions as a design constraint using optimal control; (2) the use of model predictive control (MPC) to retrofit existing controllers with real-time fault detection and diagnosis (FDD) routines; (3) hybrid hierarchical approaches to FTC taking advantage of control reconfiguration at multiple levels, or layers, enabling the possibility of set-point reconfiguration, system restructuring and path / mission re-planning. Combining these control elements in a hierarchical structure allows for the development of a comprehensive framework for prognosis based FTC.

First, the PHM-based reconfigurable controls framework presented in this thesis is given as one approach to a much larger hierarchical control scheme. This begins with a brief overview of a much broader three-tier hierarchical control architecture defined as having three layers: supervisory, intermediate, and low-level. The supervisory layer manages high-level objectives. The intermediate layer redistributes component loads

among multiple sub-systems. The low-level layer reconfigures the set-points used by the local production controller thereby trading-off system performance for an increase in remaining useful life (RUL).

Next, a low-level reconfigurable controller is defined as a time-varying multi-objective criterion function and appropriate constraints to determine optimal set-point reconfiguration. A set of necessary conditions are established to ensure the stability and boundedness of the composite system. In addition, the error bounds corresponding to long-term state-space prediction are examined. From these error bounds, the point estimate and corresponding uncertainty boundaries for the RUL estimate can be obtained. Also, the computational efficiency of the controller is examined by using the number of average floating point operations per iteration as a standard metric of comparison.

Finally, results are obtained for an avionics grade triplex-redundant electro-mechanical actuator (EMA) with a specific fault mode; insulation breakdown between winding turns in a brushless DC (BLDC) motor is used as a test case for the fault-mode. A prognostic model is developed relating motor operating conditions to RUL. Standard metrics for determining the feasibility of RUL reconfiguration are defined and used to study the performance of the reconfigured system; more specifically, the effects of the prediction horizon, model uncertainty, operating conditions and load disturbance on the RUL during reconfiguration are simulated using MATLAB[®] and Simulink[®].

The contributions of this body of work are the following:

- Define a control architecture
- Prove stability and boundedness (performance and RUL)
- Derive the control algorithm and examine its performance
- Demonstrate feasibility with an example

CHAPTER I

INTRODUCTION

In this opening chapter, a brief overview of the problem, its history, significance and current research initiatives are discussed. Beginning in Section 1.1 is the origin and history of the problem along with a brief summary of current research initiatives. Next, Section 1.2 provides a brief description of the “state of the art” in related fields. Finally, the chapter concludes in Section 1.3 with the organization for the remainder of the dissertation.

1.1 The Origin and History of the Problem

The emergence of complex and autonomous systems, such as modern aircraft, unmanned aerial vehicles (UAV), automated industrial processes, among many others, is driving the development and implementation of new control technologies that are aimed to accommodate incipient failures and maintain a stable system operation for the duration of the emergency. The primary motivation for this research topic emerged over the need for improved reliability and performance for safety critical systems, particularly in aerospace related applications. In the scope of this work, reliability is defined as [1],

Definition 1.1 (Reliability). The probability that a system will perform within specified constraints for a given period of time.

1.1.1 Relevance

Fatal accidents in the worldwide commercial jet fleet during the years 1987-2005 were due primarily to (i) controlled flight into terrain, (ii) loss-of-control in flight and (iii) system/component failure or malfunction [2]. In a coordinated effort to improve

aviation safety, industry and government worked together to reduce the number of fatal commercial aircraft accidents, which dropped by 65% during the period of 1996-2007 [3]. As a result of this effort, accidents due to controlled flight into terrain have been virtually eliminated through the addition of various safeguards, but the same cannot be said for accidents due to loss-of-control in flight and system/component failure or malfunctions. System/component failure and malfunctions are recognized as contributing factors to aircraft loss-of-control in flight, so safeguarding against such events will reduce the number of fatal accidents in the two top accident categories (ii) and (iii) respectively.

1.1.2 Current Initiatives

Military fixed wing aircraft programs drove much of the reconfigurable controls work in the 1980s and 1990s, but applications to passenger and general aviation began to receive substantial interest under the NASA aviation safety program (ASP) founded in 1997 [4]. NASA ASP research focuses on vehicle design, manufacturing, operation, and maintenance. Presently, two major NASA ASP initiatives, integrated vehicle health management (IVHM) and the integrated resilient aircraft control (IRAC) projects, are addressing these needs by developing innovative technologies, tools and methods to protect against hardware system/component failure or malfunctions.

1.1.2.1 Integrated Vehicle Health Management (IVHM) Project

The IVHM project began in 2008 to develop validated tools, technologies and techniques for automated detection, diagnosis and prognosis that enable mitigation of adverse events during flight [5]. Specific goals of the IVHM program include:

- Integrated vehicle health management
- Fault-tolerant systems
- Intelligent systems capable of self-diagnosis and reconfiguration

1.1.2.2 The Integrated Resilient Aircraft Control (IRAC) Project

The IRAC project started in 2007 to advance the state of aircraft flight control by providing on-board control resilience for ensuring safe flight in adverse conditions [6].

1.1.2.3 The Prognostics Center of Excellence (PCoE)

The PCoE is a center at NASA AMES for prognostic technology development, addressing prognostic technology gaps within the application areas of aeronautics and space exploration. Specific areas of interest include, [7],

- **Uncertainty management:** How can the information from multiple uncertainty sources be properly captured and processed?
- **Autonomic control reconfiguration:** How can local prognostic information be translated into changes at the controller level such that controller objectives are satisfied in the long term?
- **Integration:** How should information from different, interacting subsystems be combined and processed?
- **Validation and verification of prognostics:** How can the proper operation of prognostic algorithms be validated, especially on new systems?
- **Post-prognostic reasoning:** How can the information from a prognostic reasoner be turned into an action, also factoring in other considerations such as logistics information, mission information, and fleet management?

1.1.2.4 Collaborative Programs

Additional related programs exist with collaboration among academia, industry and other government agencies to leverage expertise and technological advances. The coordination and collaboration efforts include but are not limited to the integrated intelligent flight deck (IIFD) project, aircraft aging and durability (AAD) project, fundamental aeronautics (FA), exploration systems mission directorate (ESMD), joint army navy NASA air force (JANNAF) and the air force research laboratory (AFRL).

1.2 State of the Art

The current state of the art in aircraft IVHM is exemplified by the joint strike fighter (JSF) program. This program has incorporated PHM into its design using sensors, advanced processing and reasoning, and a fully integrated system of information and supplies management. The on-board JSF PHM system is hierarchical, dividing the aircraft into areas such as propulsion and mission systems. Area data is generated by a mixture of dedicated, purpose-built sensors and analysis on existing control sensors to identify degradation and failures, which are compiled and correlated by area reasoners and then correlated by system-level model-based reasoners. Maintenance data-links transmit vehicle health data to ground-based information systems focused on maintenance and management of the supply chain. Prognostic events are detected by prognostic built-in-tests, automated post-flight trending, and reasoning with an emphasis on distinguishing sources of degradation rather than failure. An autonomic logistics information system provides logistic support to the end-user and also provides off-board trending across the entire JSF fleet [8]. Although these represent significant achievements, it is widely acknowledged that more work is required to build reliable, effective health management systems that build upon detection, diagnostics, and prognostics to enable safe and efficient implementation of mitigation strategies [5].

1.3 Organization of Dissertation

The remainder of this document is organized as follows. Chapter 2 presents a literature review for fault detection and diagnosis, long-term prognosis predictions and fault tolerant control strategies. Chapter 3 outlines specific aims of this thesis, separated by chapter. Chapter 4 defines the FTC architecture. Chapter 5 studies the stability and boundedness of the reconfigured system and the RUL prediction. Chapter 6 presents the MPC algorithm used by the FTC. Chapter 7 provides general design guidelines and demonstrates the reconfigurable control algorithms on an EMA. Finally, Chapter 8 summarizes the findings and future work. Supporting material such as nomenclature, theorems and models not explicitly presented in the body of this document is provided in the Appendix.

CHAPTER II

LITERATURE REVIEW

According to the NASA ASP IVHM program, the following enabling technologies are necessary before prognosis based control can be considered: fault detection, fault diagnosis and failure prognosis [5]. First, a conceptual overview of the reconfiguration approach discussed in this dissertation is presented in Section 2.1. Next, fault detection and fault diagnosis are discussed in Section 2.2 as a combined topic in fault detection and diagnosis (FDD). Then, a background on failure prognosis and long-term prediction is given in Section 2.3. The remainder of the chapter investigates fault tolerant control (FTC) strategies, in Section 2.4, with references to applications in diagnosis and prognosis where applicable.

2.1 Conceptual Overview

In the scope of this body of work, reconfiguration is performed without directly modifying the plant, which consists of the process to be controlled and its corresponding production controller, shown in Figure 2.1(a). Traditionally, reconfiguration is performed on the production controller within the plant itself as illustrated in Figure 2.1(b). However, in some cases the plant is physically closed to the designer where access to the production controller is not available. An alternative approach allows indirect reconfiguration of the plant by modifying its external reference command, illustrated in Figure 2.1(c). An example of a system where direct access to the controller is not available and set-point reconfiguration is utilized is provided in this dissertation using an EMA.

2.1.1 Electro-Mechanical Actuator (EMA) Example

The EMA studied in this dissertation consists of a three-phase brushless-DC motor, a gear train and a flight surface (or loading mechanism) as shown in Figure 2.2.

The motor is controlled using a direct torque control (DTC) scheme based on the application of space vector modulation (SVM). The terminal voltages applied to the motor windings are calculated from the phase voltage commands, which are generated by the current controllers. Three current feedback controllers are used to match the current on each of the three winding phases. By estimating the synchronous speed and the voltage behind the transient reactance, the change in torque and flux over the switching period is calculated and used to update the current commands, accordingly. Finally, a position and velocity controller are used to track the output response (actuator position) with a reference command (desired position).

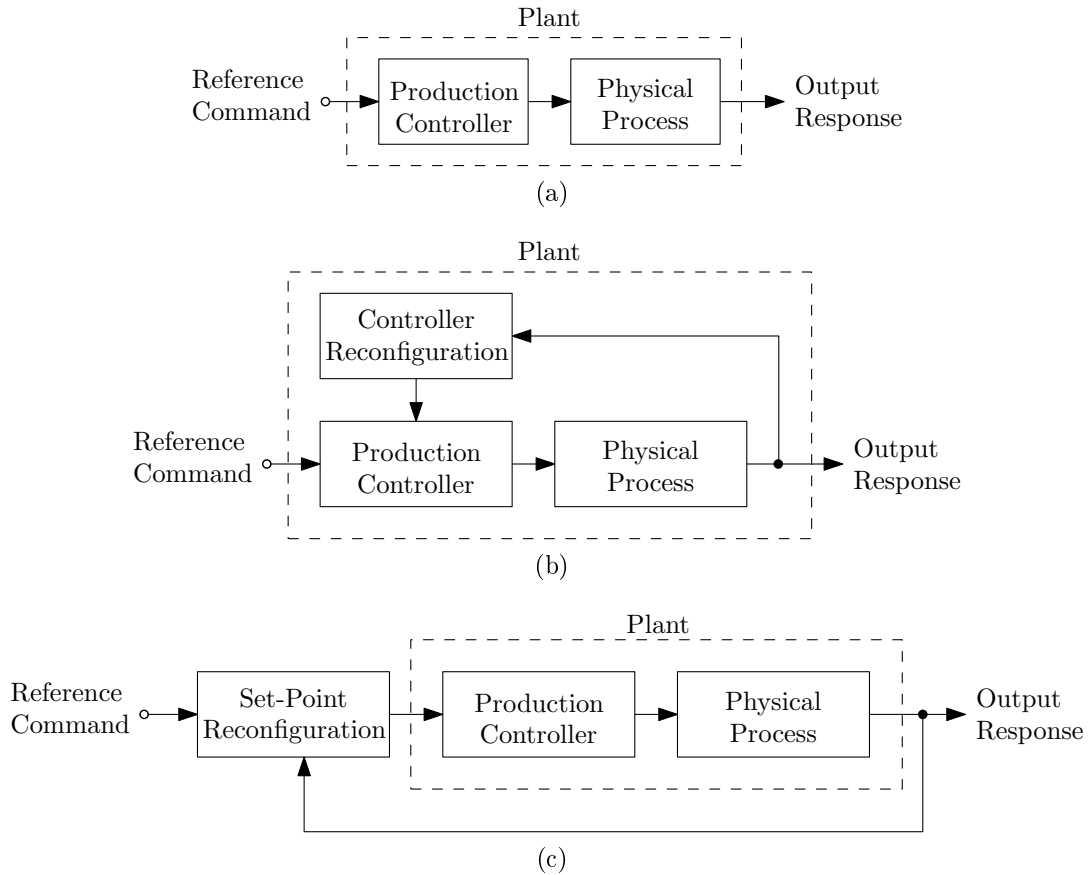


Figure 2.1: Block diagram of the (a) plant illustrating the production controller and physical process (b) plant with internal control reconfiguration and (c) plant with external set-point reconfiguration.

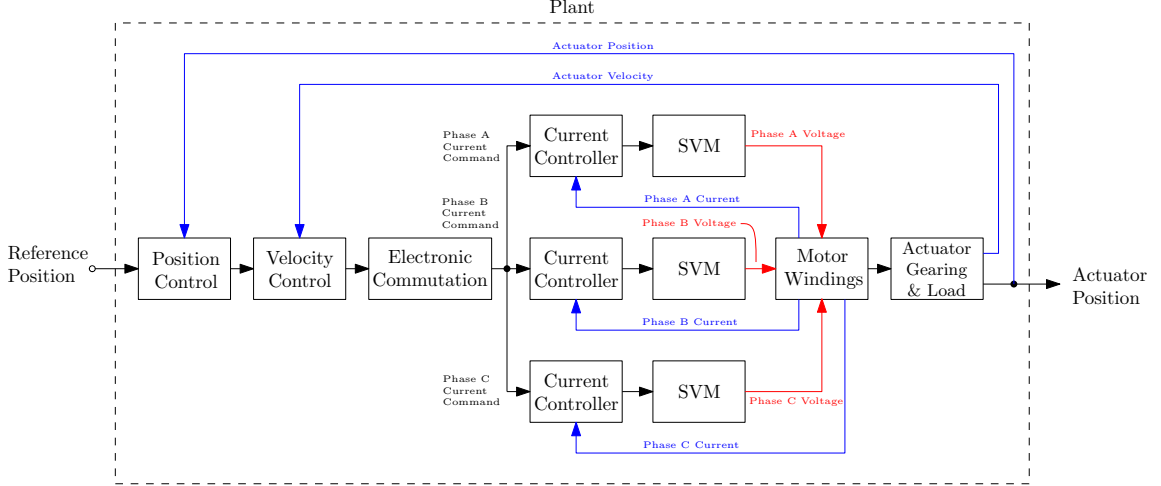


Figure 2.2: Block diagram of three-phase actuator.

2.1.2 Physical Constraints

The EMA example used in this dissertation is studied with the following physical constraints imposed by the manufacturer:

- The production controller (which includes the position, velocity and current controllers) is proprietary to the manufacturer and is inaccessible. Therefore, reconfiguration to the production controller is not a viable option.
- In the case of the EMA, only two phase currents of the three-phase motor are measured. The third phase current is inferred from the other two such that the sum of the total phase currents are zero. During a turn-to-turn winding fault condition the actual phase currents deviate from the estimate. This introduces error into the system.

To overcome these physical constraints a simplified model of the EMA (plant) is used as a reference model in set-point reconfiguration. The major problem with this approach is the plant itself changes during the occurrence of a fault and continues to change as the fault progresses. In the scope of this work, it is assumed the system is still controllable during the fault state and the discrepancy between the true plant and the reference model can be represented as a modeling error. Although imperfect, this approach will be demonstrated as a sub-optimal solution.

2.2 Fault Detection and Diagnosis (FDD)

Adverse events can lead to potentially serious consequences if they go undetected. Researchers in such diverse disciplines as medicine, engineering, the sciences, business and finance have been developing methodologies to detect fault or anomaly conditions, pinpoint or isolate which component in a system is faulty, and decide on the potential impact of a failing or failed component of the health of the system [9].

2.2.1 Preliminary Definitions

FDD consists of two elements, fault detection and fault diagnosis. The goal of the fault detection element is to apply validated technologies to detect anomalies from adverse events throughout the system [5]. According to Vachtsevanos *et al.* [10],

Definition 2.1 (Fault Detection). An abnormal operating condition that is detected and reported.

Whereas, the fault diagnosis element is developed to integrate and validate technologies to determine the causal factors, the nature and severity of an adverse event (fault identification) and to distinguish that event within a family of potential adverse events (fault isolation) [5]. Vachtsevanos *et al.* [10] define fault diagnosis as,

Definition 2.2 (Fault Diagnosis). Detection, isolation and identification of an impending or incipient failure condition—the affected component (subsystem, system) is still operational even though at a degraded mode.

Definitions 2.1 and 2.2 can be combined to formally define FDD,

Definition 2.3 (Fault Detection and Diagnosis (FDD)). Course of action by which a fault is detected and later diagnosed.

Before examining diagnosis any further its important to understand how raw data measurements can be related to diagnostic information. First, data acquisition is used as a front-end process to record raw sensor data. Next, raw sensor data is processed using low-level digital signal processing routines. Typical data-preprocessing routines include filtering, noise rejection / reduction and sensor fusion. Finally, higher-level data processing routines are invoked to generate feature vectors from pre-processed data using various digital signal-processing techniques.

2.2.2 Previous Work

Over the past three decades, the growing demand for reliability, maintainability, and survivability in dynamic systems has drawn significant research in FDD. Historically, FDD has been used in FTC to retrieve fault information from the system for use in a control recovery strategy and procedure, which is commonly referred to as reconfiguration. Preliminary research by Jiang & Patterson [11, 12] demonstrated that state estimation based schemes are most suitable for fault detection since they are inherently fast and cause a very short time delay in real-time decision making. However, the information from state estimation based algorithms may not be detailed enough for subsequent control system reconfiguration. Work presented by Wu and Zhang [13, 14] recommends that parameter estimation schemes be used for control reconfiguration and state estimation based schemes for FDD. A unified approach to state estimation/prediction and parameter estimation/identification for FDD using particle filtering was thoroughly studied by M. Orchard [15].

2.2.3 Particle Filtering Based Diagnosis

Particle filtering is of particular interest in diagnosis applications of complex dynamic systems, such as engines, gas turbines and gearboxes, because of its ability to handle non-linear behavior when operating under fault conditions. Moreover, particle filtering allows information from multiple measurement sources to be fused in a

principled manner [15]. The particle-filter-based diagnosis aims to accomplish these tasks, under general assumptions of non-Gaussian noise structures and non-linearities in process dynamic models, using a reduced particle population to represent the state pdf [16]. A compromise between model-based and data-driven techniques is accomplished by the use of a particle filter-based module built upon a non-linear dynamic model.

At any given instant of time, particle filtering provides an estimate of the probability masses associated with each fault mode, as well as a pdf estimate for physical variables in the system. A detailed example of this is presented given by M. Orchard [15]. Once this information is available within the FDD module, it is processed to generate proper fault-detection alerts / alarms with statistical confidence of the detection routine. Furthermore, pdf estimates for the system states may be used as initial conditions in failure prognostic routines. As a result, a swift transition between FDD and prognosis can occur and reliable prognosis can be achieved shortly thereafter [17]. This characteristic is one of the main advantages of the particle-filter-based diagnosis.

2.3 Failure Prognosis & Long-Term Prediction

The term prognosis has been used widely in medical practice to imply the foretelling of the probable course of a disease. In the industrial and manufacturing fields, prognosis is interpreted to answer the question, “*What is the remaining useful life (RUL) of a machine or component once an impending failure condition is detected, isolated, and identified?*” Within the context of this work, the following definition will be adopted from Vachtsevanos et al. [10] when referring to prognosis,

Definition 2.4 (Prognosis). The ability to predict accurately the RUL of a failing component or subsystem.

2.3.1 Preliminary Definitions

Definitions for failure, probability of failure and RUL must be well established before continuing the discussion on prognosis. First, the notion of a fault-dimension is defined.

Definition 2.5 (Fault Dimension). The size of a fault (eg. crack size) is referred to as the fault dimension and is commonly represented by the symbol, L .

The fault-growth rate is dependent on many factors including the current fault dimension and any operating or environmental conditions that may influence the fault which is described by a fault growth model.

Definition 2.6 (Fault Growth / Feature Mapping Models). A model in the form of a set of state-space equations to describe the progression of the fault-dimension, L , with time,

$$\begin{cases} \dot{L}(t) = f_p(L(t), \mathbf{u}_f(t), \mathbf{n}_1(t)), \\ \mathbf{f}(t) = h_p(L(t), \mathbf{u}_f(t), \mathbf{n}_2(t)), \end{cases} \quad (2.1)$$

where f_p and h_p are the fault growth and feature mappings, \mathbf{f} is a vector of measured feature values and \mathbf{u}_f is the prognostic control input. The vectors \mathbf{n}_1 and \mathbf{n}_2 correspond to the process noise and observation noise, accordingly.

Once a fault is defined, the criteria for a failure can be addressed.

Definition 2.7 (Failure). An event that corresponds to the fault-dimension, L , entering an unwanted range, or hazard-zone. The hazard-zone is defined by the upper and lower bounds, H_{ub} and H_{lb} , respectively.

The boundaries of the hazard zone are design parameters related to the false-alarm rate (type I error). It should be recognized any discussion regarding a failure over a future time horizon $t > t_0$ is stochastic in nature. Instead, the term probability of failure, defined in Definition 2.8, should be used.

Definition 2.8 (Probability of Failure). The probability of a failure occurring at some time t , represented as,

$$p_{\text{failure}}(t) = p(H_{lb} \leq L(t) \leq H_{ub}), \quad (2.2)$$

where p is a probability density function (pdf).

Finally, its often convenient to describe the minimum time-horizon corresponding to a failure with a particular level of certainty. This is formally referred to as the RUL, and represented by the symbol $t_{\text{RUL}(lb)}$.

Definition 2.9 (Remaining Useful Life (RUL)). The amount of time before a failure occurs at the initial time of prediction, t_0 . The time corresponding to the probability of failure can be expressed as,

$$t_{\text{RUL}(lb)}(t_0) \triangleq \min(t^*) \quad \text{s.t.} \quad p_{\text{failure}}(t^*|t_0) \geq \beta, \quad (2.3)$$

where $t^* \in (t_0, \infty)$ and $0 < \beta < 1$. The symbols t_0 and β refer to the initial prediction time and the type-II error associated with the prediction accordingly.

Sometimes the term confidence level is used instead of the type-II error, which is defined in Definition 2.10.

Definition 2.10 (Confidence Level (CL)). Let the upper RUL boundary, $t_{\text{RUL}(ub)}$, predicted at time t_0 be defined as,

$$t_{\text{RUL}(ub)}(t_0) \triangleq \min(t^*) \quad \text{s.t.} \quad p_{\text{failure}}(t^*|t_0) \leq 1 - \beta. \quad (2.4)$$

where $t^* \in (t_0, \infty)$. Then the CL is defined by the following probability,

$$\text{CL} = \int_{t_{\text{RUL}(lb)}}^{t_{\text{RUL}(ub)}} p_{\text{failure}}(t^*|t_0) dt^*. \quad (2.5)$$

Additionally, CL is related to β by,

$$\text{CL} = 1 - 2\beta. \quad (2.6)$$

Figure 2.3 illustrates the predicted fault growth of a system where a fault is detected at time t_{detect} and a prediction of the RUL is made at time $t_{\text{prognosis}}$. The boundaries

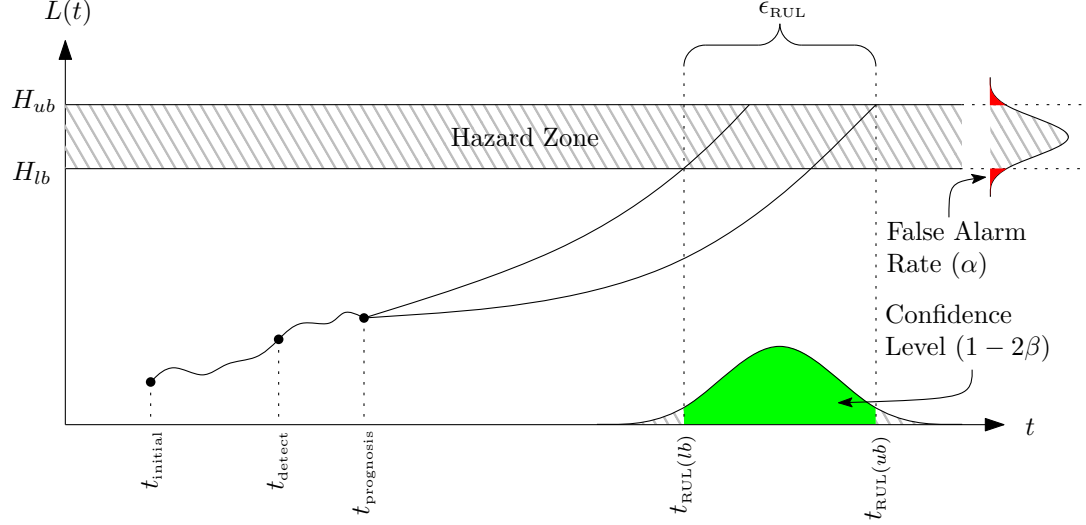


Figure 2.3: Predicted fault growth curves, hazard zone and corresponding projection on the time-axis.

of the hazard-zone are defined by H_{lb} and H_{ub} . The probability that a failure occurs outside this boundary is defined as the false-alarm rate, α . The time corresponding to each predicted fault trajectory in the hazard-zone is represented as a distribution on the time-axis. The upper and lower RUL boundary values that encompass a CL of $1 - 2\beta$ are represented as $t_{RUL(ub)}$ and $t_{RUL(lb)}$, accordingly. The width of the corresponding confidence interval is defined as,

$$\epsilon_{RUL} \triangleq t_{RUL(ub)} - t_{RUL(lb)} \quad (2.7)$$

Several approaches to prognosis have been investigated in recent years, such as model-based, data-driven, hybrid methods and particle filtering. Each approach is discussed briefly.

2.3.2 Data-Driven Prognostics

Data driven approaches use historical data to automatically learn a model of system behavior by using processed data, or features, related to system health. Data-driven approaches are appropriate when the first principles of system operation are not comprehensive or when the system is sufficiently complex such that developing an accurate model is impractical [18]. Depending on the format of the stored data,

these processes can range from signal processing of sampled measurements to queries performed on database tables [1]. Data-driven approaches include machine learning, neural networks, decision trees and support vector machines.

2.3.3 Model-Based Prognostics

Model-based prognostics attempts to incorporate physical models of the physics of failure when estimating RUL. Examples include Yu and Harris’s fatigue life model for ball bearings [19], which relates the fatigue life of a bearing to the induced stress and Paris and Erdogan’s crack growth model [20, 21]. However, purely model-based approaches rely on accurate estimates of model parameters which are seldom known a-priori and can lead to substantial uncertainty of long-term RUL predictions.

2.3.4 Hybrid-Based Prognostics

Hybrid-based prognostics combines the benefits from both data-driven and model-based approaches by utilizing off-line and on-line processes. In the off-line mode, physics-based models and knowledge of physics of failure are used to understand fault propagation. In the on-line mode, real-time data is used to estimate the fault dimension and estimate model parameters for use in prognosis.

2.3.5 Particle Filtering Based Prognostics

Particle filtering based prognostics estimates the probability of failure in a system given a hazard zone that is defined by a pdf with lower and upper bounds for the domain of the random variable, denoted as H_{lb} and H_{ub} , respectively. The probability of failure at any future time instant is estimated by combining both the weights of predicted trajectories and specifications for the hazard zone. The resulting RUL pdf estimate is composed of the probability of the RUL estimate corresponding to each particle. This provides the basis for the generation of confidence intervals and expectations for prognosis.

2.4 Fault–Tolerant Control (FTC) Strategies

Modern systems rely on sophisticated controllers to meet increased performance and safety requirements. A conventional feedback control design for a complex system may result in unsatisfactory performance, or even instability, in the event of malfunctions in actuators, sensors or other system components. To overcome such weaknesses, new approaches to control system design have been developed in order to tolerate component malfunctions while maintaining desirable stability and performance properties. According to Y. Zhang [22], FTC is defined as,

Definition 2.11 (Fault-Tolerant Control (FTC) Systems). Control systems that possess the ability to accommodate system component failures automatically [while] maintaining overall system stability and acceptable performance.

Traditionally, FTC systems are classified into two categories: *passive* and *active* [23]. Passive FTC systems (PFTCS) are designed to make a system robust against system uncertainties and anticipated faults [24]. For this reason PFTCS have a limited fault-tolerant capability. Alternatively, active FTC systems (AFTCS) react to the system component failures by reconfiguring control actions to maintain stability and acceptable system performance. In such control systems, the controller compensates for the effects of faults by selecting a pre-computed control law or synthesizing a new control scheme on-line. Analytical methods for FTC usually assume linear models of the system dynamics. For large-scale systems, this is generally a reasonable assumption since in a region of the nominal operating point, the system dynamics are approximately linear. Recent research has investigated the issue of FTC for nonlinear systems, such as using feedback linearization in a restructured digital flight control system [25]. The subsequent sections investigate several types of PFTCS and AFTCS with respect to the following attributes: stability, transient and steady-

state performance, robustness to noise, uncertainty and disturbances and interaction among other subsystems.

2.4.1 Passive Fault-Tolerant Control Systems (PFTCS)

Historically, when fault tolerance was an issue, controllers were designed targeting selected faults with specific control actions to mitigate the risk of impending failures [26]. Within such passive approaches, no fault information is required and robust control techniques are employed to ensure the closed-loop system remains insensitive to specific anticipated faults [27]. The most common and widely studied PFTCS is robust control.

A robust control is a PFTCS designed to control the system over a range of potential failure modes [28, 29]. PFTCS have been widely investigated for many years and have been demonstrated with a high level of simplicity and effectiveness for a wide range of applications; a few examples can be found in [30, 31]. PFTCS are robust to noise, large parameter variations, uncertainties/disturbances and ensure stability. Although PFTCS are widely used, they lack an active reconfiguration of the control law thus disallowing use of any external information such as FDD and prognostics. Therefore, the remaining discussion of FTC Systems will focus on AFTCS.

2.4.2 Active Fault-Tolerant Control Systems (AFTCS)

AFTCS react to system component failures by reconfiguring control actions to maintain stability and acceptable system performance. AFTCS FTC methodologies typically have two main objectives: FDD and control reconfiguration [32]. Several authors have reported on the problem of FDD [33, 34]. In such control systems, the controller compensates for the effects of faults either by selecting a pre-computed control law or by synthesizing a new control scheme on-line [35, 36]. An AFTCS consist of a reconfigurable controller, a FDD scheme and a reconfiguration mechanism [37].

2.4.2.1 Adaptive Robust Control

An adaptive robust control is a AFTCS design where the fault severity may not be known, but the system structure is known *a-priori*. This control scheme improves on PFTCS by including real-time measurements with the known structure of the system model to identify parameter variations using a model-matching scheme. For example, Ye *et al.* [38] present an adaptive fault-tolerant flight controller design methodology designed to mitigate faults caused by loss of actuator effectiveness. The approach is based on the online estimation of an eventual fault and the addition of a new control law to the nominal control law in order to reduce the fault effect without using a FDD mechanism. In the framework of a linear matrix inequality (LMI) approach, the normal tracking performance of the linear time-invariant (LTI) closed-loop system is optimized without any conservativeness and the states of the fault modes asymptotically track those of the normal mode. The adaptive control law was shown to be asymptotically stable during the presence of a fault condition by using Lyapunov's direct method. Yang *et al.* expand on this idea by applying robust control methods with \mathbf{H}_∞ and μ synthesis techniques to a faulty plant [27].

AFTCS designed using adaptive robust control techniques are insensitive to noise, uncertainties, disturbances and are shown to be mathematically stable. However, while these techniques are capable of handling many types of fault modes, they do so in a brute force way [39]. For example, if a fault condition can be modeled as a change in system parameters, an adaptive controller can be designed to monitor the changes and constantly change the control law accordingly [40, 41]. This adaptation continues indefinitely until the required control authority is no longer available leading to a failure state. Also, within the proposed framework, the adaptive fault-tolerant flight controller does not utilize any additional FDD information which may be available externally to the controller.

2.4.2.2 Expert Control

Expert control is an AFTCS design that utilizes past experience, or heuristics, in the development of control laws to provide fault accommodation for known faults. Expert systems are frequently used in large scale applications where the plant or process cannot be modeled or situations where the model is unknown. Artificial Intelligence (AI) methods have been exploited to handle model-free fault diagnosis and FTC in an expert system setting [42, 43]. Recent extensions to expert system approaches to fault tolerance include work by Wu *et al.* [44], in which past performance is used to dynamically update the database of fault controllers/parameters. Although expert control are found in a variety of FTC applications, there are no mechanisms available to demonstrate stability and boundedness in a rigorous manor.

2.4.2.3 Finite Horizon Optimal Control (FHOC)

FHOC is an AFTCS design using mathematical optimization methods over a finite time horizon, T , to derive control laws given a set of boundary constraints. Consider a generalized non-linear system,

$$\begin{cases} \dot{\mathbf{x}}(t) = f_m(\mathbf{x}(t), \mathbf{u}(t), \mathbf{n}_1(t)), \\ \mathbf{y}(t) = h_m(\mathbf{x}(t), \mathbf{u}(t), \mathbf{n}_2(t)), \end{cases} \quad (2.8)$$

where f_m is the process model, h_m is the observation model, \mathbf{x} is the state, \mathbf{u} is the control input, \mathbf{y} is the plant output, \mathbf{n}_1 is the process noise and \mathbf{n}_2 is the observation noise. An optimal control includes a cost functional, J , expressed as,

$$J(\mathbf{x}(t), \mathbf{u}(t)) = \Phi(\mathbf{x}(t_0), \mathbf{x}(t_0 + T)) + \int_{t_0}^{t_0+T} \mathcal{L}(\mathbf{x}(t), \mathbf{u}(t)) dt, \quad (2.9)$$

where \mathbf{g} is a Lagrangian (or cost operator) and Φ represents the end-point (or terminal) cost. Typically, boundary constraints on \mathbf{x} and \mathbf{u} are imposed,

$$\begin{cases} \mathbf{g}(\mathbf{x}(t), \mathbf{u}(t)) = \mathbf{0}, \\ \mathbf{h}(\mathbf{x}(t), \mathbf{u}(t)) \leq \mathbf{0}, \end{cases} \quad (2.10)$$

where \mathbf{g} and \mathbf{h} are functional mappings for the equality and inequality constraints, accordingly. However, due to the generality of the problem formulation, (2.9) may have multiple solutions. In addition, a solution to the non-linear optimal control problem is known to be prohibitively difficult, both analytically and computationally [45]. Furthermore, many numerical techniques must operate off-line which is impractical for use in on-line control reconfiguration. Instead, consider the linear optimal control problem with the linear dynamics,

$$\begin{cases} \dot{\mathbf{x}}(t) = \mathbf{A}\mathbf{x}(t) + \mathbf{B}\mathbf{u}(t) + \mathbf{n}_1(t), \\ \mathbf{y}(t) = \mathbf{C}\mathbf{x}(t) + \mathbf{n}_2(t). \end{cases} \quad (2.11)$$

Now, consider the Lagrangian operator and terminal costs replaced with quadratic terms,

$$J(\mathbf{x}(t), \mathbf{u}(t)) = \frac{1}{2} \int_{t_0}^{t_0+T} (\mathbf{x}^\top(t) \mathbf{Q}\mathbf{x}(t) + \mathbf{u}^\top(t) \mathbf{R}\mathbf{u}(t)) dt + \frac{1}{2} \mathbf{x}^\top(T) \mathbf{W}\mathbf{x}(T), \quad (2.12)$$

subject to the linear algebraic constraints,

$$\begin{cases} \mathbf{g}(\mathbf{x}) = \mathbf{0}, \\ \mathbf{h}(\mathbf{x}) \leq \mathbf{0}, \end{cases} \quad (2.13)$$

where \mathbf{Q} , and \mathbf{R} are positive definite weight matrices of constant value associated with the states and control input and \mathbf{W} is a positive semi-definite weight matrix of constant value corresponding to the terminal cost. This formulation is known as the

linear quadratic regulator (LQR), The feedback control, \mathbf{u}^* , that minimizes the cost function in (2.12) can be shown to be [46, 47, 48],

$$\mathbf{u}^*(t) = -\mathbf{K}(t) \mathbf{x}(t), \quad (2.14)$$

where \mathbf{K} is the gain matrix given by,

$$\mathbf{K}(t) = \mathbf{R}^{-1}(t) \mathbf{B}^\top(t) \mathbf{P}(t), \quad (2.15)$$

such that \mathbf{P} is found by solving the continuous time differential Riccati equation (DRE),

$$\dot{\mathbf{P}}(t) = -\mathbf{A}^\top(t) \mathbf{P}(t) - \mathbf{P}(t) \mathbf{A}(t) + \mathbf{P}(t) \mathbf{B}(t) \mathbf{R}^{-1}(t) \mathbf{B}^\top(t) \mathbf{P}(t) + \mathbf{Q}(t), \quad (2.16)$$

where $\mathbf{P} = \mathbf{P}^\top$, with the terminal boundary condition,

$$\mathbf{P}(t_k + T) = \mathbf{S}. \quad (2.17)$$

Several variants and extensions of FHOC have been used for fault-tolerant control, the most common being IHOC and MPC.

2.4.2.4 Infinite Horizon Optimal Control (IHOC)

A special case of the FHOC, where the finite time horizon T is replaced with an infinite-horizon ($T \rightarrow \infty$), is commonly encountered to reduce complexity and numerical computations [49]. The IHOC is defined by the cost function,

$$J(\mathbf{x}(t), \mathbf{u}(t)) = \frac{1}{2} \int_0^\infty (\mathbf{x}^\top(t) \mathbf{Q} \mathbf{x}(t) + \mathbf{u}^\top(t) \mathbf{R} \mathbf{u}(t)) dt. \quad (2.18)$$

where \mathbf{Q} and \mathbf{R} are positive definite weight matrices of constant value associated with the states and control input, respectively. The solution to the IHOC can be obtained from (2.16) by considering $\mathbf{P}(t) = \mathbf{P}_0$ as a constant positive definite matrix. As a result $\dot{\mathbf{P}}(t) \rightarrow \mathbf{0}$ and the DRE reduces to the following,

$$-\mathbf{A}^\top \mathbf{P}_0 - \mathbf{P}_0 \mathbf{A} + \mathbf{P}_0 \mathbf{B} \mathbf{R}^{-1} \mathbf{B}^\top \mathbf{P}_0 + \mathbf{Q} = \mathbf{0}, \quad (2.19)$$

which is also known as the algebraic Riccati equation (ARE) where the system defined by $(\mathbf{A}, \mathbf{B}, \mathbf{C})$ is assumed to be LTI. The solution, $\mathbf{u}^*(t)$ to the IHOC is the same as the FHOC,

$$\mathbf{u}^*(t) = -\mathbf{K}(t) \mathbf{x}(t), \quad (2.20)$$

where \mathbf{K} is the gain matrix given by,

$$\mathbf{K}(t) = \mathbf{R}^{-1} \mathbf{B}^\top \mathbf{P}_0, \quad (2.21)$$

An example of an IHOC controller used in an AFTCS design is given by Bogdanov *et al.* [50]. In this example, an LQR design methodology for a maximum disturbance rejection control is presented to control a servo-motor with an external load disturbance while providing a framework to consider long-term lifetime prediction as a design constraint. The winding temperature for a motor was used to meet a lifetime constraint for the winding insulation based on an estimated life remaining (or usage) model derived from historical data. The external load disturbance at the motor output is modeled as a first-order Markov process. To account for the lifetime constraint, the authors consider a parameterization of a family of infinite-horizon LQR controllers with a single parameter ρ , and then optimize the parameter to satisfy the

lifetime constraint. The infinite horizon cost function used by [50, 51] is provided as,

$$J(\mathbf{x}(t), u(t)) = \int_0^{\infty} \left([\mathbf{x}(t)]^{\top} \mathbf{Q} \mathbf{x}(t) + \rho R [u(t)]^2 \right) dt, \quad (2.22)$$

with the reported solution,

$$u^*(t) = - \underbrace{(\rho R)^{-1} \mathbf{B}^{\top} [\mathbf{P}(\rho)]}_{\mathbf{k}} \mathbf{x}(t), \quad (2.23)$$

where \mathbf{k} is the gain vector and $\mathbf{P}(\rho)$ is the solution to the modified ARE,

$$\mathbf{P} \mathbf{A} + \mathbf{A}^{\top} \mathbf{P} - \rho^{-1} \mathbf{P} \mathbf{B} R^{-1} \mathbf{B}^{\top} \mathbf{P} + \mathbf{Q} = 0. \quad (2.24)$$

Finally, the authors used the following three-step procedure to estimate the optimal value for ρ , provided in Figure 2.4. The key assumption made that RUL is inversely related to the control effort $|u|^2$. This work constitutes one of the first attempts to incorporate prognosis information into a control law for the purposes of trading off system performance to extend RUL. The LQR formulation has the advantage of providing an analytical framework not offered by the previously discussed control designs. However, the authors did not demonstrate boundedness or discuss performance constraints in the scope of their work. Instead, it was assumed that all of the available control authority could be forfeited, or traded off, to indefinitely maintain the health of the actuator. Uncertainties in lifetime estimates and their effect on the controlled system are also left unresolved.

2.4.2.5 Model Predictive Control (MPC)

A control scheme similar to FHOC which places importance on optimal performance [52, 53] subject to boundary constraints. MPC generates a discrete-time controller which takes action at regularly spaced, discrete time instances. The sampling instants,

1. **Set** $\rho = 1$ and solve the LQR problem to compute the gain \mathbf{k} .
2. **Check** if the estimated lifetime is greater than the desired lifetime.
If this condition is true then stop, otherwise continue to the next step.
3. **Solve** for ρ using the bisections algorithm.

Figure 2.4: Procedure to estimate the lifetime adjustment parameter ρ .

k , correspond to the time-instants at which the controller acts. The time between sampling instants is defined as the sampling period, T_s . An illustration of the MPC sampling instants and corresponding control actions is provided in Figure 2.5, where the current measured output, $\mathbf{y}[k]$, and the previous measurements, $\mathbf{y}[k-1]$, $\mathbf{y}[k-2]$, \dots , are known at time-instant k . To calculate the next control input the controller operates in two phases, estimation and optimization [54, 55],

1. **Estimation.** The controller needs to know the current state. This includes the true value of the controlled variable, \mathbf{y}_k and any internal variables that influence the future trend, (i.e. $\mathbf{y}_{k+1}, \dots, \mathbf{y}_{k+p}$), where p is the prediction horizon.
2. **Optimization.** Values of set points, measured disturbances, and constraints are specified over a finite horizon of future sampling instants, $k+1, k+2, \dots, k+p$ where $p \in \mathbb{Z}^+$. The controller computes m modes $\mathbf{u}[k], \mathbf{u}[k+1], \dots, \mathbf{u}[k+m-1]$, where $1 \leq m \leq p$. The symbol, m , is referred to as the control horizon.

The MPC formulation maximizes the system performance by minimizing the tracking error between the desired input reference \mathbf{r} and the measured plant output \mathbf{y} [56, 57]. Consider the general non-linear state equation from (2.8). An illustration of the non-linear system with MPC is provided in Figure 2.6 [58, 59]. The MPC is obtained by

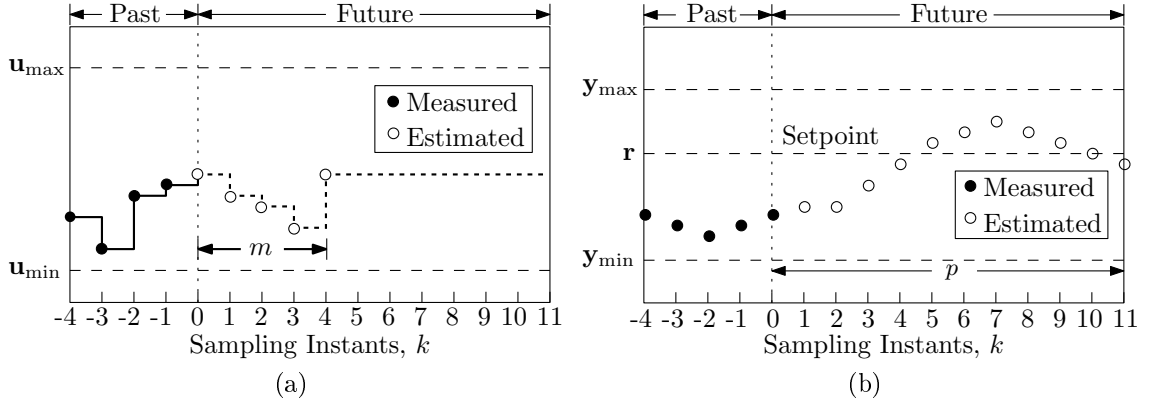


Figure 2.5: MPC controller state at the k^{th} sampling instant showing (a) adjusted set-points of the MPC for p -steps ahead at time k and (b) predicted output of the MPC for p -steps ahead at time k .

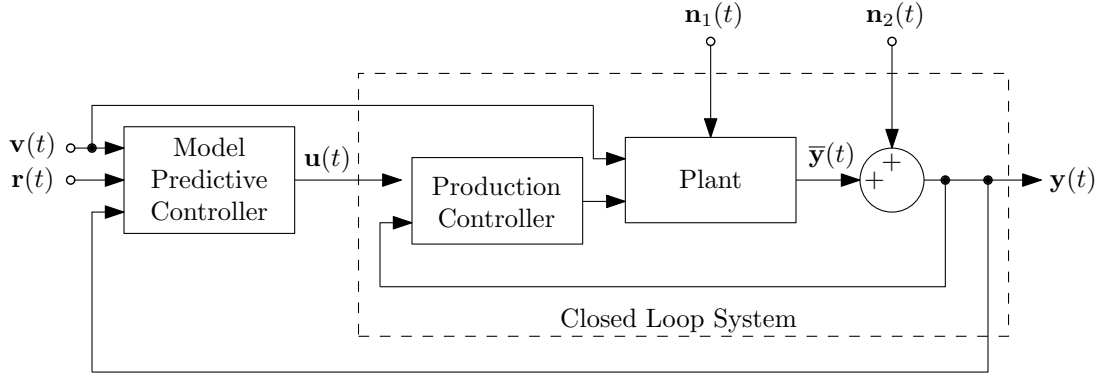


Figure 2.6: Block diagram of MPC with plant and signals

solving the optimization problem at time t_0 over the fixed time horizon, $T = pT_s$,

$$J(\mathbf{y}(t), \Delta \mathbf{u}(t)) = \int_{t_0}^{t_0+T} \left[(\mathbf{r}(t) - \mathbf{y}(t))^T \mathbf{Q} (\mathbf{r}(t) - \mathbf{y}(t)) + [\Delta \mathbf{u}(t)]^T \mathbf{R} \Delta \mathbf{u}(t) \right] dt, \quad (2.25)$$

where the vector $\Delta \mathbf{u}$ corresponds to the applied set-point adjustment. The weight matrices \mathbf{Q} and \mathbf{R} are defined *a-priori* as the inverse of the maximum allowable tracking error and control correction, respectively. The additional symbol $\bar{\mathbf{y}}$ in Figure 2.6 refers to the deterministic plant output.

For systems where on-line computation is feasible, MPC has proved quite successful [60, 61]. Monaco *et al.* [40] demonstrated an MPC based framework used to retrofit

the F/A-18 fleet support flight control computer (FSFCC) with an adaptive flight controller. The authors utilize a constrained parameter identification algorithm to provide on-line model corrections to account for uncertainties or changes in the current aircraft dynamics. The updated estimates are utilized in a MPC to provide increments to pilot commands. The increments from the adaptive control law reduce tracking error given the closed-loop dynamics of the aircraft. The adaptation is only significant if the aircraft behavior differs appreciably from the intended closed-loop flying qualities.

2.4.2.6 Hybrid Control Architectures

An AFTCS design combining modeling with AI and expert systems [62]. Many existing reconfigurable control strategies fall naturally into this category [63, 64]. More recently, hybrid hierarchical approaches to FTC have been proposed [65, 66, 67]. For example, in N. S. Clements [68], the high-level of the architecture includes situation awareness and fault diagnosis routines. The middle-level consists of three modules that actively reconfigure the controls, subsystem interconnections and local controller gains. The low-level consists of the individual components and their corresponding controllers [69]. In another manifestation, the high-level performs mission adaptation functions [70, 71, 72]. Other recent analytical approaches employ a mathematical model in which failures are captured as uncertainties in the model parameters [73], or controller reconfiguration is effected by considering the redirection of control authority between parts of the system [74].

CHAPTER III

RESEARCH AIMS

It is evident from the literature that a well defined interface for incorporating prognosis information into a control system is non-existent. However, there have been a few proposed attempts to describe what that interface may look like and how it may be implemented. The first is by Gokdere et *al.* where prognosis is incorporated into the control law using IHOC [51]. The second is by Monaco et *al.* where an MPC based framework was used to retrofit an existing control system with an adaptive controller [40]. These two concepts will be extended to accomplish the following research objective:

Objective:

Define a robust control architecture which utilizes (or retrofits) an existing physical process and controller (or plant) with prognostic health management information to extend Remaining Useful Life by trading off performance.

Specific elements of the research objective are broken up into specific aims to ensure the overall research objective is achieved. Each of these aims is discussed briefly in the following sections.

3.1 Aim #1 – Define a Control Architecture

A clear and concise definition for a control architecture which utilizes prognosis information is required. This begins in Chapter 4 by first defining the performance criteria for any such control system. Extending the work from N. Clements [68], a family of potential control schemes are presented in a three-tier hierarchical scheme. The main emphasis of this work is on a low-level reconfigurable controller designed to retrofit an existing controller using MPC. The architecture defines the interfaces between the controller, prognostic module and MPC. The architecture utilizes the MPC to adjust the set-points sent to the production controller. The set-points are adjusted by minimizing a quadratic cost function which incorporates the prognostic information into the control law. This allows future trajectories to be computed which maximizes the RUL while operating within fixed performance boundaries.

3.2 Aim #2 – Prove Stability and Boundedness

Its essential that the stability and boundedness of the reconfigurable control architecture is demonstrated in a robust manor. This is addressed in Chapter 5 where the stability of the composite plant / reconfigurable controller is studied. The overall stability and corresponding boundaries on the tracking error are examined by applying the assumptions set by the control architecture. Next, long-term prediction boundaries for the estimated plant state are studied. Additionally, boundaries for long-term RUL prediction are defined in the context of the estimated plant states. Finally, metrics are proposed to describe the effects of uncertainty associated with the estimated plant state.

3.3 Aim #3 – Derive and Benchmark the MPC Algorithm

The MPC algorithm has been extensively studied and successfully applied for several decades. However, the MPC algorithm used by this specific reconfigurable control scheme, discussed in Chapter 6, differs from the conventional algorithm. In this specific implementation, the MPC does not regulate the tracking error, rather, only the cost associated with the system state and set-point adjustment. Also, the only constraints are imposed on the set-point adjustments. Therefore, the resulting algorithm can be simplified accordingly. Details for the derivation of the MPC algorithm are given in Appendix C. The section concludes by investigating the computational efficiency of the MPC algorithm.

3.4 Aim #4 – Demonstrate Feasibility with an Example

In Chapter 7, an example application using an EMA with a known fault-mode is studied to demonstrate the MPC algorithm and feasibility of the claim that RUL can be extended through set-point reconfiguration. General design criteria along with proposed metrics are used to examine the feasibility of the control approach to a general system. Once it's determined that reconfiguration is achievable, the effects of model uncertainty, prediction horizon, reference input and measured load disturbance on the RUL are examined. Simulation results are provided to demonstrate the effectiveness of the reconfigurable control scheme in extending RUL.

CHAPTER IV

CONTROL ARCHITECTURE

The purpose of this chapter is to outline a PHM-based FTC architecture. This begins in Section 4.1 with an introduction which includes a definition of performance criteria and a qualitative overview of the desired reconfiguration action on performance and RUL. Next, in Section 4.2 a general PHM-based control architecture consisting of a three-tier hierarchical control scheme is presented. Each tier is briefly discussed along with its associated advantages and disadvantages. Finally, Section 4.3 focuses on the lower-tier in detail by defining and analyzing each module of the reconfigurable control architecture.

4.1 Introduction

The problem of incorporating prognosis in a control system can be approached in a variety of ways. The efficacy of any one approach depends on the problem formulation and the specific application. Therefore, fixed performance criteria are necessary to compare any two designs. In the scope of this work, the controller performance criteria are determined by the ability to prevent a failure while minimizing the impact on overall system performance over a well-defined time horizon. Let these criteria be evaluated by the cost function, Θ ,

$$\Theta(\Phi, \Psi) = \Phi(t_f) + \int_{t_0}^{t_f} \Psi(\mathbf{e}(t)) dt, \quad (4.1)$$

where the terminal cost is defined as,

$$\Phi = \begin{cases} \infty & : p_{\text{failure}}(t_f) \geq \beta, \\ 0 & : \text{otherwise.} \end{cases} \quad (4.2)$$

The mappings Φ and Ψ represent the cost associated with the performance and the final damage. The symbols L and \mathbf{e} refer to the fault dimension, and tracking error, accordingly.

4.1.1 Qualitative Example

Consider the plots in Figure 4.1 for the fault dimension, L , probability of failure, p_{failure} and tracking error, e , versus time for three different scenarios. The illustration of this example is simplified by considering a single-input single-output (SISO) case. Let the symbols e_{\min} and e_{\max} be constant boundaries for the tracking error and $t_{\text{RUL}(lb)}$ represent the lower confidence bound of the RUL. In scenario (a) the performance criteria is not relaxed and the RUL is not achieved. That is, the probability of failure exceeds β before time t_{mission} . In scenario (b) the performance criteria is relaxed, more specifically e_{\min} and e_{\max} are extended to e_{\min}^+ and e_{\max}^+ , to achieve the RUL. However, the performance criteria is relaxed by more than what is actually necessary. In scenario (c) the performance criteria is relaxed such that the RUL requirement is satisfied, but not as much as scenario (b). This is the desired solution, which raises the following questions,

- Existence: Under what conditions is this solution feasible?
- Uncertainty: How does uncertainty affect the existence of such a solution?

These questions are too vague to answer without first defining the scope of the problem in the context of the system to be controlled and the available control authority. The framework is discussed in the remaining sections.

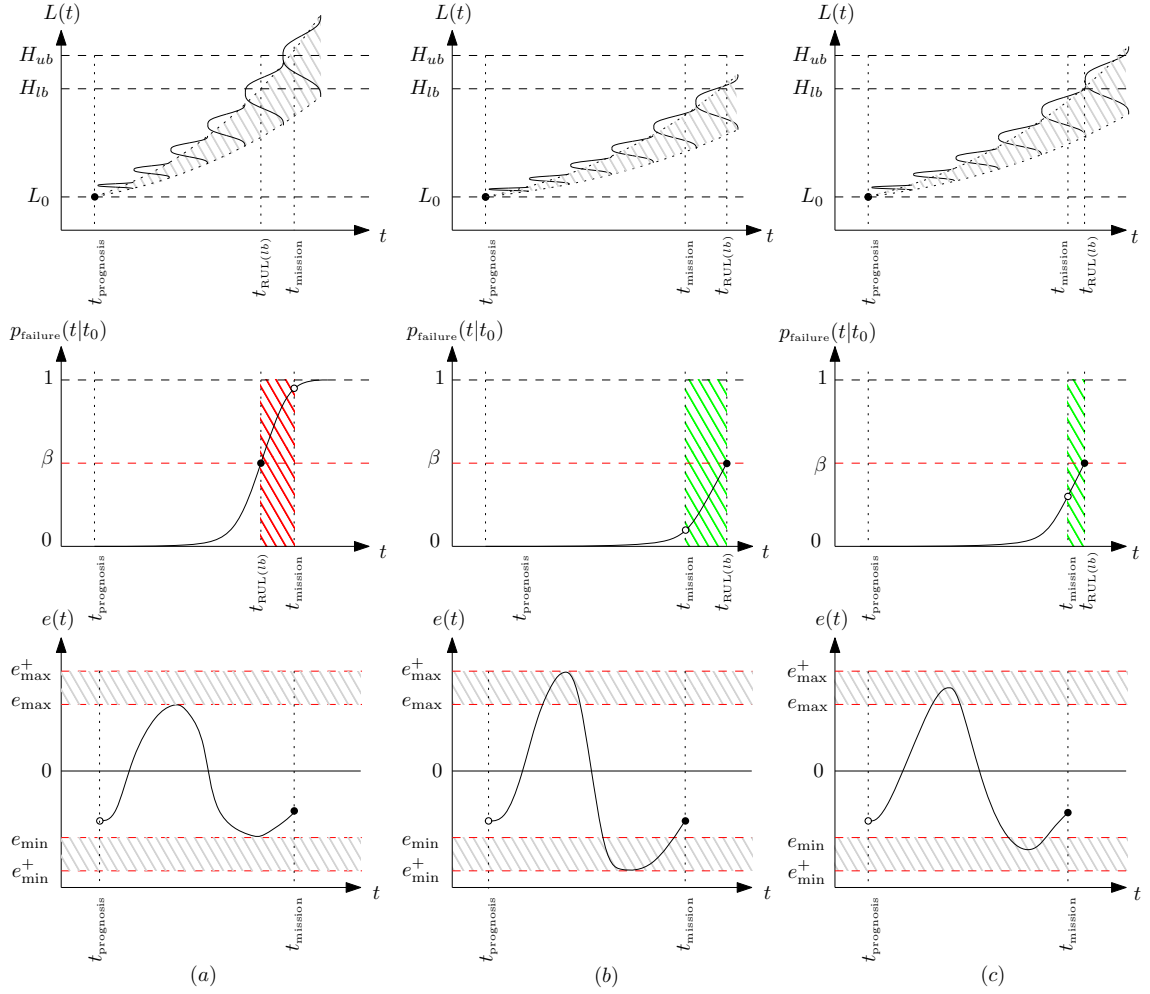


Figure 4.1: Conceptual plots for the fault dimension, L , probability of failure predicted at time $t_{\text{prediction}}$ and the tracking error, e , versus time for three different reconfiguration scenarios: (a) $t_{\text{RUL}(lb)} < t_{\text{mission}}$, (b) $t_{\text{RUL}(lb)} > t_{\text{mission}}$ but the control is overcompensated leading to an unnecessary increase in tracking error and (c) $t_{\text{RUL}(lb)} > t_{\text{mission}}$ and the tracking error is minimized.

4.2 Hierarchical PHM Control Architecture

The proposed FTC architecture is comprised of three levels: A low-level, a middle-level and a high-level, as illustrated in Figure 4.2. Each level of the control hierarchy is responsible for different tasks where the three levels are coordinated via supervisory routines and contribute to system fault tolerance.

The overall fault-tolerant control architecture begins with reconfiguration at the low-level since the impact of reconfiguration is localized to the individual component. If component reconfiguration is not sufficient to meet the mission objectives, control redistribution is performed at the middle-level. The impact of control redistribution affects all components within the subsystem. This action provides flexibility over component reconfiguration at the expense of increased computational complexity. Finally, if the previous actions are insufficient in achieving the desired objectives, mission adaptation is performed at the high-level. During this action, lower-priority mission objectives are compromised or traded-off to achieve higher priority objectives.

4.2.1 Low-Level Control Reconfiguration

The first corrective action considered occurs at the low-level (or component-level) as control reconfiguration. The objective is to determine if set-point adjustments can be applied to the production controller of the physical process to extend the RUL past the desired RUL while ensuring required performance characteristics. Further detail regarding low-level control reconfiguration is provided in Section 4.3.

Note: Low-level control reconfiguration is the primary focus of this body of work. However, only a subset of fault instances may be resolved using this approach. For such scenarios, control redistribution and mission adaptation maybe considered as alternative solutions.

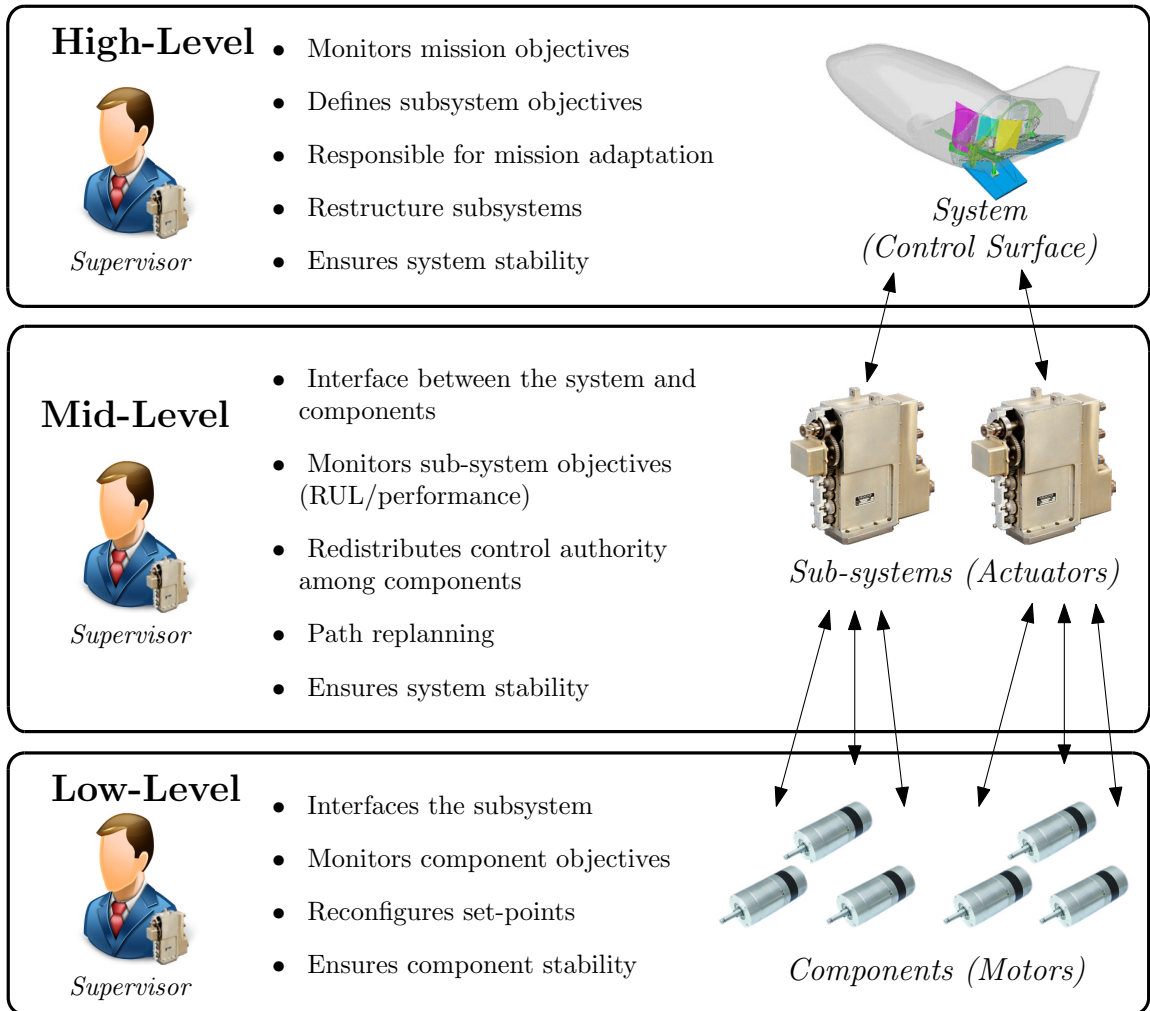


Figure 4.2: Reconfigurable control architecture 3-tier hierarchical strategy highlighting the low-level reconfiguration, mid-level redistribution and high-level mission adaptation.

4.2.2 Mid-Level Control Redistribution

The mid-level control redistribution module is reserved for systems consisting of multiple active components each with a corresponding controller. At this level, redistribution of the available control authority among healthy and faulty component is sought to extend the RUL.

4.2.3 High-Level Mission Adaptation

The high level of the fault-tolerant control hierarchy is intended to safeguard strict mission objectives through the deployment of mission adaptation mechanisms. Mission adaptation allows the control architecture to relax low-priority mission objectives to achieve greater vehicle (or system) usefulness and complete high-priority goals. Such a control action is necessary when the middle and low-level fault-tolerant control schemes are not capable of achieving such objectives due to the severity of the fault.

4.3 Reconfigurable Control Architecture

The main elements of the reconfigurable control architecture are depicted in Figure 4.3. The control architecture is comprised of the plant (physical process and production controller), reconfigurable controller and a PHM module. Initially, the production controller is utilized with no modification while the PHM module continuously monitors the system for one (or more) fault mode(s). Once a fault is detected, the RUL is evaluated by the PHM module. If the estimated RUL is greater than the desired RUL, no action is taken. During this period the RUL is re-evaluated periodically. However, if the estimated RUL is less than the desired RUL, a reconfiguration action is triggered. The reconfigurable controller relaxes constraints on the error boundaries by adjusting the weight matrices in the MPC cost function. This continues until either the RUL is satisfied or the weight matrices can no longer be adapted. The remainder of this section presents a detailed description of each module in the reconfigurable control architecture.

4.3.1 Plant (Nominal System)

The plant consists of the production controller and physical process with a control input, \mathbf{u} , internal state, \mathbf{x} , measured disturbance, \mathbf{v} and output response \mathbf{y} , illustrated in Figure 4.3. Prognosis based control can only be considered once it's established the RUL of the plant can be directly controlled and observed. As a result, two important questions arise, "Under what conditions can the RUL of the plant be controlled? ...observed?" These questions are answered by well defined criteria for RUL controllability and RUL observability given in Definitions 4.1 and 4.2, accordingly.

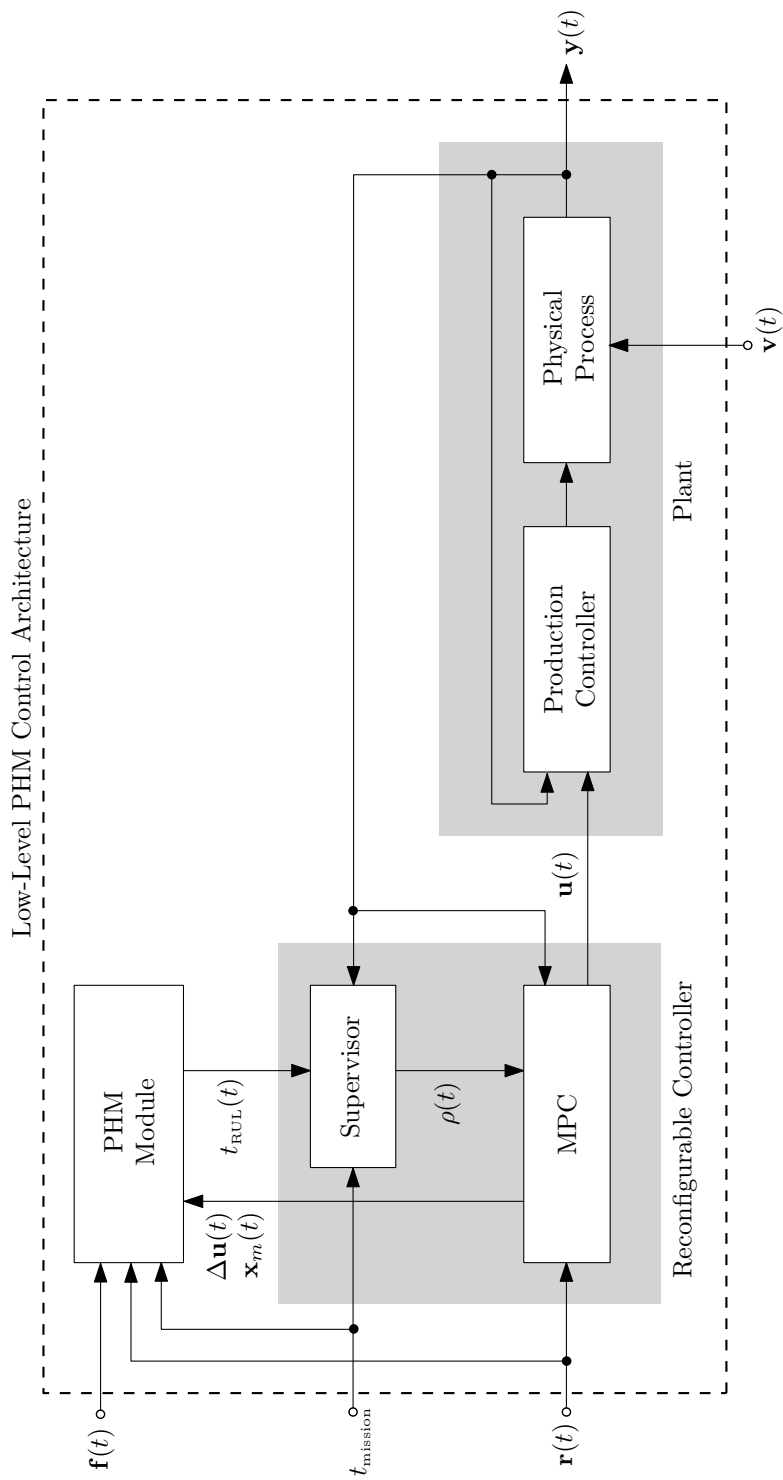


Figure 4.3: Reconfigurable controller illustrating the internal MPC controller and supervisor elements in addition to the external PHM module and connected plant.

Definition 4.1 (RUL Controllability). A system is RUL controllable at time t_0 if there exists a control input, $\mathbf{u}(t) \in \mathcal{U}$ on the interval $t \in [t_0, t_f]$ such that any initial RUL $t_{\text{RUL}}(t_0)$ can be driven to any desired RUL value, $t_{\text{RUL}}(t_f) \in \mathcal{T}_{\text{RUL}}$.

Remark 4.1. \mathcal{T}_{RUL} in Definition 4.1 is defined as $\mathcal{T}_{\text{RUL}} \in \{\forall t \leq T^*\}$ for some constant T^* such that $(t_f - t_0) \leq T^* \leq \infty$.

Definition 4.2 (RUL Observability). A system is RUL observable at time t_0 if for any initial state in the state space $\mathbf{x}(t_0) \in \mathcal{X}$ and a given control input $\mathbf{u}(t) \in \mathcal{U}$ defined on the interval $t \in [t_0, t_f]$ the RUL, t_{RUL} , can be determined for $[t_0, t_f]$.

Remark 4.2. If the conditions for RUL controllability and observability are simultaneously satisfied, then the system is said to be RUL stabilizable.

Definition 4.3 (RUL Stabilizable). A system is RUL stabilizable if for any initial state in the state space $\mathbf{x}(t_0) \in \mathcal{X}$ and any control input $\mathbf{u}(t) \in \mathcal{U}$ defined on the interval $t \in [t_0, t_f]$ the plant is simultaneously RUL controllable and RUL observable.

Remark 4.3. A system is RUL-stabilizable *if and only if* it is RUL controllable and RUL observable.

4.3.1.1 Assumptions

The assumptions regarding the plant are as follows:

► **Assumption 4.1** (State-Space Representation).

A state-space model for the plant exists in the following form,

$$\begin{cases} \dot{\mathbf{x}}(t) = f(\mathbf{x}(t), \mathbf{u}(t), \mathbf{v}(t)) + \mathbf{n}_1(t), & \mathbf{x}(0) = \mathbf{x}_0, \\ \mathbf{y}(t) = h(\mathbf{x}(t), \mathbf{v}(t)) + \mathbf{n}_2(t). \end{cases} \quad (4.3)$$

where $\mathbf{u} \in \mathbb{R}^{n_u}$ is the reference input, $\mathbf{x} \in \mathbb{R}^{n_x}$ are the internal states, $\mathbf{y} \in \mathbb{R}^{n_y}$ is the output signal and $\mathbf{v} \in \mathbb{R}^{n_d}$ is the disturbance input. The mapping $f(\mathbf{x})$ is locally Lipschitz, and $h(\mathbf{x})$ is continuous over \mathbf{x} . The vectors $\mathbf{n}_1 \in \mathbb{R}^{n_x}$ and $\mathbf{n}_2 \in \mathbb{R}^{n_y}$ represent the process and observation noise respectively.

► **Assumption 4.2** (Set-Point Tracking).

The plant is designed to track the system output, \mathbf{y} , with a reference signal, \mathbf{r} .

► **Assumption 4.3** (Exponentially Stable Tracking Error).

By design, the dynamics of the plant tracking error follows,

$$\dot{\mathbf{e}}(t) = \mathbf{A}_e \mathbf{e}(t), \quad (4.4)$$

where \mathbf{A}_e is Hurwitz and $\mathbf{e} = \mathbf{0}$ is an exponentially stable equilibrium point.

► **Assumption 4.4** (Controllability / Observability).

The plant is both controllable and observable. (See Definitions B.1 and B.2 on page 106)

► **Assumption 4.5** (RUL Stabilizable).

The plant is RUL stabilizable.

► **Assumption 4.6** (Nominal Tracking Error Boundaries).

The tracking error of the plant,

$$\mathbf{e}(t) \triangleq \mathbf{r}(t) - \mathbf{y}(t), \quad (4.5)$$

is originally bounded by the vectors \mathbf{e}_{\min} and \mathbf{e}_{\max} , such that,

$$-\infty < \mathbf{e}_{\min} \leq \mathbf{e}(t) \leq \mathbf{e}_{\max} < \infty, \quad \text{for } \forall t \geq 0. \quad (4.6)$$

► **Assumption 4.7** (Extended Tracking Error).

The minimum and maximum tracking error, \mathbf{e}_{\min} and \mathbf{e}_{\max} , can be extended to \mathbf{e}_{\min}^+ and \mathbf{e}_{\max}^+ such that,

$$-\infty < \mathbf{e}_{\min}^+ < \mathbf{e}_{\min} \leq \mathbf{e}(t) \leq \mathbf{e}_{\max} < \mathbf{e}_{\max}^+ < \infty, \quad (4.7)$$

► **Assumption 4.8** (Discretized Set-Point Adjustments).

The applied set-point adjustment is represented by the accumulation of discrete incremental changes of period T_s ,

$$\Delta \mathbf{u}(t) = \int_{t_0}^t \boldsymbol{\delta}_u[k] \cdot \delta(v - kT_s) dv, \quad (4.8)$$

where $\boldsymbol{\delta}_u$ represents the incremental changes in $\Delta \mathbf{u}$ and δ is the Dirac-delta function, defined in Appendix B.1.1. In addition the time-derivative of $\Delta \mathbf{u}$ can be found by applying the second fundamental theorem of integral calculus to arrive at,

$$\Delta \dot{\mathbf{u}}(t) = \boldsymbol{\delta}_u[k] \cdot \delta(t - kT_s). \quad (4.9)$$

► **Assumption 4.9** (Set-Point Adjustment Rate Limit).

The rate of change of the set-point adjustment is bounded by,

$$\boldsymbol{\delta}_{\min} \leq \Delta \mathbf{u}(t + kT_s) - \Delta \mathbf{u}(t + (k - 1)T_s) \leq \boldsymbol{\delta}_{\max}, \quad (4.10)$$

where $\boldsymbol{\delta}_{\min}$ and $\boldsymbol{\delta}_{\max}$ are constants. This is equivalent to,

$$\boldsymbol{\delta}_{\min} \leq \boldsymbol{\delta}_u[k] - \boldsymbol{\delta}_u[k - 1] \leq \boldsymbol{\delta}_{\max}, \quad \forall k \in \mathbb{Z}^+. \quad (4.11)$$

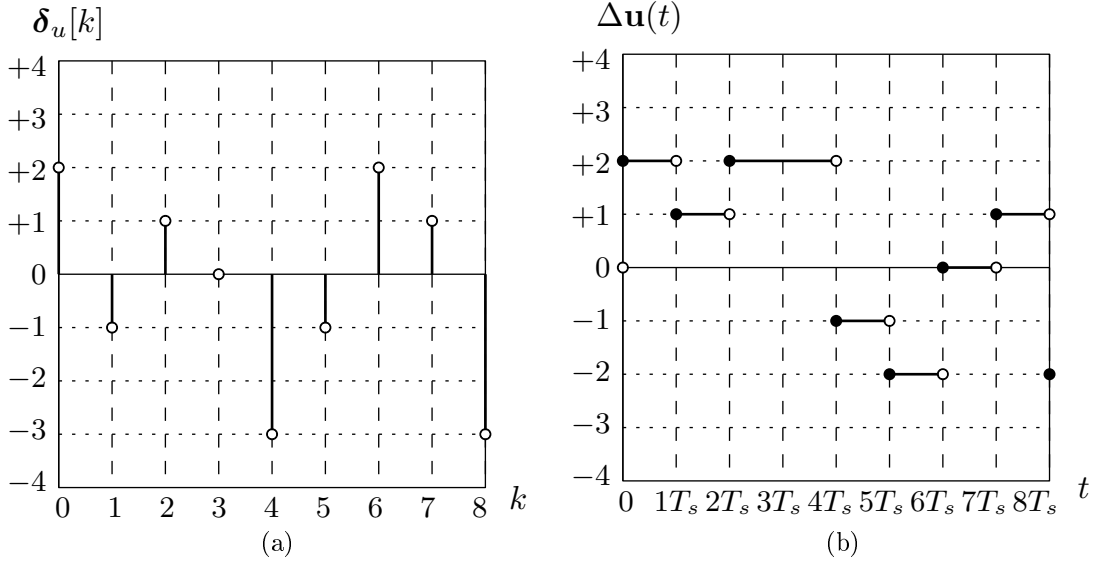


Figure 4.4: Illustrative example for a given set of (a) incremental set-point adjustments, δ_u and (b) the corresponding set-point adjustment, $\Delta \mathbf{u}$.

► **Assumption 4.10** (PHM Module).

A PHM module for the identified fault-mode(s) is available in the form of a fault-growth / feature mapping model in (2.1).

► **Assumption 4.11** (Direct State-Space / Fault-Growth Relationship).

When $\mathbf{n}_1 \equiv \mathbf{0}$, a direct relationship exists between the fault-growth mapping, f_p , and the state, \mathbf{x} ,

$$\left. \frac{\partial f_p}{\partial \mathbf{x}} \right|_{\mathbf{n}_1 \equiv \mathbf{0}} \geq \mathbf{0}. \quad (4.12)$$

4.3.2 Reconfigurable Controller

The two elements of the reconfigurable controller include the low-level supervisor and the MPC controller.

4.3.2.1 Supervisor

A logical unit, referred to as the low-level supervisor, is used to continuously monitor the output of the MPC controller (as shown in Figure 4.3) to ensure it meets the

desired RUL and set-point requirements. More specifically, if the measured RUL, t_{RUL} , is greater than the desired mission time, t_{mission} , then no reconfiguration is necessary; otherwise new acceptable minimum and maximum allowable tracking errors, $\mathbf{e}_{\text{min}}^+$ and $\mathbf{e}_{\text{max}}^+$, are adopted. Then, the adjusted set-point, $\Delta \mathbf{u}$, and modeled state estimate, \mathbf{x}_m , are passed to the PHM module to estimate, t_{RUL} . This estimate is used as an input to the adaptation function, Γ , to update the adaptation parameter, ρ . The cost function is updated using a new value for ρ at time-instant k . When the estimated RUL, t_{RUL} , is less than the desired mission time, t_{mission} , the adaptation parameter, ρ , increases, otherwise it decreases. This process is re-iterated until $\rho \geq \rho_{\text{max}}$. When this occurs, the controller makes no further adaptation attempts. An outline of this process is shown as a flowchart in Figure 4.5.

4.3.2.2 Model Predictive Controller (MPC)

The purpose of the reconfigurable controller is to make adjustments to the control signal, \mathbf{u} , thereby altering the internal states, \mathbf{x} , and causing the RUL to increase. A system that exhibits this property is RUL controllable. In the scope of this work, constraints are imposed on the maximum allowable tracking error, \mathbf{e} . Foreshadowing briefly to the next chapter, it can be proven if \mathbf{e} is constrained according to Assumption 4.7, then $\Delta \mathbf{u}$ must belong to \mathcal{U}_δ ,

$$\mathcal{U}_\delta \in \{ \Delta \mathbf{u}_{\text{min}} \leq \Delta \mathbf{u}(t) \leq \Delta \mathbf{u}_{\text{max}} | \forall t \in [t_0, t_{\text{RUL}(lb)}] \}, \quad (4.13)$$

where,

$$\begin{cases} \Delta \mathbf{u}_{\text{min}} &= \mathbf{e}_{\text{min}}^+ - \mathbf{e}_{\text{min}}, \\ \Delta \mathbf{u}_{\text{max}} &= \mathbf{e}_{\text{max}}^+ - \mathbf{e}_{\text{max}}. \end{cases} \quad (4.14)$$

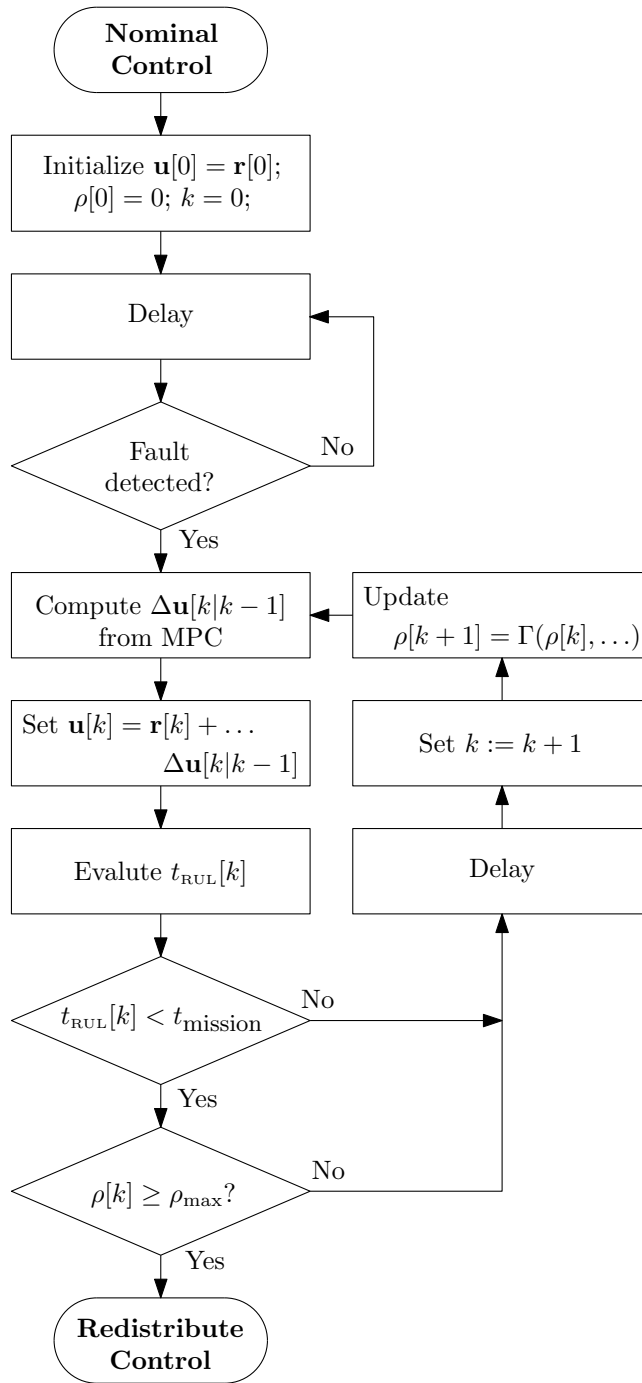


Figure 4.5: Flowchart of the low-level supervisor.

Now, the optimal set-point adjustment $\Delta \mathbf{u}$ is found by minimizing the quadratic cost function,

$$J(\mathbf{x}(t), \Delta \mathbf{u}(t)) = \min_{\Delta \mathbf{u} \in \mathcal{U}_\delta} \left\{ \int_{t_0}^{t_0+T} \left[(\mathbf{x}^*(t) - \mathbf{x}(t))^\top (\mathbf{Q}\rho[k]) \cdots \right. \right. \\ \left. \left. (\mathbf{x}^*(t) - \mathbf{x}(t)) + \Delta \mathbf{u}^\top(t) \mathbf{R} \Delta \mathbf{u}(t) \right] dt \right\}, \quad (4.15)$$

where \mathbf{x}^* is the desired state-space value. The weight matrices \mathbf{Q} and \mathbf{R} are of size $n_x \times n_x$ and $n_r \times n_r$, respectively.

4.3.3 PHM Module

In the scope of this work, the PHM module is external to the reconfigurable controller. In general, the prognostic control input to the PHM model includes the reference signal, \mathbf{r} , modeled state estimate, \mathbf{x}_m , and set-point adjustment $\Delta \mathbf{u}$,

$$\mathbf{u}_f(t) = \left[\mathbf{r}^\top(t) \quad \Delta \mathbf{u}^\top(t) \quad \mathbf{x}_m^\top(t) \right]^\top. \quad (4.16)$$

Additional inputs to the PHM module include the feature vector, \mathbf{f} . The output of the PHM module is the RUL estimate, t_{RUL} .

4.3.3.1 Parameter Adaptation Function

The interface between the PHM module and the reconfigurable controller is governed by the adaptation function, Γ , defined in Definition 4.4. This function is used to update the adaptation parameter, ρ , thereby allowing the PHM module to indirectly affect $\Delta \mathbf{u}$ by changing the cost associated with the state.

Definition 4.4 (Parameter Adaptation Function). The adaptation function, Γ , is a function of t_{RUL} , t_{mission} and previous values of the adaptation parameter, ρ ,

$$\dot{\rho}(t) = \Gamma(\rho(t), t_{\text{RUL}}(t), t_{\text{mission}}) \quad (4.17)$$

where the function Γ has the following property,

$$\begin{cases} \Gamma(t) < 0 & : t_{\text{RUL}} \geq t_{\text{mission}}, \\ \Gamma(t) > 0 & : \text{otherwise,} \end{cases} \quad (4.18)$$

bounded by,

$$0 \leq \Gamma(\rho(t), t_{\text{RUL}}(t), t_{\text{mission}}) \leq \rho_{\text{max}}, \quad (4.19)$$

with the initial condition $\rho(0) = \rho_0$. During periods of no set-point reconfiguration, $\rho = 0$.

CHAPTER V

STABILITY AND UNCERTAINTY ANALYSIS

The qualitative overview of the reconfigurable control architecture in the previous chapter provides a basis for a quantitative study of set-point reconfiguration with respect to stability and boundedness. This begins in Section 5.1 by defining a reference model used by the MPC. Next, in Section 5.2, a composite system comprised of the MPC and plant is described. Then, Section 5.3 analyzes the stability and boundedness corresponding to the tracking error of the composite system and the prediction error of the reference model. In Section 5.4, the prediction error of the reference model is used to identify prediction boundaries for the estimated plant state. Finally, Section 5.5 defines RUL metrics to describe the effects of uncertainty on the estimated plant state.

5.1 Reference Model

The MPC requires a reference model of the plant to predict the future set-point adjustments for control reconfiguration. Ideally, the reference model is equivalent to the non-linear plant dynamics in (4.3). Since this is not realistically achievable, the next best alternative is to define a reference model which follows a similar form to the non-linear plant dynamics,

$$\begin{cases} \dot{\mathbf{x}}_m(t) = f_m(\mathbf{x}_m(t), \mathbf{u}(t), \mathbf{v}(t)) + \mathbf{n}_1(t), & \mathbf{x}_m(0) = \mathbf{x}_{m0}, \\ \mathbf{y}_m(t) = h_m(\mathbf{x}_m(t), \mathbf{v}(t)) + \mathbf{n}_2(t), \end{cases} \quad (5.1)$$

where f_m and h_m correspond to the non-linear modeling dynamics of the plant, $\mathbf{x}_m \in \mathbb{R}^{n_x}$ is the modeling state and $\mathbf{y}_m \in \mathbb{R}^{n_r}$, is the modeled output. However, using a linear reference model reduces the complexity of the optimal control problem. A

linearization of (5.1) is realized as,

$$\begin{cases} \dot{\mathbf{x}}_m(t) = \mathbf{A}_m \mathbf{x}_m + \mathbf{B}_{m,r} \mathbf{r}(t) + \mathbf{B}_{m,v} \mathbf{v}(t), & \mathbf{x}_m(0) = \mathbf{x}_{m0} \\ \mathbf{y}_m(t) = \mathbf{C}_m \mathbf{x}_m + \mathbf{D}_{m,v} \mathbf{v}(t) \end{cases}, \quad (5.2)$$

where the matrices \mathbf{A}_m , $\mathbf{B}_{m,r}$, $\mathbf{B}_{m,v}$, \mathbf{C}_m and $\mathbf{D}_{m,v}$ are obtained from the first-order linear expansions of f_m and h_m ,

$$\begin{cases} \mathbf{A}_m &= \frac{\partial}{\partial \mathbf{x}} f_m(\mathbf{x}_m(t), \mathbf{u}(t), \mathbf{v}(t)) \in \mathbb{R}^{n_x \times n_x}, \\ \mathbf{B}_{m,r} &= \frac{\partial}{\partial \mathbf{u}} f_m(\mathbf{x}_m(t), \mathbf{u}(t), \mathbf{v}(t)) \in \mathbb{R}^{n_x \times n_r}, \\ \mathbf{B}_{m,v} &= \frac{\partial}{\partial \mathbf{v}} f_m(\mathbf{x}_m(t), \mathbf{u}(t), \mathbf{v}(t)) \in \mathbb{R}^{n_x \times n_v}, \\ \mathbf{C}_m &= \frac{\partial}{\partial \mathbf{x}} h_m(\mathbf{x}_m(t), \mathbf{v}(t)) \in \mathbb{R}^{n_y \times n_x}, \\ \mathbf{D}_{m,v} &= \frac{\partial}{\partial \mathbf{v}} h_m(\mathbf{x}_m(t), \mathbf{v}(t)) \in \mathbb{R}^{n_y \times n_v}. \end{cases} \quad (5.3)$$

5.2 Composite System

The composite system is comprised of the plant and MPC, as shown in Figure 5.1. In this section, the interaction between the state observer, reference model and optimizer is discussed.

5.2.1 Plant

The control input to the plant, \mathbf{u} , is defined as,

$$\mathbf{u}(t) = \mathbf{r}(t) + \Delta\mathbf{u}(t), \quad (5.4)$$

where $\Delta\mathbf{u}$ is a set-point adjustment computed by the MPC. The output of the plant and corresponding tracking error are represented by \mathbf{y} and \mathbf{e} , accordingly.

5.2.2 MPC Controller

The MPC consists of a linear reference model, state observer and an optimizer. The state observer accepts the current control input, \mathbf{u} , and plant output, \mathbf{y} , as inputs. The output of the state observer, \mathbf{x}_m , is used to initialize the reference model. The reference model is used to predict future state estimates for a given set of future input references over a prediction horizon and takes the form of (5.2). The optimizer solves for a set-point adjustment $\Delta\mathbf{u}$ by minimizing the cost function in (4.15).

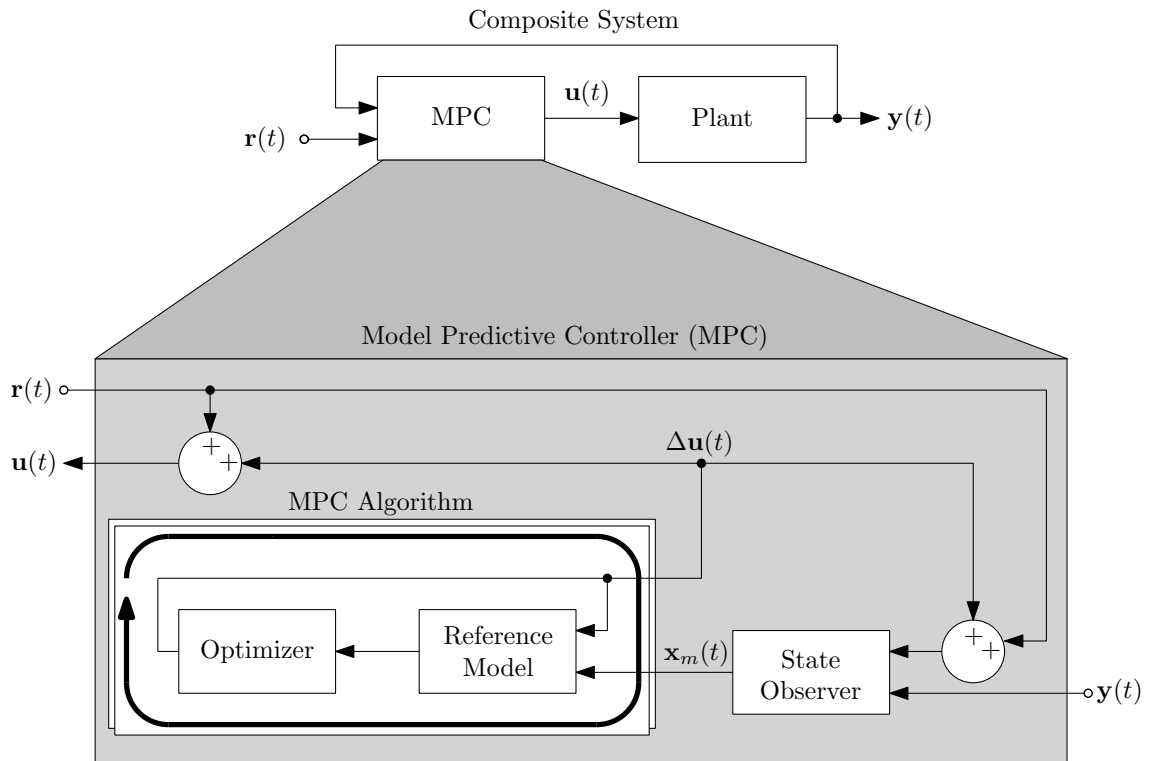


Figure 5.1: Block diagram of the composite system showing the inner-connections between the state observer, reference model and optimizer within the MPC.

5.3 Error Analysis

Two types of errors are analyzed in this section: tracking error and modeling error. The tracking error, defined in the previous chapter, corresponds to the difference between the desired input reference, \mathbf{r} , and plant output, \mathbf{y} . The modeling error, represented by the symbol \mathbf{e}_m , corresponds to the error in the state estimates that occur as a result of model mismatches propagated over the prediction horizon.

5.3.1 Tracking Error

The tracking error of the composite system, \mathbf{e}^+ (referred to as the extended tracking error in the previous chapter), is described by the differential equation

$$\dot{\mathbf{e}}^+(t) = \mathbf{A}_e \mathbf{e}^+(t) + \boldsymbol{\delta}_u[k] \cdot \delta(t - kT_s). \quad (5.5)$$

where \mathbf{A}_e is Hurwitz and $\mathbf{e}^+(t_0) = \mathbf{e}(t_0)$. The following theorem provides the boundaries for the tracking error of the composite system.

Theorem 5.1 (Tracking Error Boundaries with MPC). Let the tracking error of the composite system be described by (5.5). If the set-point adjustment, $\Delta \mathbf{u}$, is uniformly bounded in time by $\Delta \mathbf{u}_{\min} \leq \Delta \mathbf{u}(t) \leq \Delta \mathbf{u}_{\max}$, then the tracking error of the composite system, \mathbf{e}^+ , must also be uniformly bounded in time by, $\mathbf{e}(t_0) + \Delta \mathbf{u}_{\min} \leq \mathbf{e}^+(t) \leq \mathbf{e}(t_0) + \Delta \mathbf{u}_{\max}$.

Proof. First, the explicit solution of (5.5) can be found,

$$\mathbf{e}^+(t) = \exp(\mathbf{A}_e(t - t_0)) \mathbf{e}(t_0) + \int_{t_0}^t \exp(\mathbf{A}_e(t - \tau)) (\boldsymbol{\delta}_u[k] \cdot \delta(\tau - kT_s)) d\tau. \quad (5.6)$$

Applying the translation property of the Dirac-delta function gives,

$$\mathbf{e}^+(t) = \exp(\mathbf{A}_e(t - t_0)) \mathbf{e}(t_0) + \sum_{n=0}^k \boldsymbol{\delta}_u[n] \cdot \exp(\mathbf{A}_e(t - nT_s)). \quad (5.7)$$

Since $\Delta \mathbf{u}$ is uniformly bounded, the cumulative sum of $\boldsymbol{\delta}_u$ is bounded by,

$$\Delta \mathbf{u}_{\min} \leq \sum_{n=0}^k \boldsymbol{\delta}_u[n] \leq \Delta \mathbf{u}_{\max}. \quad (5.8)$$

Now, consider the worst case when $\text{eig}(\mathbf{A}_e) \rightarrow \mathbf{0}^-$. Under this condition, the explicit expression for \mathbf{e}^+ (5.7) becomes,

$$\mathbf{e}^+(t) = \mathbf{e}(t_0) + \sum_{n=0}^k \boldsymbol{\delta}_u[n]. \quad (5.9)$$

By applying (5.8) to (5.9), the boundary for the case when $\text{eig}(\mathbf{A}_e) \rightarrow \mathbf{0}$ can be given as,

$$\mathbf{e}(t_0) + \Delta \mathbf{u}_{\min} \leq \mathbf{e}^+(t) \leq \mathbf{e}(t_0) + \Delta \mathbf{u}_{\max}. \quad (5.10)$$

Finally, if \mathbf{A}_e is Hurwitz, then (5.7) must always be less than or equal to (5.9) for all $t \geq t_0$. Therefore, by the comparison theorem, (5.7) must also be bounded by (5.10). \square

5.3.2 Modeling Error

The observation and prediction errors are sources of uncertainty in the state estimate, \mathbf{x}_m . The observation error, \mathbf{e}_o , arises when an approximate model is used to estimate the state of the system. The prediction error, \mathbf{e}_p , occurs as a result of the reference model predicting the state estimate over a future time horizon. The sum of both errors is referred to as the modeling error, \mathbf{e}_m , which is defined as,

$$\mathbf{e}_m(t) \triangleq \mathbf{e}_o(t) + \mathbf{e}_p(t). \quad (5.11)$$

5.3.2.1 Observation Error

The state can be estimated by using the reference model from (5.1) in the following observation equation,

$$\dot{\mathbf{x}}_m(t) = f_m(\mathbf{x}_m(t), \mathbf{u}(t), \mathbf{v}(t)) + \mathbf{L}[\mathbf{y}(t) - h_m(\mathbf{x}_m(t), \mathbf{v}(t))], \quad (5.12)$$

where \mathbf{x}_m is the modeled plant state and $\mathbf{L} \in \mathbb{R}^{n_x \times n_r}$ is the observer gain. The observation error is defined as,

$$\mathbf{e}_o(t) \triangleq \mathbf{x}(t) - \mathbf{x}_m(t), \quad (5.13)$$

with the corresponding dynamics,

$$\begin{aligned} \dot{\mathbf{e}}_o(t) = & [f(\mathbf{x}(t), \mathbf{u}(t), \mathbf{v}(t)) - f_m(\mathbf{x}_m(t), \mathbf{u}(t), \mathbf{v}(t))] - \dots \\ & \mathbf{L}[h(\mathbf{x}(t), \mathbf{v}(t)) - h_m(\mathbf{x}_m(t), \mathbf{v}(t))]. \end{aligned} \quad (5.14)$$

The stability of the observer error dynamics is ensured by the following theorem:

Theorem 5.2 (Observer Stability for an Unmatched Non-Linear System). Consider a non-linear model for the closed-loop system with the modeling offsets, $\Delta\mathbf{A}_m$, $\Delta\mathbf{B}_{m,r}$, $\Delta\mathbf{B}_{m,v}$ and $\Delta\mathbf{C}_m$,

$$\begin{cases} f(\mathbf{x}(t), \mathbf{u}(t), \mathbf{v}(t)) = (\mathbf{A}_m + \Delta\mathbf{A}_m)\mathbf{x}(t) + (\mathbf{B}_{m,r} + \Delta\mathbf{B}_{m,r})\mathbf{u}(t) + \dots \\ \quad (\mathbf{B}_{m,v} + \Delta\mathbf{B}_{m,v})\mathbf{v}(t) + \psi_{\text{nl}}(\mathbf{x}(t)) \\ h(\mathbf{x}(t), \mathbf{v}(t)) = (\mathbf{C}_m + \Delta\mathbf{C}_m)\mathbf{x}(t) \end{cases} \quad (5.15)$$

for the corresponding reference model in (5.2) such that $\mathbf{D}_{m,v} \equiv \mathbf{0}$. If the following function, Δ_o , defined as,

$$\Delta_o(t) = (\Delta \mathbf{A}_m - \mathbf{L} \Delta \mathbf{C}_m) \mathbf{x}(t) + \Delta \mathbf{B}_{m,r} \mathbf{u}(t) + \Delta \mathbf{B}_{m,v} \mathbf{v}(t) + \psi_{\text{nl}}(\mathbf{x}(t)),$$

is uniformly bounded for $\mathbf{x} \in \mathcal{X}$, $\mathbf{u} \in \mathcal{U}$, $\mathbf{v} \in \mathcal{V}$ and the matrix $\mathbf{A} - \mathbf{L}\mathbf{C}$ is Hurwitz, then the observation error has an exponentially stable equilibrium point. Moreover, the equilibrium point of the observation error, $\bar{\mathbf{e}}_o$, can be found using (5.17).

Proof. By substituting (5.15) and (5.2) into (5.14) the observer error dynamics can be written as,

$$\begin{aligned} \dot{\mathbf{e}}_o(t) &= (\mathbf{A}_m - \mathbf{L}\mathbf{C}_m) \mathbf{e}_o(t) + \dots \\ &\quad \underbrace{(\Delta \mathbf{A}_m - \mathbf{L} \Delta \mathbf{C}_m) \mathbf{x}(t) + \Delta \mathbf{B}_{m,r} \mathbf{u}(t) + \Delta \mathbf{B}_{m,v} \mathbf{v}(t) + \psi_{\text{nl}}(\mathbf{x}(t))}_{\Delta_o(t)}. \end{aligned} \quad (5.16)$$

Let $\bar{\mathbf{e}}_o$ represent the equilibrium point of (5.16),

$$\bar{\mathbf{e}}_o = -(\mathbf{A}_m - \mathbf{L}\mathbf{C}_m)^{-1} \bar{\Delta}_o. \quad (5.17)$$

where,

$$\bar{\Delta}_o = (\Delta \mathbf{A}_m - \mathbf{L} \Delta \mathbf{C}_m) \bar{\mathbf{x}} + \Delta \mathbf{B}_{m,r} \bar{\mathbf{u}} + \Delta \mathbf{B}_{m,v} \bar{\mathbf{v}} + \psi_{\text{nl}}(\bar{\mathbf{x}}) \quad (5.18)$$

such that $\bar{\mathbf{x}}$, $\bar{\mathbf{u}}$ and $\bar{\mathbf{v}}$ are equilibrium points for \mathbf{x} , \mathbf{u} and \mathbf{v} . Now, consider the error dynamics shifted at the equilibrium point, $\tilde{\mathbf{e}}_o = \mathbf{e}_o - \bar{\mathbf{e}}_o$ so that,

$$\dot{\tilde{\mathbf{e}}}_o(t) = (\mathbf{A}_m - \mathbf{L}\mathbf{C}_m) [\tilde{\mathbf{e}}_o(t) - \bar{\mathbf{e}}_o]. \quad (5.19)$$

If the matrix $\mathbf{A}_m - \mathbf{L}\mathbf{C}_m$ is Hurwitz and Δ_o is uniformly bounded for $\mathbf{x} \in \mathcal{X}$, $\mathbf{u} \in \mathcal{U}$,

$\mathbf{v} \in \mathcal{V}$, then for any $\bar{\mathbf{x}} \in \mathcal{X}$, $\bar{\mathbf{u}} \in \mathcal{U}$ and $\bar{\mathbf{v}} \in \mathcal{V}$, $\bar{\mathbf{e}}_o$ is an exponentially stable equilibrium point. \square

5.3.2.2 Prediction Error

Since a linear reference model is used to make future state predictions of a non-linear system, error in the prediction is unavoidable. Therefore, its essential to understand how the prediction error evolves in time. Let the model prediction error, \mathbf{e}_p , be defined as,

$$\mathbf{e}_p(t_{k+p} | t_k) \triangleq \mathbf{x}(t_{k+p} | t_k) - \mathbf{x}_m(t_{k+p} | t_k), \quad \text{s.t. } t_k = t_0 + kT_s. \quad (5.20)$$

A boundary for the prediction error can be found using Theorem 5.3.

Theorem 5.3 (Prediction Error for an Unmatched Non-Linear System). If the state observer in Theorem 5.2 is exponentially stable then there exists a constant $\bar{\mathbf{e}}_p$ such that $|\mathbf{e}_p(t_{k+p} | t_k)| \leq \bar{\mathbf{e}}_p$ over the finite prediction horizon $t \in [t_k, t_{k+p}]$.

Proof. First, define $\mathbf{x}(t_{k+p} | t_k)$ and $\mathbf{x}_m(t_{k+p} | t_k)$ as,

$$\mathbf{x}(t_{k+p} | t_k) = \int_{t_k}^{t_{k+p}} f(\mathbf{x}(\tau), \mathbf{u}(\tau), \mathbf{v}(\tau)) d\tau \quad (5.21)$$

$$\mathbf{x}_m(t_{k+p} | t_k) = \int_{t_k}^{t_{k+p}} f_m(\mathbf{x}_m(\tau), \mathbf{u}, \mathbf{v}(\tau)) d\tau. \quad (5.22)$$

Next, substitute (5.15) and (5.2) into (5.21) and (5.22). Substituting the resulting expressions into (5.20) and simplifying gives,

$$\mathbf{e}_p(t_{k+p} | t_k) = \int_{t_k}^{t_{k+p}} \Delta_p(\tau) d\tau, \quad (5.23)$$

where,

$$\Delta_p(t) = \Delta \mathbf{A}_m \mathbf{x}(t) + \Delta \mathbf{B}_{m,r} \mathbf{u}(t) + \Delta \mathbf{B}_{m,v} \mathbf{v}(t) + \psi(\mathbf{x}(t)). \quad (5.24)$$

Now, by applying the integral comparison property, that is $|\int (\cdot)| \leq \int |(\cdot)|$, to the expression in (5.23), \mathbf{e}_p can be bounded by,

$$\mathbf{0} \leq |\mathbf{e}_p(t_{k+p} | t_k)| \leq \int_{t_k}^{t_{k+p}} |\Delta_p(\tau)| d\tau \quad (5.25)$$

Finally, if Theorem 5.2 is true then, \mathbf{x} , \mathbf{u} and \mathbf{v} are uniformly bounded, $\Delta \mathbf{A}_m$, $\Delta \mathbf{B}_{m,r}$ and $\Delta \mathbf{B}_{m,v}$ are real-valued matrices, the non-linear mapping $\psi(\mathbf{x})$ is bounded in \mathbf{x} , and there exists a constant $\bar{\mathbf{x}}_m$ such that $\mathbf{x}_m \leq \bar{\mathbf{x}}_m < \infty$. Imposing these restrictions on (5.24) implies that Δ_p must also be uniformly bounded; that is there exists a value for $\Delta_{p,\max}$ such that $\Delta_{p,\max} = \sup_{t_k \leq t \leq t_{k+p}} |\Delta_p(t)| < \infty$. Therefore, by invoking (5.25) the prediction error must be bounded by, $\mathbf{0} \leq |\mathbf{e}_p(t_{k+p} | t_k)| \leq \bar{\mathbf{e}}_p$, where $\bar{\mathbf{e}}_p \triangleq (pT_s) \cdot \Delta_{p,\max}$. □

5.4 State-Variable Adjustment Analysis

Now that the error of the reference model is considered for an unmatched reference over the prediction horizon, the effects of set-point adjustment on the future state values can be studied.

5.4.1 Ideal (Matched) Case

First, consider the following definition for the change in the state-variable,

$$\Delta \mathbf{x}(t) \triangleq \mathbf{x}^+(t) - \mathbf{x}(t), \quad (5.26)$$

where \mathbf{x} is the state of the system if $\Delta \mathbf{u} \equiv \mathbf{0}$ and \mathbf{x}^+ is the reconfigured state of the system if a set-point adjustment $\Delta \mathbf{u}$ were applied. Now, consider the case where the linear reference model matches the dynamics of the plant. The predicted change in the state-variable after reconfiguration can be found using Theorem 5.4.

Theorem 5.4 (State Adjustment (Matched Model)). Consider a closed-loop system which matches the linear-deterministic reference model described by (5.2). The estimated change in the state, $\Delta \hat{\mathbf{x}}$, at time t_{k+q} given at time t_k can be computed by,

$$\Delta \hat{\mathbf{x}}(t_{k+q}|t_k) = e^{\mathbf{A}_m(t_{k+q}-t_k)} \Delta \mathbf{x}_0 + \int_{t_k}^{t_{k+q}} [e^{\mathbf{A}_m(t-\tau)} \cdot \mathbf{B}_{m,r} \Delta \mathbf{u}(\tau)] d\tau, \quad (5.27)$$

Proof. The dynamics of the reconfigured state can be expressed as,

$$\dot{\mathbf{x}}^+(t) = \mathbf{A}_m \mathbf{x}^+(t) + \mathbf{B}_{m,r} \mathbf{r}(t) + \mathbf{B}_{m,r} \Delta \mathbf{u}(t). \quad (5.28)$$

Next, taking the time derivative of (5.26) and substituting the first-order dynamics

of \mathbf{x} and \mathbf{x}^+ gives,

$$\Delta \dot{\mathbf{x}}(t) = \mathbf{A}_m \Delta \mathbf{x}(t) + \mathbf{B}_{m,r} \Delta \mathbf{u}(t), \quad (5.29)$$

The explicit solution to this first-order differential equation is found as,

$$\Delta \mathbf{x}(t) = e^{\mathbf{A}_m(t-t_0)} \Delta \mathbf{x}_0 + \int_{t_0}^t [e^{\mathbf{A}_m(t-\tau)} \cdot \mathbf{B}_{m,r} \Delta \mathbf{u}(\tau)] d\tau. \quad (5.30)$$

Finally, since this is assumed to be a perfectly matched model, $\Delta \hat{\mathbf{x}} \equiv \Delta \mathbf{x}$. Therefore, the state estimate at time t_{k+q} given at time t_k can be found by using (5.30). □

5.4.2 Non-Ideal (Unmatched) Case

The estimated change in the state at time t_{k+q} given at time t_k when the reference model does not match the closed-loop system dynamics can be found if the structure of the reference and the closed-loop system models are assumed.

Claim 5.1 (State Adjustment (Unmatched Model)). Consider the case of the unmatched reference model in (5.15). If the requirements in Theorem 5.2 and Theorem 5.3 are satisfied then, the actual change in the state at time t_{k+q} given at time t_k is bounded by,

$$\Delta \mathbf{x}_{lb} \leq \Delta \mathbf{x}(t_{k+q}|t_k) \leq \Delta \mathbf{x}_{ub}. \quad (5.31)$$

where,

$$\begin{cases} \Delta \mathbf{x}_{lb} &= \Delta \hat{\mathbf{x}}(t_{k+q}|t_k) - |\mathbf{e}_m| \\ \Delta \mathbf{x}_{ub} &= \Delta \hat{\mathbf{x}}(t_{k+q}|t_k) + |\mathbf{e}_m| \end{cases} \quad (5.32)$$

5.5 RUL Analysis

In the previous chapter, the modeling error was used to arrive at uncertainty boundaries, $\Delta \mathbf{x}$, for the plant state given an applied set-point adjustment $\Delta \mathbf{u}$. Given these boundaries, the best-case and worst-case prediction boundaries for RUL estimates are studied in a stochastic manner.

5.5.1 Boundary Conditions

The absolute upper and lower-boundary conditions for each state vector at time t are defined as \mathbf{x}_{ub} and \mathbf{x}_{lb} ,

$$\begin{aligned} \{\mathbf{x}_{ub}(t_{k+p}|t_k)\}_i = & \\ & \begin{cases} \{\mathbf{x}_m(t) + \Delta \mathbf{x}_{ub}\}_i : |\{\mathbf{x}_m(t) + \Delta \mathbf{x}_{ub}\}_i| \geq |\{\mathbf{x}_m(t) + \Delta \mathbf{x}_{lb}\}_i| \\ \{\mathbf{x}_m(t) + \Delta \mathbf{x}_{lb}\}_i : |\{\mathbf{x}_m(t) + \Delta \mathbf{x}_{ub}\}_i| < |\{\mathbf{x}_m(t) + \Delta \mathbf{x}_{lb}\}_i| \end{cases}, \end{aligned} \quad (5.33)$$

$$\begin{aligned} \{\mathbf{x}_{lb}(t_{k+p}|t_k)\}_i = & \\ & \begin{cases} \{\mathbf{x}_m(t) + \Delta \mathbf{x}_{ub}\}_i : |\{\mathbf{x}_m(t) + \Delta \mathbf{x}_{ub}\}_i| \leq |\{\mathbf{x}_m(t) + \Delta \mathbf{x}_{lb}\}_i| \\ \{\mathbf{x}_m(t) + \Delta \mathbf{x}_{lb}\}_i : |\{\mathbf{x}_m(t) + \Delta \mathbf{x}_{ub}\}_i| > |\{\mathbf{x}_m(t) + \Delta \mathbf{x}_{lb}\}_i| \end{cases}, \end{aligned} \quad (5.34)$$

where $i \in [0, n_x - 1]$. By Assumption 4.11, since $\frac{\partial f}{\partial \mathbf{x}} \geq \mathbf{0}$, the lower boundary (or worst case conditions) for RUL must occur when $\mathbf{x} = \mathbf{x}_{ub}$,

$$t_{\text{RUL}(lb)}^* = t_{\text{RUL}(lb)} \Big|_{\mathbf{x}=\mathbf{x}_{ub}}. \quad (5.35)$$

Similarly, the upper boundary (or best-case condition) for RUL occurs when $\mathbf{x} = \mathbf{x}_{lb}$,

$$t_{\text{RUL}(ub)}^* = t_{\text{RUL}(ub)} \Big|_{\mathbf{x}=\mathbf{x}_{lb}}. \quad (5.36)$$

By applying the lower-bound as the most conservative estimate for t_{RUL} , the resulting RUL gained after reconfiguration is defined as,

$$\Delta t_{\text{RUL}(lb)} \triangleq t_{\text{RUL}(lb)}^* - t_{\text{RUL}(lb)}. \quad (5.37)$$

Additionally, the corresponding confidence interval width of the reconfigured RUL is defined as,

$$\epsilon_{\text{RUL}}^* = t_{\text{RUL}(ub)}^* - t_{\text{RUL}(lb)}^*. \quad (5.38)$$

An illustration of the predicted fault growth curves for nominal, best-case reconfiguration and worst-case reconfiguration conditions is provided in Figure 5.2.

5.5.2 Metrics

In this section, metrics are presented to evaluate the effectiveness of the reconfiguration routine.

5.5.2.1 Remaining Life Increase (RLI)

RLI is a standardized measure of the relative net increase in RUL, defined as,

$$RLI \triangleq \frac{t_{\text{RUL}(lb)}^* - t_{\text{RUL}(lb)}}{t_{\text{RUL}(lb)}}. \quad (5.39)$$

Note: For the case when $RLI < 0$, the RUL decreases ($\Delta t_{\text{RUL}} < 0$) thereby leading to an implausible or undesirable reconfiguration action.

5.5.2.2 Prediction Uncertainty Increase (PUI)

PUI is a standardized measure of the relative net increase in the width of the RUL confidence interval, defined as,

$$PUI \triangleq \frac{\epsilon_{\text{RUL}}^* - \epsilon_{\text{RUL}}}{\epsilon_{\text{RUL}}}. \quad (5.40)$$

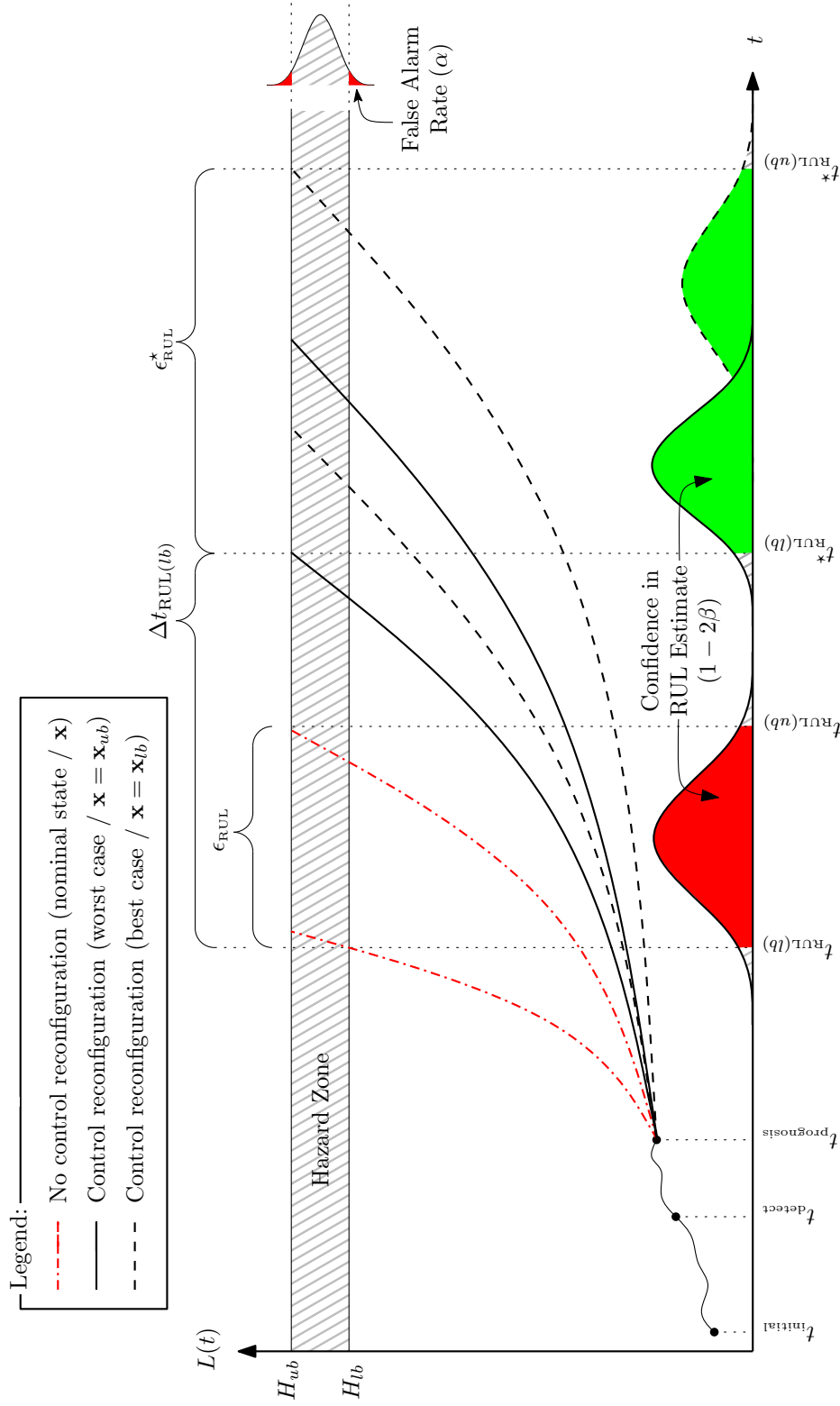


Figure 5.2: Predicted fault-growth curves, hazard zone and corresponding projection on the time axis for the best-case and worst-case reconfiguration boundaries.

CHAPTER VI

MPC ALGORITHM

In this chapter, the elements of the MPC control algorithm are presented in detail. First in Section 6.1, the discrete-time linear prediction model is defined. Then, Section 6.2 gives an overview of the MPC algorithm with a brief description of its core elements. The chapter concludes in Section 6.3 where the cost function is defined, conditions for optimality are presented and numerical techniques to solve the quadratic programming problem are provided.

6.1 Reference / Prediction Model

Recall from the previous chapter the reference model for the plant is a linear time-invariant system. By discretizing the reference model, a discrete-time state predictor can be described by the difference equation,

$$\begin{aligned} \mathbf{x}_m^d [k + j + 1 | k] = & \mathbf{A}_m^d \mathbf{x}_m^d [k + j | k] + \mathbf{B}_{m,r}^d (\mathbf{r}^d [k + j | k] + \Delta \mathbf{u}^d [k + j | k]) \\ & + \mathbf{B}_{m,v}^d \mathbf{v}^d [k + j | k], \end{aligned} \quad (6.1)$$

where the vectors $\mathbf{x}_m^d [k + j + 1 | k]$, $\Delta \mathbf{u}^d [k + j | k]$, $\mathbf{r}^d [k + j | k]$ and $\mathbf{v}^d [k + j | k]$ represent the discrete-time versions of the predicted state, computed set-point adjustment, reference signal and measured disturbance at time-instant k predicting j time-instances ahead. Additionally, the matrices $\mathbf{A}_m^d \in \mathbb{R}^{n_x \times n_x}$, $\mathbf{B}_{m,r}^d \in \mathbb{R}^{n_x \times n_r}$ and $\mathbf{B}_{m,v}^d \in \mathbb{R}^{n_x \times n_v}$, represent the discretized state transition, control input, and disturbance input matrices from (5.2), respectively. Now, define the concatenated vectors \mathbf{x}_p , $\Delta \mathbf{u}_p$, \mathbf{r}_p and \mathbf{v}_p representing the discrete-time predicted states, computed set-point adjustments, reference signal and measured disturbance at time-instant k

over the prediction horizon p for $j \in [0, p - 1]$,

$$\begin{aligned}
\mathbf{x}_p[k] &= \begin{bmatrix} (\mathbf{x}_m^d[k+1|k])^\top & \dots & (\mathbf{x}_m^d[k+p|k])^\top \end{bmatrix}^\top \in \mathbb{R}^{pn_x} \\
\Delta \mathbf{u}_p[k] &= \begin{bmatrix} (\Delta \mathbf{u}^d[k|k])^\top & \dots & (\Delta \mathbf{u}^d[k+p-1|k])^\top \end{bmatrix}^\top \in \mathbb{R}^{pn_r}, \\
\mathbf{r}_p[k] &= \begin{bmatrix} (\mathbf{r}^d[k|k])^\top & \dots & (\mathbf{r}^d[k+p-1|k])^\top \end{bmatrix}^\top \in \mathbb{R}^{n_r}, \\
\mathbf{v}_p[k] &= \begin{bmatrix} (\mathbf{v}^d[k|k])^\top & \dots & (\mathbf{v}^d[k+p-1|k])^\top \end{bmatrix}^\top \in \mathbb{R}^{n_v}.
\end{aligned} \tag{6.2}$$

Then, estimates for the predicted states and plant output can be found as,

$$\mathbf{x}_p[k] = \mathbf{S}_x \mathbf{x}_{m0}^d[k] + \mathbf{S}_u (\mathbf{r}_p[k] + \Delta \mathbf{u}_p[k]) + \mathbf{H}_{vx} \mathbf{v}_p[k], \tag{6.3}$$

where the vector $\mathbf{x}_{m0}^d \in \mathbb{R}^{n_x}$ represents the initial, or observed, state at time-instant k . See Appendix C on page 107 for definitions of the remaining matrix constants.

6.2 Description

MPC is based on two main steps, estimation and optimization. The process of obtaining future set-point adjustments, $\Delta \mathbf{u}_p$, is outlined in Figure 6.1 as a block diagram and further explained as an iterative series of three steps:

1. Future states, \mathbf{x}_p , are predicted at each time-instant k using a linear reference model with the current state estimate, \mathbf{x}_{m0}^d , and the future values for the reference signals, \mathbf{r}_p , and measured disturbances, \mathbf{v}_p .
2. The vector of future set-point adjustments, $\Delta \mathbf{u}_p$, is calculated by optimizing a specific cost function in order to keep \mathbf{x}_p as close as possible to the desired state values \mathbf{x}_p^* while minimizing $\Delta \mathbf{u}_p$.
3. The set-point adjustment, $\Delta \mathbf{u}$ at time-instant k is set as $\Delta \mathbf{u}_p[k]$. The remaining predictions of $\Delta \mathbf{u}_p$ are discarded because at the next sampling instant the state estimates are updated with a new state estimate, \mathbf{x}_{m0}^d . Finally, step 1 is repeated for the next time-instant, $k + 1$.

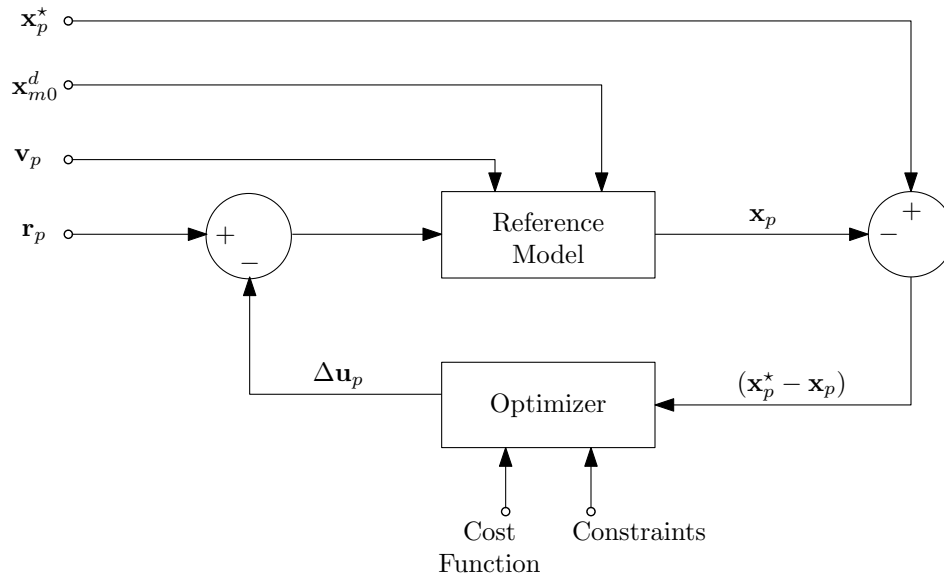


Figure 6.1: MPC showing common elements.

6.3 Optimizer

The optimizer consists of an objective (or cost) function, boundary conditions and an algorithm to find the optimal solution to the defined objective function.

6.3.1 Objective Function

In the scope of this work, a quadratic cost function, J , is used to minimize a quadratic cost associated with the difference between the predicted and desired plant state and the applied set-point adjustment,

$$J = \min_{\mathbf{M}\Delta\mathbf{u}_p \leq \mathbf{c}} \left[(\mathbf{x}_p^* - \mathbf{x}_p[k])^\top \mathbf{Q}_p \rho[k] (\mathbf{x}_p^* - \mathbf{x}_p[k]) + (\Delta\mathbf{u}_p^\top[k]) \mathbf{R}_p \Delta\mathbf{u}_p[k] \right], \quad (6.4)$$

where the constraints imposed by the linear matrix inequality are discussed in Section C.3 and \mathbf{x}_p^* is defined as,

$$\mathbf{x}_p^*[k] = \left[(\mathbf{x}^*[k+1|k])^\top \dots (\mathbf{x}^*[k+p|k])^\top \right]^\top \in \mathbb{R}^{pm_x}. \quad (6.5)$$

According to Assumption 4.11, the rate of fault-growth decreases monotonically for each state element. Therefore, setting $\mathbf{x}_p^* = \mathbf{0}$ is guaranteed to minimize the rate of fault growth and simplifies (6.4) to the following,

$$J = \min_{\mathbf{M}\Delta\mathbf{u}_p \leq \mathbf{c}} \left[\mathbf{x}_p^\top[k] (\mathbf{Q}_p \rho[k]) \mathbf{x}_p + (\Delta\mathbf{u}_p^\top[k]) \mathbf{R}_p \Delta\mathbf{u}_p[k] \right]. \quad (6.6)$$

This can be rewritten explicitly for $\Delta\mathbf{u}_p$ in quadratic form as,

$$J = \min_{\mathbf{M}\Delta\mathbf{u}_p \leq \mathbf{c}} \left[\frac{1}{2} \Delta\mathbf{u}_p^\top[k] (\mathbf{H}_0[k]) \Delta\mathbf{u}_p[k] + \mathbf{b}_0^\top \Delta\mathbf{u}_p[k] + f_0[k] \right], \quad (6.7)$$

where \mathbf{H}_0 is positive definite. The matrix \mathbf{H}_0 and vector \mathbf{b}_0 are defined in Section C.2.

- Find a feasible starting point
- **Repeat** until "optimal enough"
 - Solve the equality problem defined by the active set (approximately)
 - Compute the Lagrange multipliers of the active set
 - Remove a subset of the constraints with negative Lagrange multipliers
 - Search for infeasible constraints
- **End.**

Figure 6.2: Pseudo-code for the active set algorithm.

6.3.2 Medium-Scale Quadratic Programming

Several algorithms exist for solving the linear inequality constraints posed by the MPC. In this section the active set approach is discussed in a qualitative manner. Then, Dantzig-Wolfe's algorithm is presented as an extension to the active set solution.

6.3.2.1 Active Set

The active set is particularly important in optimization theory as it determines which constraints will influence the final result of optimization. In general an active set algorithm has the structure outlined in Figure 6.2.

6.3.2.2 Dantzig-Wolfe algorithm

The Dantzig-Wolfe algorithm is used to solve the convex quadratic program using Dantzig-Wolfe's active set method [75, 76]. The solution is usually found after $n + r$, where $n = \dim(\Delta \mathbf{u}_p) = p \cdot n_r$ is the number of optimization variables and $r = \dim(\mathbf{c})$ is the number of constraints. According to Dantzig et al. more than $3(n + r)$ iterations are rarely required [77].

6.3.2.3 Computational Requirements

Computational requirements for the MPC algorithm were benchmarked using the “quadprog.m” function provided by MATLAB as the average number of double-precision floating-point operations per each iteration of the MPC for relatively small model dimensions, $n_x \leq 5$ with one reference input, one measured disturbance and one output. The total number of such operations for a given size prediction horizon can be found in Figure 6.3. The data was generated using randomly generated matrices where the system described by the triplex $(\mathbf{A}_m^d, \mathbf{B}_{m,r}^d, \mathbf{C}_m^d)$ is in reachable canonical form with negative eigenvalues to ensure a stable system. Ten different prediction horizons were used and the model dimension was increased from $n_x = 1$ to 5. The time between each optimization was recorded and repeated 30 times for each prediction horizon and model dimension with a different randomly generated system. According to the results, the average number of floating-point operations required per iteration of the MPC algorithm increases logarithmically with the size of the prediction horizon, p . The total number of floating-point operations percent can be computed by dividing the average number of floating-point operations required per iteration of the MPC algorithm by the sample-time, T_s .

6.3.3 Aliasing

In signal processing aliasing refers to an effect that causes different signals to become indistinguishable when sampled. Applying the discrete-time solution generated by the MPC algorithm to offset the reference input to the closed-loop system can have unintended effects on the RUL performance if the problem of aliasing is not properly considered. Aliasing occurs when the signal is sampled at a rate lower than twice its maximum frequency. Therefore, upper-bound of the frequency range, f_{ub} , that can

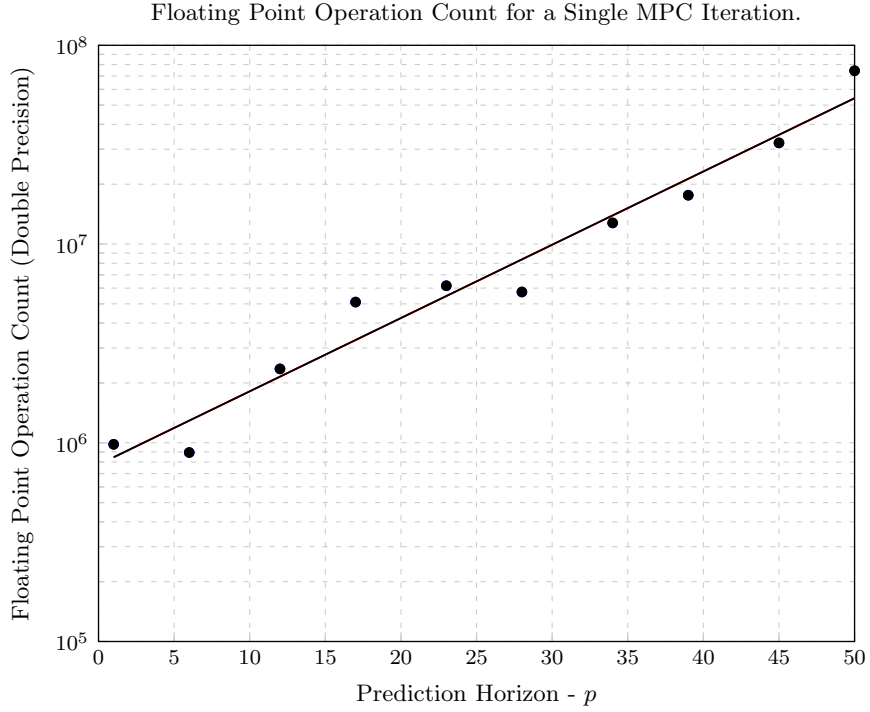


Figure 6.3: Average floating point operation count for different size prediction horizons for $n_x \leq 5$.

be effectively reconfigured is given as,

$$f_{ub} = \frac{1}{2T_s} \tag{6.8}$$

CHAPTER VII

EXAMPLE APPLICATION

The previous chapters provided the groundwork for the PHM-based reconfigurable control architecture, stability / boundedness guarantees and the MPC algorithm. This chapter begins with a general design criteria outline presented in Section 7.1. In Section 7.2 the design criteria is applied to an example application, an electro-mechanical actuator (EMA). A metric for determining RUL feasibility for the reconfiguration procedure is presented along with a few examples. The remainder of the chapter studies the specific example of the motor winding insulation fault with respect to extending RUL through set-point reconfiguration. Section 7.3 provides a procedure to determine the weight matrices for the MPC cost function. Section 7.4 examines an adaptation function for the EMA example and evaluates its performance for a set of operating conditions. Section 7.5 studies the effect of linear model uncertainty on modeling error associated with the state estimate. Section 7.6 utilizes these uncertainties to make long-term state predictions with error boundaries. Section 7.7 uses the long-term state predictions as inputs to the prognostic model to arrive at RUL estimates with uncertainty boundaries. Finally, the chapter concludes in Section 7.8 with a discussion on the applied load disturbance and its affect on the RUL estimates.

7.1 General Design Criteria

Several system-specific criteria need to be evaluated to determine if the PHM-based reconfigurable controller is a feasible candidate to extend RUL. An outline of the evaluation criteria is provided in Figure 7.1. The main criteria are separated into three categories: (a) system model and evaluation, (b) constraints and operating conditions and (c) RUL feasibility.

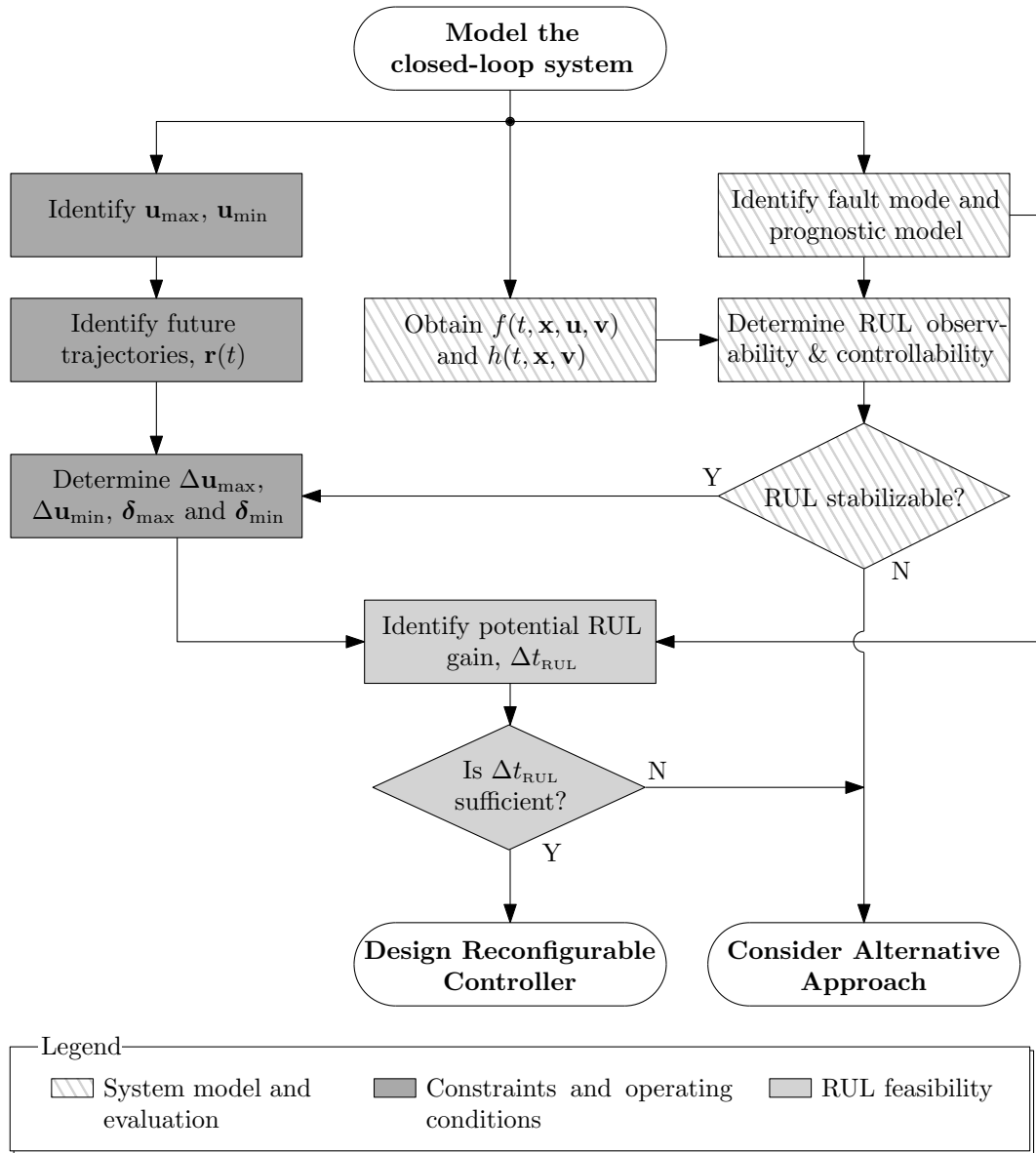


Figure 7.1: Flowchart used to determine feasibility criteria for the reconfigurable control design.

7.1.1 System Model and Evaluation

First, it's assumed a model for the plant and the identified fault-mode are known. These models are evaluated to see if the system is RUL stabilizable. If the system is not RUL stabilizable reconfiguration cannot be achieved and another design approach is needed.

7.1.2 Constraints and Operating Conditions

After the plant is shown to be RUL stabilizable, the available control authority and operating conditions are defined. The constraints consist of the minimum and maximum possible values for the control input, \mathbf{u} , set-point adjustments, $\Delta\mathbf{u}$, and the rate of set-point adjustments, δ . The expected or anticipated operating conditions are application specific and are known (or estimated) a-priori.

7.1.3 RUL Feasibility

Finally, once the system model and corresponding constraints are identified, the RUL is evaluated for feasibility. This is done by using the estimated (or anticipated) future set-point trajectories, \mathbf{r} , adjusted set-point boundaries, and plant model with the PHM module to estimate the relative change in RUL, Δt_{RUL} , as a consequence of the reconfiguration action. If Δt_{RUL} is not sufficient then another approach is required. Otherwise, the reconfiguration architecture can be applied.

7.1.3.1 Performance Metric

Evaluation of RUL feasibility can be difficult to explicitly quantify. A quick estimate of the relative increase in RUL can be made by evaluating the relative change in the cost associated with the plant state before and after reconfiguration. First, define the cost corresponding to the weight ρ as,

$$J(\rho, \mathbf{x}_p, \Delta \mathbf{u}_p) = \min_{\Delta \mathbf{u} \in \mathcal{U}_\delta} \left\{ J_x(\rho, \mathbf{x}_p, \mathbf{Q}_p) + J_{\Delta u}(\Delta \mathbf{u}_p, \mathbf{R}_p) \right\}, \quad (7.1)$$

where,

$$J_x(\rho, \mathbf{x}_p, \mathbf{Q}_p) = \rho \mathbf{x}_p^\top \mathbf{Q}_p \mathbf{x}_p, \quad (7.2)$$

and,

$$J_{\Delta u}(\Delta \mathbf{u}_p, \mathbf{R}_p) = \Delta \mathbf{u}_p^\top \mathbf{R}_p \Delta \mathbf{u}_p. \quad (7.3)$$

Now, the percent change in the cost before and after reconfiguration, η , can be computed,

$$\eta(\rho) = \frac{J_x(0, \mathbf{x}_p, \mathbf{Q}_p) - J_x(\rho, \mathbf{x}_p, \mathbf{Q}_p)}{J_x(0, \mathbf{x}_p, \mathbf{Q}_p)}, \text{ for } \rho \in (0, \infty), \quad (7.4)$$

where $\eta > 0$ corresponds to a net increase in RUL and $\eta < 0$ corresponds to a net reduction in RUL.

7.2 Electro-Mechanical Actuator (EMA) Design Criteria

In this section an EMA is examined as an example for PHM-based control reconfiguration. An EMA was selected in part due to its availability and its emergence as a solution of choice for future flight control actuation systems. More specifically, the rudder of the NASA X-38 crew re-entry vehicle, shown in Figure 7.2, was selected as the system of interest. A failure modes, effects and criticality analysis (FMECA) of the X-38 rudder actuator was examined to identify the most critical component, degradation of the motor winding insulation.

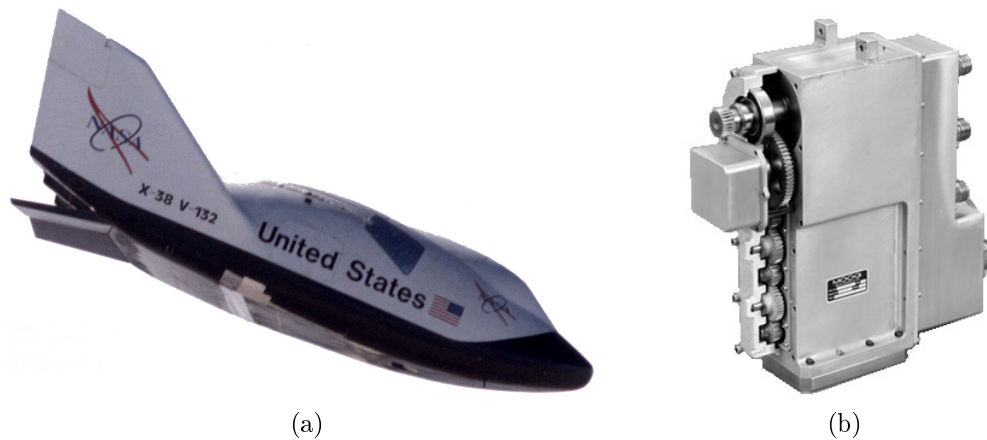


Figure 7.2: Photo of the (a) X-38 crew re-entry vehicle and its (b) corresponding rudder actuator.

7.2.1 System Model and Evaluation

Two models for the X38 actuator, the system and prognostic models, are provided in the appendix. The dynamics of the system are presented as a 5th order state-space model, given in Appendix D on page 114. The corresponding prognostic model for the motor winding insulation fault is provided in Appendix E on page 118.

7.2.1.1 Controllability / Observability

The plant is shown to be controllable and observable using the modeling parameters in Table D.1. This can be shown by applying Definitions B.1 and B.2, accordingly.

Table 7.1: Actuator constraints applied to system reconfiguration.

Type of Constraint	Min Value	Max Value
Control input	$\mathbf{u}_{\min} = -60 \text{ deg}$	$\mathbf{u}_{\max} = 60 \text{ deg}$
Set-point adjustment	$\Delta \mathbf{u}_{\min} = -5.0 \text{ deg}$	$\Delta \mathbf{u}_{\max} = 5.0 \text{ deg}$
Set-point adjustment rate	$\delta_{\min} = -2.5 \text{ deg}$	$\delta_{\max} = 2.5 \text{ deg}$
Motor current	$i_{m,\min} = -20 \text{ A}$	$i_{m,\max} = 20 \text{ A}$

7.2.1.2 RUL Controllability / RUL Observability

The prognostic model for the motor winding insulation fault is given in (E.9). According to the model, the critical inputs are the ambient temperature, T_a , and motor current, i_m . The motor current can be directly manipulated and measured as a state of the plant. Also, the ambient temperature can be measured. Therefore by Definition 4.2, the plant is shown to be RUL observable. Finally, if it's assumed that T_a is negligible compared to the contribution of i_m to RUL, then by Definition 4.1 the plant can be said to be RUL controllable. Therefore, by Definition 4.3 the plant is RUL stabilizable.

7.2.2 Constraints and Operating Conditions

7.2.2.1 Constraints

The constraints on the possible control values, set-point adjustment and rate applied set-point adjustment for the actuator are provided in Table 7.1.

7.2.2.2 Operating Conditions

The sampling period of the digital controller is set to $T_s = 0.02\text{s}$ to match the update rate of the production controller in the X38 actuator.

7.2.3 RUL Feasibility

RUL feasibility is demonstrated for the X38 actuator by using the metric defined in (7.4) with the linear plant model provided in Appendix D.

7.2.3.1 Steady-State Conditions

The steady-state conditions for the state vector $\bar{\mathbf{x}}_m$ can be found using the linear reference model,

$$\bar{\mathbf{x}}_m = -(\mathbf{A}_m^{-1}\mathbf{B}_{m,r}) \cdot \theta_{\text{ref}}. \quad (7.5)$$

According to the model, the steady-state conditions yield, $\bar{\mathbf{x}}_m = [0 \ 8 \ 0 \ 1 \ 0]^T \cdot \theta_{\text{ref}}$, indicating that $\bar{i}_m = \bar{\omega}_m = \bar{\omega}_\ell = 0$ and $\bar{\theta}_m = 8\bar{\theta}_\ell$. That is, at steady-state conditions in the absence of an external load, the motor current, motor speed and load speed are zero, and the steady-state motor position is a multiple of the steady-state load position by a factor of eight.

7.2.3.2 Dynamic Conditions

Next, dynamic conditions are studied by applying a series of ramp reference signals of constant slope to the linear actuator model. The slopes of each ramp input ranges from 10 rad/s to 50 rad/s . Results of the simulation, shown in Figure 7.3, indicate the motor current increases linearly with the slope of each ramp input. Every 1 rad/s increase in the ramp slope corresponds to an increase in motor current by 1.8 A . A similar plot is generated for a set of sinusoidal inputs with a frequency ranging from 0.1 Hz to 10 Hz and an amplitude of 60 deg , shown in Figure 7.4. The amount of current increases at higher reference frequencies due to the increased rate of change similar to that observed by the increased ramp rate. Both of these instances indicates reconfiguration is plausible under dynamic conditions.

Next, to illustrate the effect of reconfiguration, a sinusoidal input with a frequency of

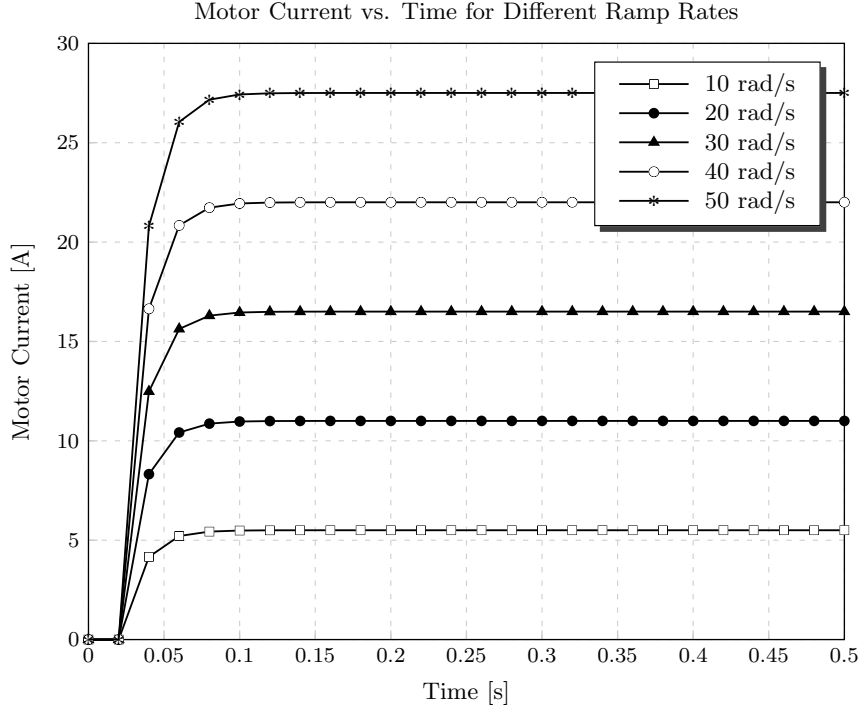


Figure 7.3: Simulated plots of motor current versus time for a set of ramp inputs with a constant slope. The slope of each ramp input ranged from 10 rad/s to 50 rad/s .

2 Hz and an amplitude of 60 deg is applied to the linear actuator model. This time, the MPC controller is utilized with a matched linear-reference model where $p = 5$, $\rho = \text{"high"}$, $\mathbf{Q} = \text{diag}([1 \ 0 \ 0 \ 0 \ 0])$ and $\mathbf{R} = 1$. The results of the simulation are shown in Figure 7.5. The position command is shown to be reconfigured to stay within the pre-defined set-point boundaries while reducing the overall motor current. A value of $\eta_{\text{high}} = 0.19$ was computed from the simulation. Selection of \mathbf{Q} and \mathbf{R} are explained in the next section.

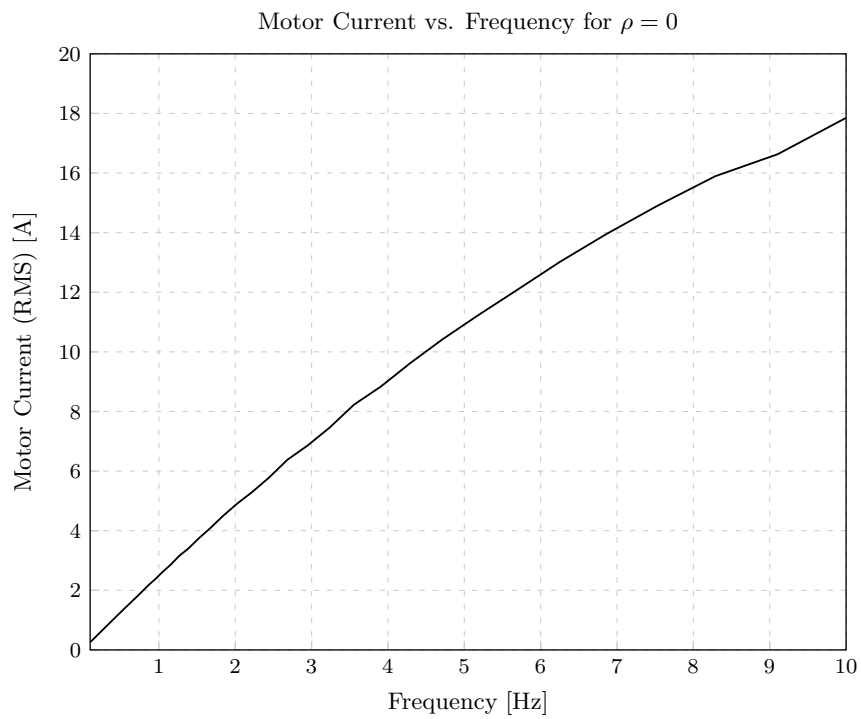
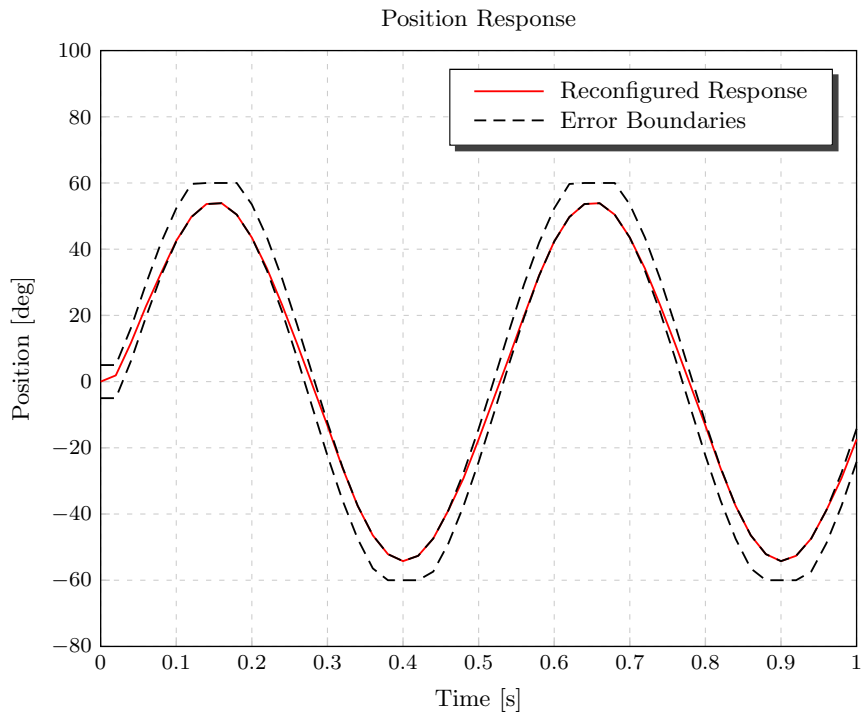
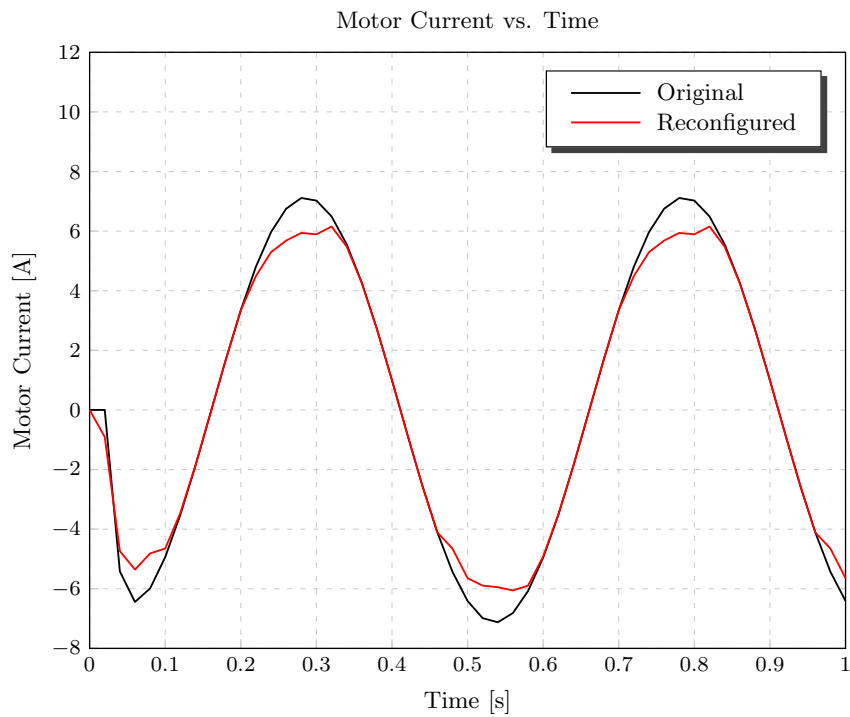


Figure 7.4: Simulated plots of motor current (RMS) versus time for a set of sinusoidal reference inputs. The frequency ranged from 0.1 Hz to 10 Hz.



(a)



(b)

Figure 7.5: Simulated plots of (a) actuator position and (b) motor current before and after applying the MPC controller.

7.3 Determining MPC Weights

There are several ways that the positive semi-definite weight matrices \mathbf{Q} and \mathbf{R} can be selected. First, consider the matrix, \mathbf{Q}' , which is selected to reflect the quadratic cost on the components of \mathbf{x} which are related to the RUL. For example, in the case of the X38 actuator example, the variable corresponding to RUL controllability and observability is the motor current, i_m . The simplest quadratic cost function is i_m^2 . To generate this cost from the state vector \mathbf{x} , a weight matrix \mathbf{Q}' is selected as,

$$\mathbf{Q}' = \begin{bmatrix} 1 & 0 & 0 & 0 & 0 \\ 0 & 0 & 0 & 0 & 0 \\ 0 & 0 & 0 & 0 & 0 \\ 0 & 0 & 0 & 0 & 0 \\ 0 & 0 & 0 & 0 & 0 \end{bmatrix}. \quad (7.6)$$

Next, the weight matrix \mathbf{R}' is defined. In general the matrix, \mathbf{R}' , is set to reflect the quadratic costs on the components of \mathbf{u} that can manipulate the RUL. Since only one reference input is used in this application, $\mathbf{R}' = 1$. Finally, the weight matrices are normalized by the following,

$$\mathbf{Q} = \mathbf{Q}' \left(\frac{1}{\mathbf{x}_{\max}^T \mathbf{Q}' \mathbf{x}_{\max}} \right) \quad \text{and} \quad \mathbf{R} = \frac{\mathbf{R}'}{\Delta \mathbf{u}_{\max}^T \mathbf{R}' \Delta \mathbf{u}_{\max}}. \quad (7.7)$$

Now, assume that $|i_{m,\max}| \geq |i_{m,\min}|$ and $|\Delta \mathbf{u}_{\max}| \geq |\Delta \mathbf{u}_{\min}|$. Then, in this example, by using the boundaries defined in Table 7.1 with the knowledge that $\mathbf{x}_{\max} = [i_{m,\max} \quad \star \quad \star \quad \star \quad \star]^T$, the following weight matrices are obtained,¹

$$\mathbf{Q} = \text{diag} (1.778 \times 10^{-4}, 0, 0, 0, 0) \quad \text{and} \quad \mathbf{R} = 131.3. \quad (7.8)$$

¹The vector elements denoted by the symbol “ \star ” are regarded as “don’t care” values.

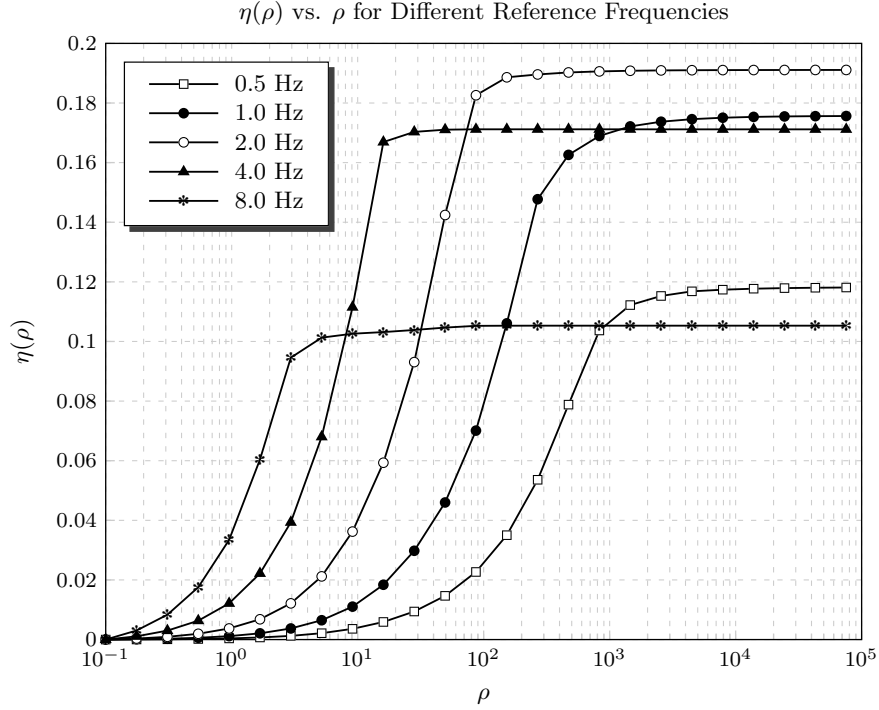


Figure 7.6: Simulated plots of η versus ρ for 5 different sinusoidal reference inputs.

Using these weight matrices, a series of simulations were run to compute η for different values of ρ . A set of five sinusoidal reference inputs were used to generate the plots of η for different values of ρ , shown in Figure 7.6. Each sinusoidal reference maintained a fixed amplitude of 60 deg and varied between 0.5 Hz to 8 Hz. According to the results, there is a wide range in behavior between η and ρ for different frequencies. The results also demonstrate that $\frac{d\eta}{d\rho} \geq 0$ and $\lim_{\rho \rightarrow \infty} \left(\frac{d\eta}{d\rho}\right) = 0$ for each reference input.

7.4 Selecting an Adaptation Function

The primary purpose of the adaptation function is to find the optimal value for the adaptation parameter, denoted as ρ^* , which maximizes η while minimizing $\Delta \mathbf{u}$. In the previous section it was shown that η reaches a maximum when $\rho \rightarrow \infty$. However, large values of ρ results in the maximum allowable reduction in performance. An alternative selection criteria is sought to find the smallest possible value for ρ which approaches the maximum value for η . First, recall the observations made in the previous section from Figure 7.6 where η increases at an increasing rate for small values of ρ and increases at a decreasing rate for large values of ρ . An approximation for ρ^* can be made near the point of inflection where $d^2\eta/d\rho^2 = 0$. This value for ρ^* can be found by applying the following optimization criteria,

$$\rho^* = \min(\rho') \quad \text{s.t.} \quad \frac{d^2\eta}{d\rho'^2} \leq 0 \quad \text{and} \quad \rho_{\min} \leq \rho' \leq \rho_{\max}. \quad (7.9)$$

One possible way to numerically solve for ρ^* is by applying the adaptation function,

$$\Gamma(\rho[k]) = \begin{cases} \rho[k] & : \text{if } \text{mod}(k, N) \neq 0, \\ \rho[k] + \gamma_\rho \text{sign}(\eta[k] - \eta[k - N]) & : \text{elseif } \left| \eta[k] - \eta[k - N] \right| \geq \epsilon_\eta, \\ \rho[k] + \varpi[k] & : \text{otherwise,} \end{cases} \quad (7.10)$$

where γ_ρ is an adaptation gain, ϵ_η is the adaptation threshold and ϖ is a random variable following a Gaussian distribution with a variance of σ_ϖ^2 . Values for ρ are be updated by,

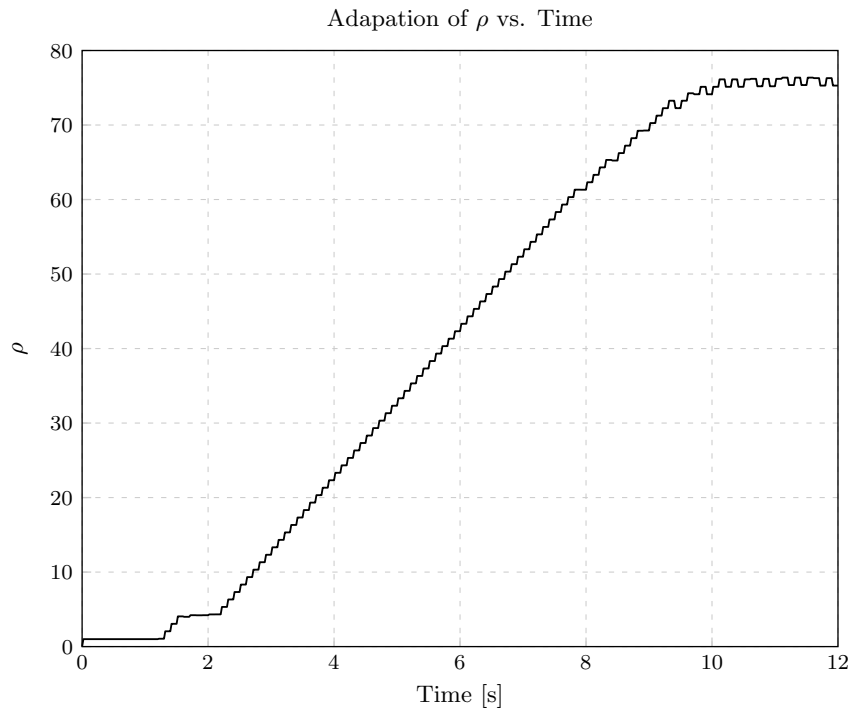
$$\rho[k + 1] = \max(\min(\Gamma(\rho[k]), \rho_{\max}), \rho_{\min}). \quad (7.11)$$

This adaptation scheme is simulated by applying a sinusoidal input with a frequency of 2 Hz and an amplitude of 60 deg to the linear actuator model. The parameters of the adaptation function used during the simulation are provided in Table 7.2 along

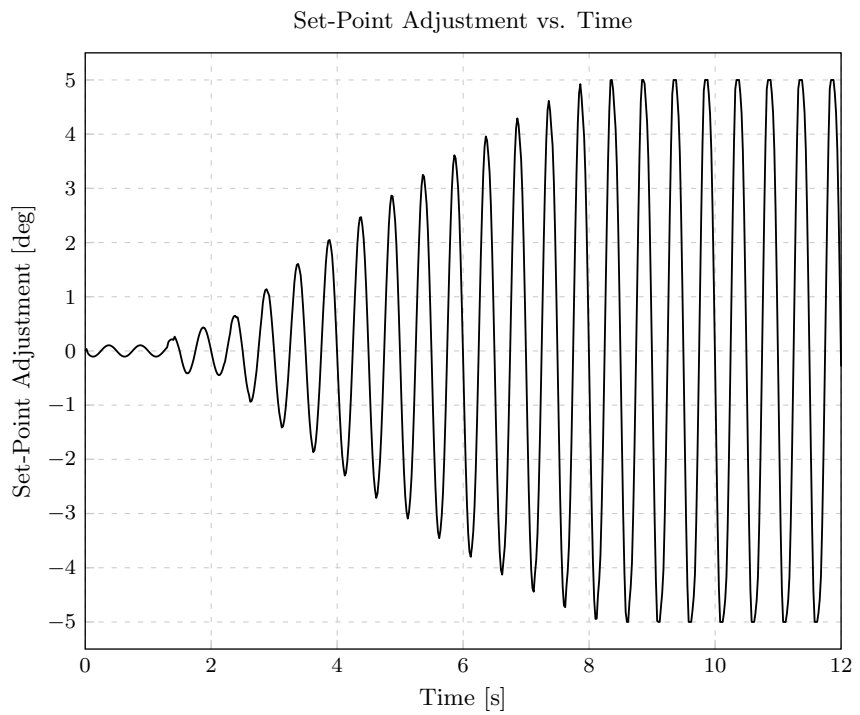
Table 7.2: Adaptation function parameters.

Parameter	Value
Minimum adaptation parameter	$\rho_{\min} = 1$
Maximum adaptation parameter	$\rho_{\max} = 1 \times 10^5$
Adaptation gain	$\gamma_p = 1$
Adaptation variance	$\sigma_{\varpi}^2 = 1 \times 10^{-2}$
Adaptation threshold	$\epsilon_{\eta} = 1 \times 10^{-3}$

with the initial condition, $\rho[0] = 1$. Plots for ρ , the change in motor position and change in motor current are given in Figure 7.7. According to Figure 7.7(a), the adaptation parameter increases until it reaches a steady-state value of approximately $\rho = 75$. This is reflected in Figure 7.7(b) where the magnitude of the applied set-point adjustment increases with ρ . The corresponding changes in actuator position and motor current before and after applying the MPC controller with parameter adaptation are given in Figure 7.8.

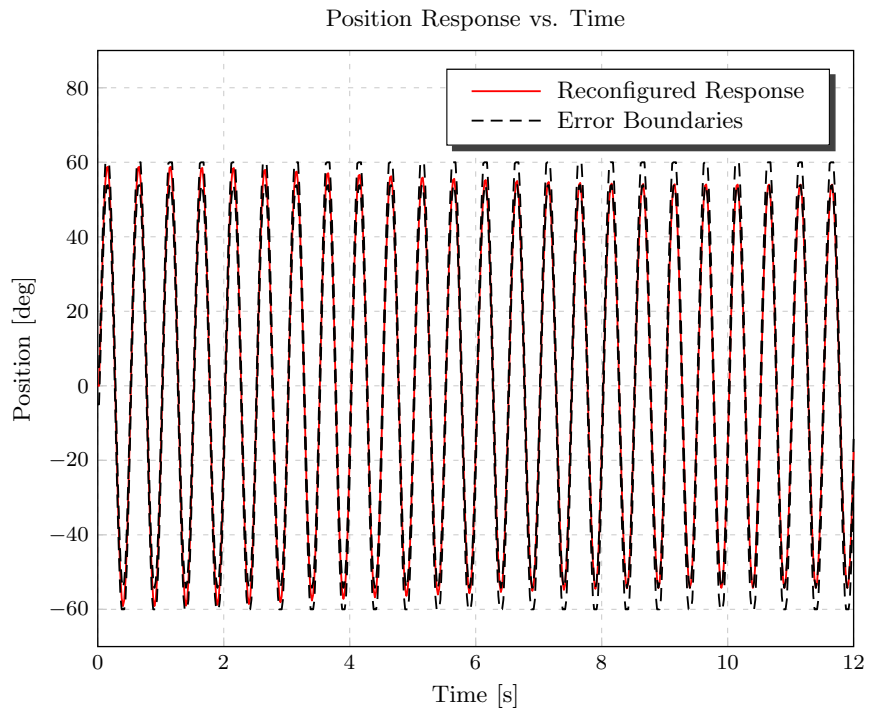


(a)

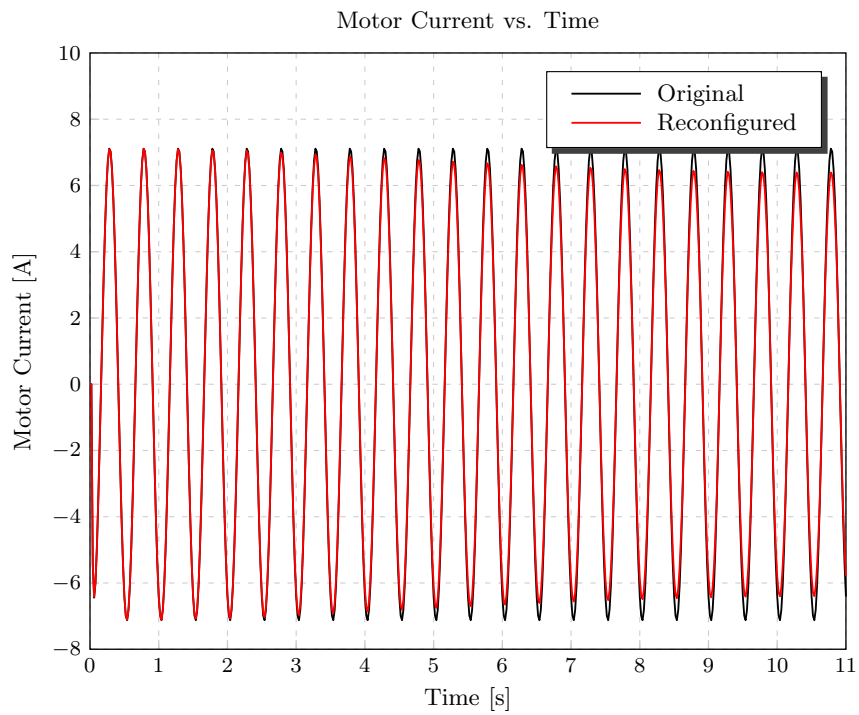


(b)

Figure 7.7: Plots of the (a) adaptation parameter (b) applied set-point adjustment vs time after applying the MPC controller with parameter adaptation.



(a)



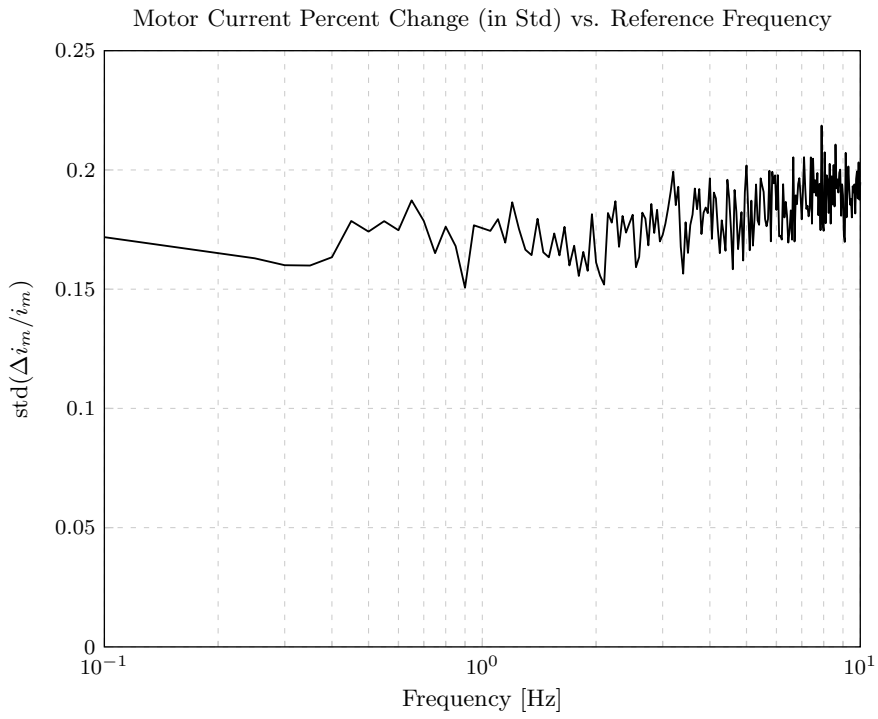
(b)

Figure 7.8: Plots of the (a) actuator position and (b) motor current vs time before and after applying the MPC controller with parameter adaptation.

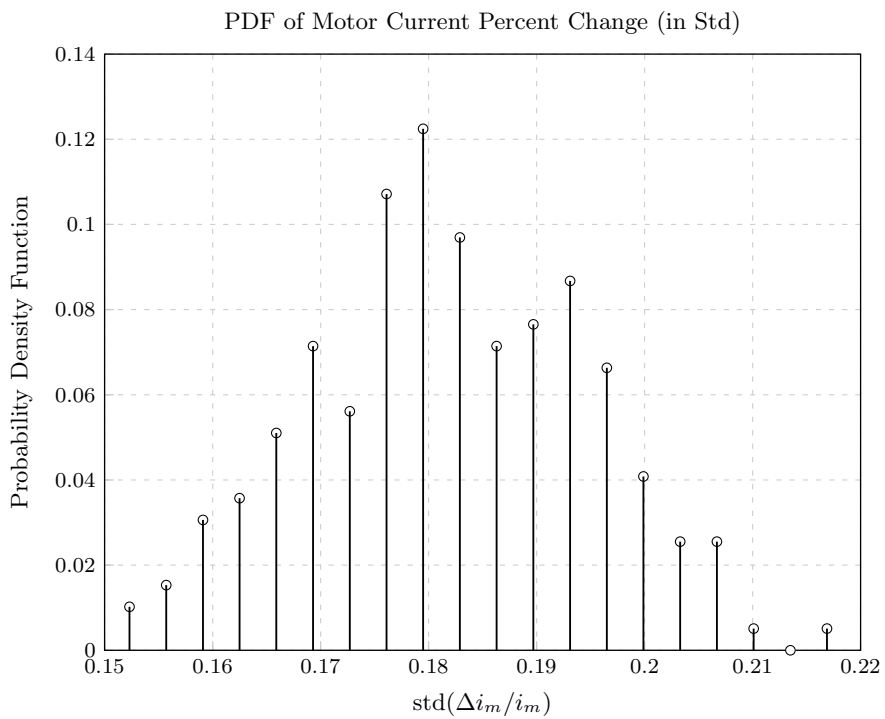
7.5 Model Uncertainty

Recall the definition for the modeling error, \mathbf{e}_m , defined earlier in (5.11). It was proven in Theorem 5.1 and later demonstrated in Figure 7.5 that if the set-point reconfiguration is uniformly bounded in time then the output must also be uniformly bounded in time. A similar claim was proven in Theorem 5.2 and Theorem 5.3 for the observation error, \mathbf{e}_o , and prediction error, \mathbf{e}_p . In the scope of this application, since the states are directly observable as measurements, $\mathbf{e}_o \rightarrow \mathbf{0} \implies \mathbf{e}_m \rightarrow \mathbf{e}_p$.

Consider the effects of model uncertainty on \mathbf{e}_p for a linear system with an unmatched linear reference model. In this example only the motor current is of interest; therefore, consideration of the entire state estimate is simplified to the scalar quantity, i_m . Values for $\Delta\mathbf{A}_m$ and $\Delta\mathbf{B}_{m,r}$ are obtained by using new values for the modeling parameters after adjusting each corresponding model parameter (i.e. k_e, J_m, \dots) randomly to within its uncertainty, provided in Table D.1. A sinusoidal input with an amplitude of 60 deg was used as the reference applied to the linear actuator model. The sample-time between predictions was set at $T_s = 0.05$ s. Monte Carlo simulations were conducted for a range of frequencies from 0.1 Hz to 10 Hz. The percent change in motor current vs. reference frequency was estimated from each set of Monte Carlo simulations. The results are shown in Figure 7.9. According to the results, the standard deviation of the percent change in motor current is approximately less than 0.2014 for 95% of the simulations.



(a)



(b)

Figure 7.9: Plots for (a) the maximum percent change versus frequency and (b) corresponding histogram.

7.6 Long-Term State Predictions with Uncertainty

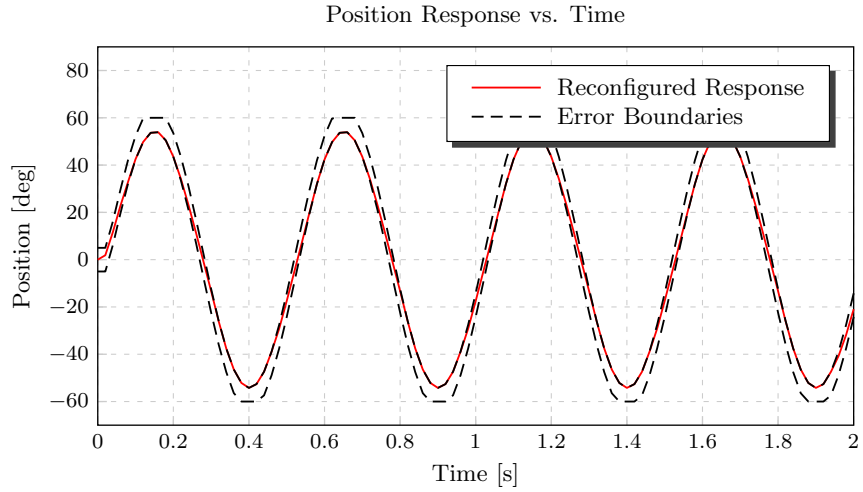
In Section 5.4, analysis was presented to predict the state with uncertainty boundaries for a set-point adjustment trajectory, $\Delta \mathbf{u}(t)$, over a long-term prediction horizon, q . It was shown in Theorem 5.4 for a perfectly matched linear model, the estimated change in the state over the prognostic prediction horizon, q , can be computed using (5.27). This is followed up in Section 5.4.2 for the case of the unmatched linear model by applying $\pm \mathbf{e}_p$ as the upper and lower boundaries. From the previous section, it can be shown the modeling error corresponding to a 95% confidence interval is approximately,

$$-0.395\hat{i}_m \leq \mathbf{e}_m(t) \leq 0.395\hat{i}_m(t) \quad (7.12)$$

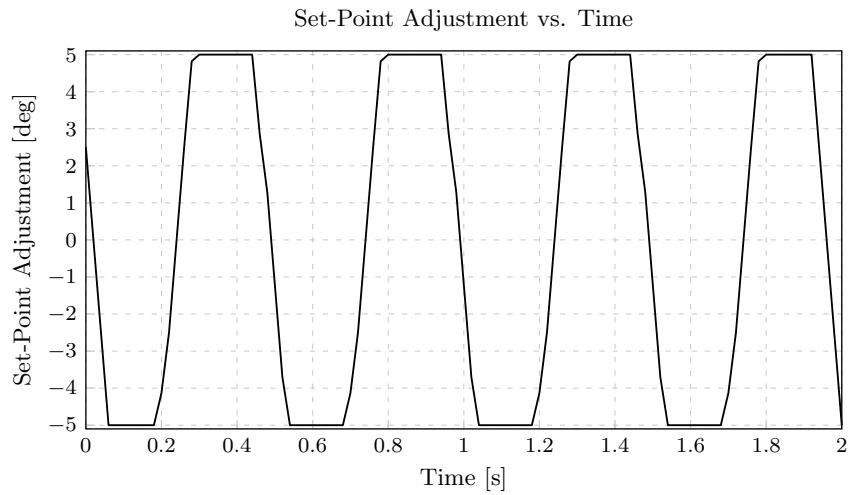
where \hat{i}_m is the estimated value of the motor current. By applying (5.34) and (5.33), a 95% confidence interval for the motor current can be expressed as,

$$0.605\hat{i}_m(t) \leq i_m(t) \leq 1.395\hat{i}_m(t). \quad (7.13)$$

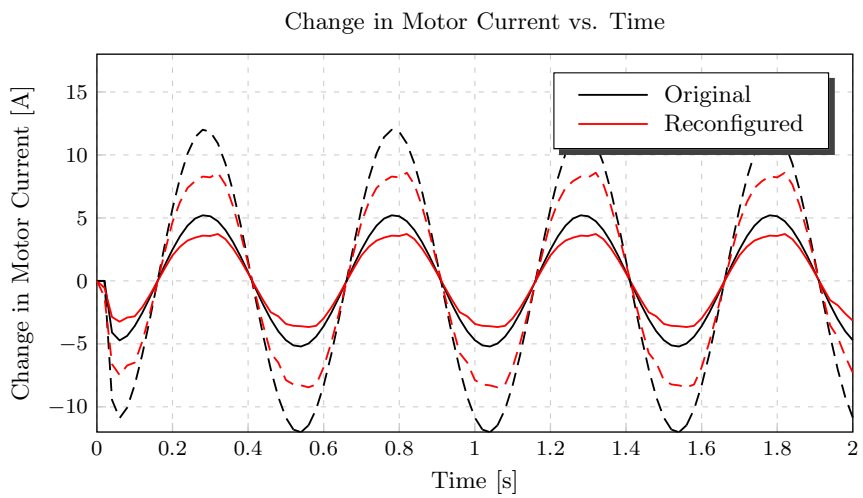
To demonstrate this boundary, consider the actuator example with the maximum reconfiguration possible, which corresponds to an adaptation parameter $\rho \gg 1$. Let the reference signal be sinusoidal with an amplitude of 60 deg and a fixed frequency of 2 Hz. The corresponding actuator position reference signal before and after reconfiguration is shown in Figure 7.10. Also shown is the set-point adjustment applied to the reference signal and the corresponding motor current with uncertainty boundaries. The uncertainty boundaries are used with the prognostic model to determine the uncertainty in the RUL estimate, discussed next.



(a)



(b)



(c)

Figure 7.10: Plots of the (a) actuator position (b) applied set-point adjustment and (c) corresponding motor current with 95% uncertainty boundaries. Dashed / solid lines correspond to the upper / lower 95% confidence boundaries.

7.7 RUL Estimation & Uncertainty

In this section, RUL estimation and uncertainty are studied for two types of reference signals. The first, a sinusoidal input reference of constant frequency and amplitude, is studied to provide an analytical understanding in estimating RUL and uncertainty. The second example, an aperiodic signal, is presented to show how the algorithm handles a dynamic situation.

7.7.1 Sinusoidal Signals with Fixed Amplitude and Frequency

First, consider the prognostic model for the winding insulation fault, provided in Appendix E where $T_a = 300^\circ\text{K}$. The input to the prognostic model is the squared current value, i_m^2 . Next, recall the cost function is directly proportional to i_m^2 . After reconfiguration, it was shown the cost function reduces by a factor of η . Therefore, the quantity $(1 - \eta) \cdot i_m^2$ can be used to represent the input to the prognostic model after reconfiguration. This can be demonstrated using a simple example. Let the reference signal be a sinusoidal input with a frequency of 2 Hz and an amplitude of 60 deg. According to Figure 7.6, $\eta \approx 0.19$ for large values of ρ . Also, according to Figure 7.4(b) the corresponding RMS value of current is approximately 5 A, which corresponds to,

$$i_m(t) = 7.07 \sin(4\pi ft). \quad (7.14)$$

For the nominal case when $\rho = 0$, the current is bounded by,

$$4.277 \sin(4\pi t) \leq i_m(t) \leq 9.863 \sin(4\pi t). \quad (7.15)$$

and the input to the prognostic model is bounded by,

$$18.29 \sin^2(4\pi t) \leq i_m^2(t) \leq 97.27 \sin^2(4\pi t). \quad (7.16)$$

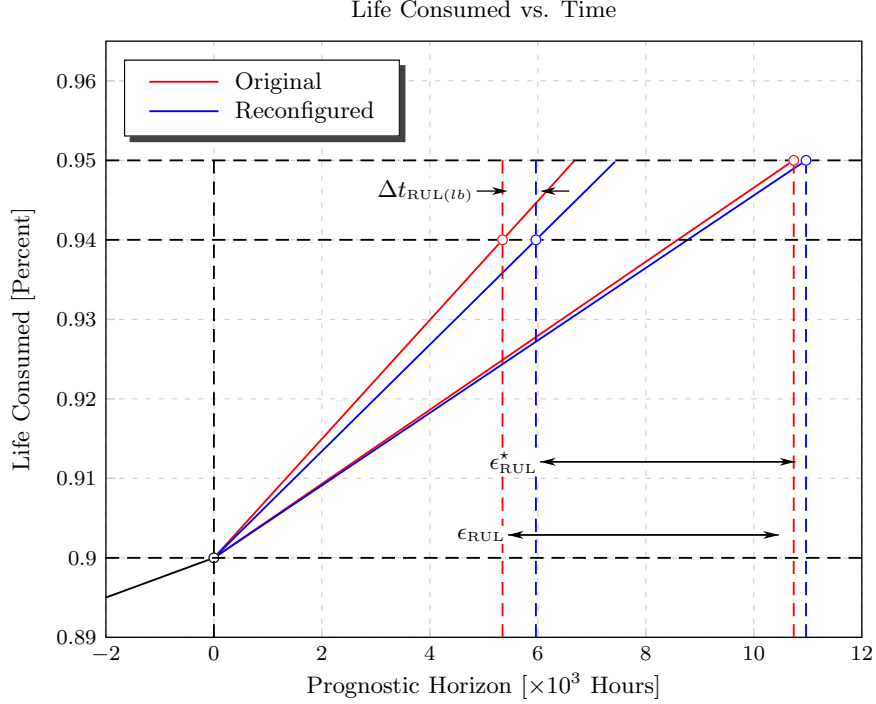


Figure 7.11: Plot of life consumed versus prognostic horizon before and after reconfiguration for a sinusoidal reference input with a frequency of 2 Hz and an amplitude of 60 deg.

Similarly, for the case when $\rho \gg 1$ and $\eta = 0.19$, the input to the prognostic model is adjusted by a factor of $(1 - \eta)$, which becomes,

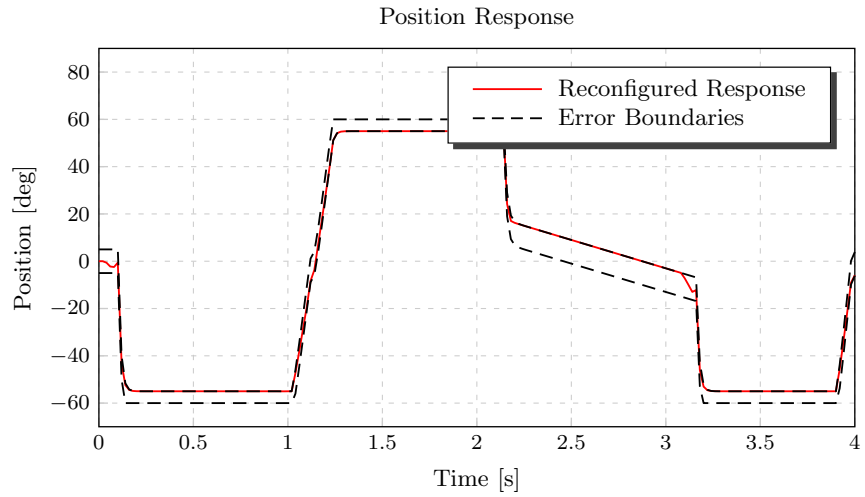
$$14.82 \sin^2(4\pi t) \leq i_m^2(t) \leq 78.79 \sin^2(4\pi t). \quad (7.17)$$

Applying these boundaries to the input of the prognostic model in (E.9), a plot of the fault dimension (life consumed) versus the prognostic horizon can be obtained for the cases before and after reconfiguration, provided in Figure 7.11. From the plot values for Δt_{RUL} , ϵ_{RUL} and ϵ_{RUL}^* are computed as 6.178×10^2 hrs, 5.393×10^3 hrs and 5.003×10^3 hrs, accordingly. This allows the metrics RLI and PUI to be computed as 0.116 and -0.080 , respectively.

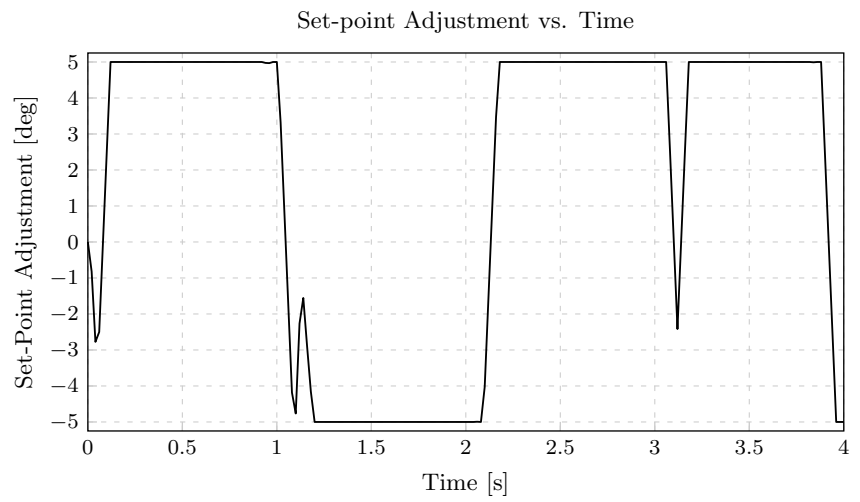
7.7.2 Aperiodic Signal

Consider an example for an aperiodic reference signal, shown in Figure 7.12(a). Applying this reference signal to the MPC controller for a prediction horizon of $p = 5$ and a sample-time of $T_s = 0.02$ s produces the set-point adjustment in Figure 7.12(b). Plots of the motor current generated before and after reconfiguration is shown in Figure 7.12(c). From the simulation it was computed that $\eta = 0.185$ for large values of ρ .

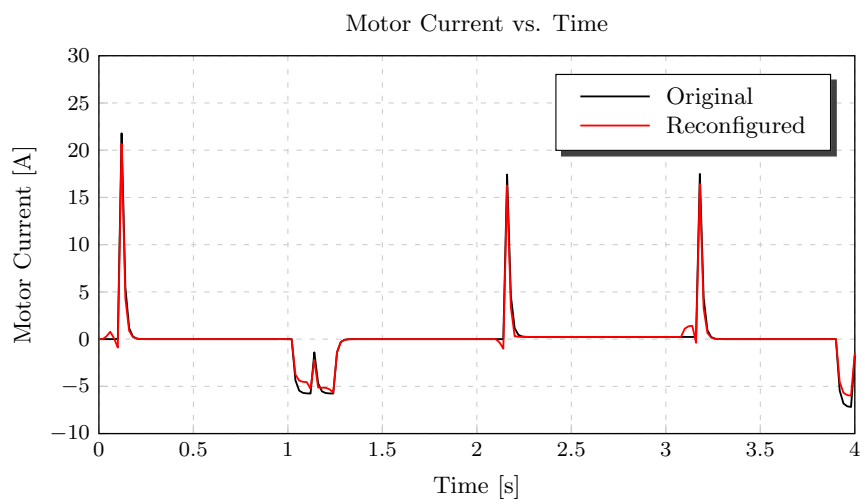
Next, recall the uncertainty constraint found in (7.13). Its assumed since this constraint holds for the frequency range 0.1 Hz to 10 Hz, then it should hold for the reference signal discussed in this section. Applying these boundaries to the input of the prognostic model in (E.9), a plot of the fault dimension (life consumed) versus the prognostic horizon can be obtained for the cases before and after reconfiguration. From the plot values for Δt_{RUL} , ϵ_{RUL} and ϵ_{RUL}^* are computed as 2.709×10^2 hrs, 3.305×10^3 hrs and 3.107×10^3 hrs, accordingly. This allows the metrics RLI and PUI to be computed as 0.032 and -0.060 , respectively. Although a positive gain in RUL is realized, the RLI of this example is approximately a factor of three less than the previous example. This is because the relative change in the peak motor current values are substantially less than the previous example with the sinusoidal reference.



(a)



(b)



(c)

Figure 7.12: Plots of the (a) actuator position signal, (b) applied set-point adjustment and (c) motor current before and after applying the MPC controller.

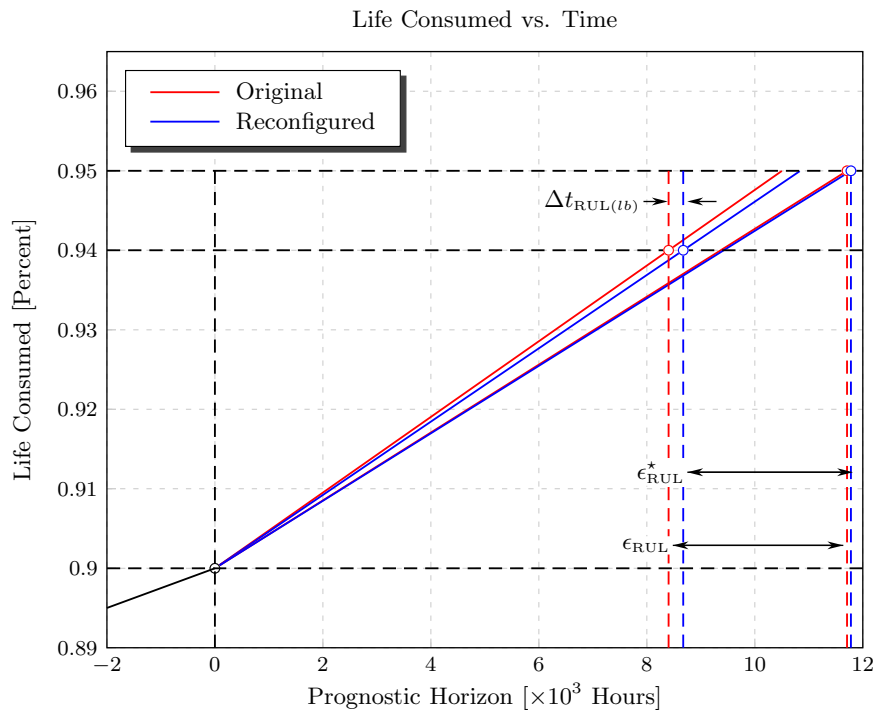


Figure 7.13: Plot of life consumed versus prognostic horizon before and after reconfiguration for a reference input using Figure 7.12(a) as a repeated sequence.

7.8 Load Disturbances

The reconfiguration routine is ideal for conditions of zero-load. Realistically however, the load disturbance affects the RUL of the system and cannot be directly controlled by the MPC. At best, the MPC can use a measure of the load-disturbance to determine the optimal set-point adjustments to help minimize the effect of the load on RUL. This is illustrated by studying the effects of reconfiguration using a sinusoidal input with a frequency of 2 Hz and an amplitude of 60 deg when applied to the linear actuator model. The MPC controller is utilized with a matched linear-reference model where $p = 5$ and $\rho = \text{"high"}$. The corresponding actuator position and motor current before and after reconfiguration for zero-load disturbance are provided in Figure 7.14(a) and (c), accordingly. Next, the actuator position and motor current before and after reconfiguration for a constant load disturbance of $\mathbf{v}(t) = 50 \text{ in} \cdot \text{lbs}$ is provided in Figure 7.14(b) and (d), respectively. According to the results, the position reconfiguration appears to produce similar set-point adjustments. When comparing the reconfiguration efficiency, $\eta = 0.190$ for the zero-load disturbance case and $\eta = 0.056$ for the case when $T_{\text{load}} = 50 \text{ in} \cdot \text{lbs}$.

For the same conditions a plot of η vs T_{load} was generated for a range of load disturbances varying from $1.00 \times 10^{-1} \text{ in} \cdot \text{lbs}$ to $1.00 \times 10^2 \text{ in} \cdot \text{lbs}$, provided in Figure 7.15. According to the plot, the effect of T_{load} on η does not become significant until the load disturbance exceeds $10 \text{ in} \cdot \text{lbs}$. Although this implies the RUL of the reconfigured system can be reduced even with the load-disturbance, the realized reduction in RUL will be less for increasing T_{load} .

The constant load disturbance has the effect of offsetting the motor current. This offset can be explained by revisiting the zero-load disturbance steady-state conditions from Section 7.2.3.1. Instead, now consider the steady-state conditions with a non-

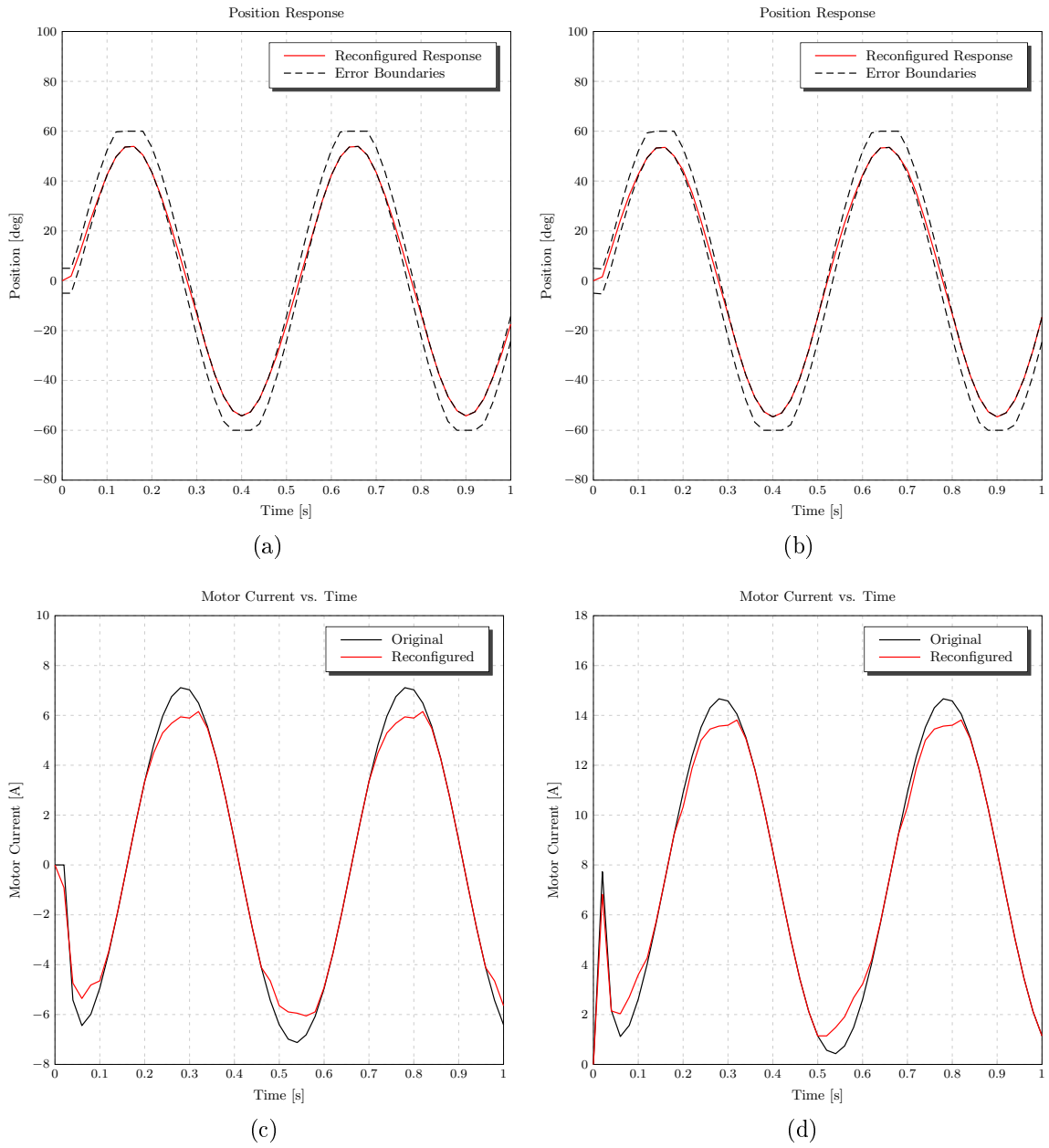


Figure 7.14: Plots of (a) actuator position and (b) motor current before and after applying the MPC controller when $T_{\text{load}} = 0 \text{ in} \cdot \text{lbs}$. Also shown are plots of (c) actuator position and (d) motor current before and after applying the MPC controller when $T_{\text{load}} = 50 \text{ in} \cdot \text{lbs}$.

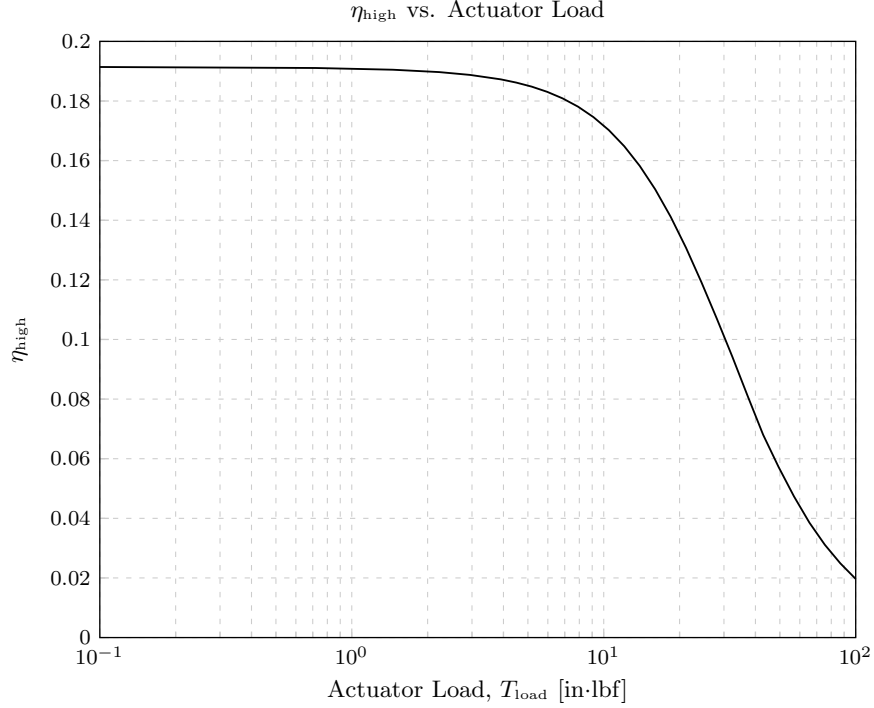


Figure 7.15: Plot of η_{high} vs. a actuator load over a range of T_{load} from 1.00×10^{-1} in · lbs to 1.00×10^2 in · lbs.

zero steady-state load disturbance,

$$\bar{\mathbf{x}}_m = -\mathbf{A}_m^{-1} \left[\mathbf{B}_{m,r} \mid \mathbf{B}_{m,v} \right] \begin{bmatrix} \theta_{\text{ref}} \\ T_{\text{load}} \end{bmatrix}. \quad (7.18)$$

According to the model, the steady-state condition yields,

$$\bar{\mathbf{x}}_m = \begin{bmatrix} 0 \\ 8 \\ 0 \\ 1 \\ 0 \end{bmatrix} \theta_{\text{ref}} + \begin{bmatrix} 1.51 \times 10^{-1} \\ -1.10 \times 10^{-3} \\ 0 \\ -1.00 \times 10^{-4} \\ 0 \end{bmatrix} T_{\text{load}}, \quad (7.19)$$

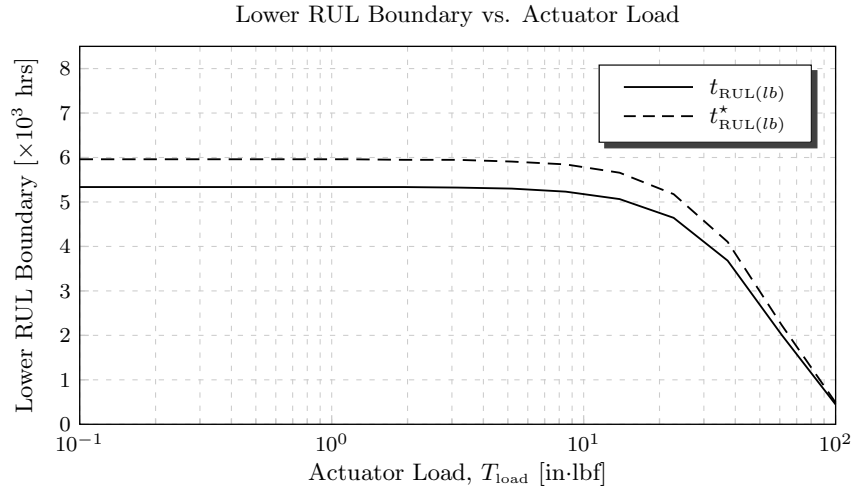
indicating that $\bar{i}_m = (1.51 \times 10^{-1}) T_{\text{load}}$, $\bar{\omega}_m = 0$, $\bar{\theta}_m = 8\theta_{\text{ref}} - (1.10 \times 10^{-3}) T_{\text{load}}$, $\bar{\omega}_\ell = 0$ and $\bar{\theta}_\ell = \theta_{\text{ref}} - (1.00 \times 10^{-4}) T_{\text{load}}$. Now, under steady-state conditions, when

Table 7.3: Computed values for t_{RUL} , t_{RUL}^* , Δt_{RUL} and RLI for different applied load disturbances, T_{load} .

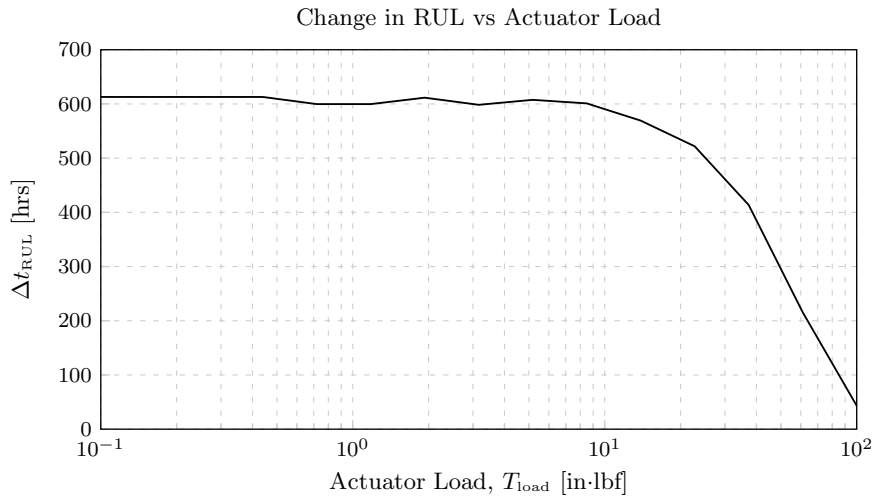
T_{load} [in · lbs]	t_{RUL} [hrs]	t_{RUL}^* [hrs]	Δt_{RUL} [hrs]	RLI
1.00×10^{-1}	5.46×10^3	6.07×10^3	6.13×10^2	0.112
4.44×10^{-1}	5.46×10^3	6.07×10^3	6.13×10^2	0.112
1.18×10^0	5.44×10^3	6.05×10^3	6.11×10^2	0.112
5.18×10^0	5.41×10^3	6.02×10^3	6.08×10^2	0.112
2.23×10^1	4.75×10^3	5.27×10^3	5.22×10^2	0.110
6.11×10^1	2.05×10^3	2.27×10^3	2.16×10^2	0.105
1.00×10^2	4.53×10^2	4.96×10^2	4.33×10^1	0.096

$T_{\text{load}} = 50$ in · lbs the corresponding steady-state current becomes $\bar{i}_m = 7.56$ A, which is approximately the offset observed in Figure 7.14(d).

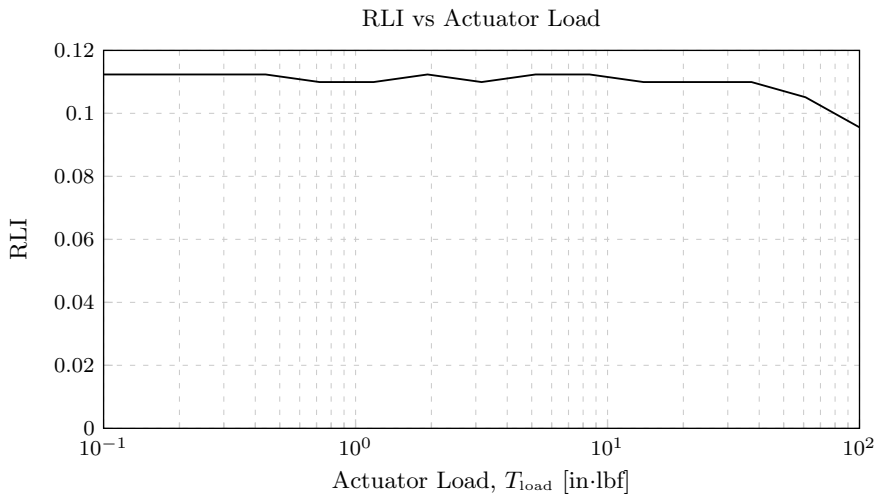
Finally, the RUL was studied for an example where the load disturbance is varied. This is illustrated by studying the effects of reconfiguration using a sinusoidal input with a frequency of 2 Hz and an amplitude of 60 deg when applied to the linear actuator model. The MPC controller is utilized with a matched linear-reference model where $p = 5$ and $\rho = \text{"high"}$. The corresponding lower RUL boundaries before and after reconfiguration, represented by the symbols t_{RUL} and t_{RUL}^* , are shown in Figure 7.16(a) over a range of T_{load} from 1.00×10^{-1} in · lbs to 1.00×10^2 in · lbs. Similarly, the change in RUL, Δt_{RUL} and computed values for RLI are given in Figure 7.16(b) and(c) over the same range of T_{load} . A summary of the computed values for t_{RUL} , t_{RUL}^* , Δt_{RUL} and RLI values for different applied load disturbances, T_{load} , is provided in Table 7.3. As expected, the RUL reduced as a result of an increase in T_{load} . However, in this example for this reference input, the RLI remained relatively constant over the range of applied load disturbances. This indicates that, although the RUL reduced with T_{load} , the relative percent change in the RUL as a result of reconfiguration remained approximately constant.



(a)



(b)



(c)

Figure 7.16: Plots of the (a) lower RUL boundary (b) change in RUL and (c) RLI vs. actuator load over a range of T_{load} from 1.00×10^{-1} in · lbs to 1.00×10^2 in · lbs.

CHAPTER VIII

CONCLUSIONS

This body of work constitutes a significant effort regarding the specific role of RUL in control systems. The PHM-based reconfigurable controls framework presented in this dissertation is one approach to a much larger hierarchical control scheme. The overall control scheme was discussed briefly as a three-tier hierarchical control architecture. More specifically, the role of the low-level layer was emphasized as a module which adjusts the reference set-points to the local production controller in order to sacrifice a fixed amount of performance to achieve an increase in RUL. The modules of the reconfigurable controller, the MPC and state observer, were defined mathematically and analyzed to demonstrate stability and boundedness. The MPC algorithm was derived and its performance studied. Finally, the reconfigurable control framework was evaluated using an EMA Simulink model. Results acquired from the simulation demonstrated the feasibility of the approach.

However, additional issues must still be addressed. First, the utility of the proposed approach is application specific. Other modules of the integrated fault-tolerant control hierarchy, such as the control redistribution and mission adaptation, are only briefly discussed; These modules can contribute significantly towards the development of high-confidence systems. Second, the assumptions made in this thesis may need refining. For example, it is assumed through the definitions of RUL controllability and observability that a state model exists for the system and the RUL can be observed and controlled by the states. However, in practice, the RUL can rarely be represented by a state space model alone. Finally, even though the MPC algorithm was evaluated in Simulink for an EMA example, hardware implementation is required to validate the results obtained through simulation.

APPENDIX A

NOTATION

A.1 Functional Notation

The formal description of a function involves the function's name, its domain, its codomain, and a rule of correspondence. For example, consider the function, $f : \mathbb{R}^{n_x} \times \mathbb{R}^{n_r} \rightarrow \mathbb{R}$ defined as,

$$f(\mathbf{x}(t), \mathbf{r}(t)) = \|\mathbf{x}(t)\| + [\mathbf{r}(t)]^T \mathbf{r}(t), \quad (\text{A.1})$$

where $\mathbf{x} \in \mathbb{R}^{n_x}$ and $\mathbf{r} \in \mathbb{R}^{n_r}$. The function name is “ f ” and reads “ f as a function of \mathbf{x} and \mathbf{r} ”. The domain are the vectors \mathbf{x} and \mathbf{r} of dimension n_x and n_r , respectively. The codomain of f is a real-valued number. Finally, the rule of correspondence is read as, “ \mathbf{x} and \mathbf{r} maps to $\|\mathbf{x}\| + \mathbf{r}^T \mathbf{r}$ ”.

A.1.1 Continuous-Time Functions

Continuous-time functions are defined by enclosing the domain by parentheses, (\cdot) . For example, $f(\mathbf{x}(t))$ represents a continuous-time functions.

A.1.2 Discrete-Time Functions

Discrete-time functions are defined by enclosing the domain by brackets, $[\cdot]$. For example, $f[\mathbf{x}[k]]$ represents a discrete-time function.

A.1.3 Zero-Order Hold (ZOH) Discretization

The prediction model is obtained from a linear state space model represented in continuous time. One such discretization is the ZOH,

$$\mathbf{x}[k] = \mathbf{x}(kT_s) \quad \text{s.t.} \quad kT_s \leq t < (k+1)T_s, \quad (\text{A.2})$$

where T_s is the period between each sample. The equivalent transfer function of the ZOH is,

$$G_{\text{ZOH}}(s) = \frac{1 - e^{-sT_s}}{T_s s}, \quad (\text{A.3})$$

which maps the eigenvectors from the s -plane, λ_i , to the z -plane by the following mapping,

$$z_i = e^{\lambda_i T_s}. \quad (\text{A.4})$$

A.1.3.1 Differential-to-Difference Equation Approximation

According to the mean-value theorem,

$$\exists t^* \in [kT_s, (k+1)T_s] \quad \text{s.t.} \quad \dot{\mathbf{x}}(t^*) = \frac{\mathbf{x}((k+1)T_s) - \mathbf{x}(kT_s)}{T_s} \quad (\text{A.5})$$

where $k \in \mathbb{Z}^+$. If T_s is sufficiently small compared to $\|\ddot{\mathbf{x}}(t)\|$, then

$$\dot{\mathbf{x}}(t) \cong \frac{1}{T_s} (\mathbf{x}[k+1] - \mathbf{x}[k]) \quad (\text{A.6})$$

A.2 Symbolic Notation

The following symbolic notations are used throughout this document (unless otherwise specified),

A.2.1 Variable Types

A.2.1.1 Scalars

Scalars are assumed to be real numbers represented in italicized “UPPERCASE” or “lowercase” type (e.g. k_1, R_0, ω and ϵ)

A.2.1.2 Vectors

Vectors are represented in **bold** “lowercase” type (e.g. \mathbf{x}, \mathbf{b} and \mathbf{c}). All vectors are assumed to be column-vectors of n real numbers defined by the notation \mathbb{R}^n where n is an integer number. (e.g. $\mathbf{x} \in \mathbb{R}^6$ defines a column vector \mathbf{x} containing 6 elements).

A.2.1.3 Matrices

Matrices are represented in **bold** “UPPERCASE” type (e.g. \mathbf{A}, \mathbf{G} and \mathbf{R}). All matrices are assumed to be of size $n \times m$ where all elements are real numbers. Both rectangular and square matrices are defined using the notation where m and n are integer numbers denoting the number of rows and columns, respectively. (e.g. $\mathbf{A} \in \mathbb{R}^{3 \times 3}$ defines a square matrix \mathbf{A} of size 3×3 whereas $\mathbf{G} \in \mathbb{R}^{2 \times 4}$ denotes a rectangular matrix \mathbf{G} of size 2×4).

A.2.2 Common Constants

A.2.2.1 Ones Vector

Represents a column vector of n unity-elements denoted by $\mathbf{1}_n$.

A.2.2.2 Identity Matrix

Represents a square matrix of dimension $n \times n$ denoted by \mathbf{I}_n where each element along the main diagonal has a value of unity and zero elsewhere.

A.2.2.3 Zero Matrix

Represents a rectangular matrix of dimension $n \times m$ denoted by $\mathbf{0}_{n \times m}$ where each element in the matrix has a value of zero.

A.2.2.4 Zeros Vector

Represents a column vector of n zero-elements denoted by $\mathbf{0}_n$.

A.2.3 Vector Operations

Consider the following vector operations for a column vector,

$$\mathbf{v} = \begin{bmatrix} v[1] & v[2] & \dots & v[k-1] \end{bmatrix}^T \in \mathbb{R}^k \quad \text{s.t.} \quad k \in \mathbb{Z}^+. \quad (\text{A.7})$$

A.2.3.1 Indexing

Indexing is used to denote a particular element or series of elements in a vector. Let $m, n \in \mathbb{Z}^+$ s.t. $0 \leq m < n \leq k - 1$. Then, vector indexing of one element is denoted by,

$$\{\mathbf{v}\}_m = v[m] \in \mathbb{R}. \quad (\text{A.8})$$

Indexing can also be represented for a continuous sequence of vector of elements,

$$\{\mathbf{v}\}_m^n = \begin{bmatrix} v[m] & v[m+1] & \dots & v[n-1] & v[n] \end{bmatrix}^T \in \mathbb{R}^{n-m+1}. \quad (\text{A.9})$$

A.2.3.2 Equalities

Every vector element can be defined using a shorthand notation utilizing the indexing operation. For example, equating every element of a vector \mathbf{v} to zero can be represented by the following,

$$\{\mathbf{v}\}_0^{k-1} = 0 \implies v[\ell] = 0 \quad \text{for } \forall \ell \in [0, k-1]. \quad (\text{A.10})$$

Vector elements can also be related to a set of inequalities as well. Another example shows how to equate all elements of a vector \mathbf{v} to be less than the real number b can be represented by the following,

$$\{\mathbf{v}\}_0^{k-1} \leq b \implies v[\ell] \leq b \quad \text{for } \forall \ell \in [0, k-1]. \quad (\text{A.11})$$

A.2.3.3 Concatenation

Concatenation is an operation that creates a vector where its entries encompass that of two or more vector elements. In the scope of this document, concatenation is used to generate a new vector element by repeating the entries of another vector element n times and is defined by,

$$\text{concat} \{\mathbf{v}, n\} = \underbrace{\left[\mathbf{v}^\top \quad \mathbf{v}^\top \quad \dots \quad \mathbf{v}^\top \right]^\top}_{\text{repeated } n \text{ times}} \in \mathbb{R}^{n \cdot k}, \quad (\text{A.12})$$

where $n \geq 2$.

APPENDIX B

DEFINITIONS & THEOREMS

This appendix outlines definitions properties of commonly used functions.

B.1 Function Definitions

B.1.1 Dirac-delta Function

The Dirac delta can be loosely thought of as a function on the real line, $v \in \mathbb{R}$, which is zero everywhere except at the origin, where it is infinite,

$$\delta(v) \triangleq \begin{cases} \infty & : v = 0, \\ 0 & : v \neq 0. \end{cases} \quad (\text{B.1})$$

B.1.1.1 Properties

One important property of the Dirac-delta function is the translation property. Consider a function $f : [0, \infty) \rightarrow \mathbb{R}^n$. The translation property is as follows,

$$f(t) = \int_0^\infty f(\tau) \delta(t - \tau) d\tau, \quad (\text{B.2})$$

where $t \in [0, \infty)$.

B.1.2 Norm Function

The most common norm is the Euclidean norm represented by,

$$\|\mathbf{u}\| = \sqrt{\mathbf{u}^T \mathbf{u}} \quad (\text{B.3})$$

The Euclidean norm (otherwise referred to as just the norm) is used to measure the size of a vector.

B.1.2.1 Properties

The norm of a vector $\mathbf{u} \in \mathbb{R}^m$ represented by $\|\mathbf{u}\| \in \mathbb{R}$, where m is a positive integer which has the three properties,

1. **Zero point:** The following case holds:

$$\|\mathbf{u}\| = \begin{cases} \mathbf{0} & : \mathbf{u} \equiv \mathbf{0} \\ > \mathbf{0} & : \text{otherwise} \end{cases} \quad (\text{B.4})$$

2. **Scaling:** For $a > 0$ and any vector \mathbf{u} , the equality $\|a\mathbf{u}\| = a\|\mathbf{u}\|$ is always true.
3. **Triangle inequality:** The form satisfies the inequality $\|\mathbf{u}_1 + \mathbf{u}_2\| \leq \|\mathbf{u}_1\| + \|\mathbf{u}_2\|$ for $\mathbf{u}_1, \mathbf{u}_2 \in \mathbb{R}^m$.

B.1.3 System Properties

In this section definitions are given for system controllability and observability.

Definition B.1 (Controllability). If a system is controllable at time, t_0 then there exists a control sequence sequence $\mathbf{u}(t) \in \mathcal{U}$ on the interval $t \in [t_0, t_f]$ such that any initial-state of the closed-loop system, $\mathbf{x}(t_0) \in \mathcal{X}$ on the same interval can be driven to any desired terminal state, $\mathbf{x}(t_f) \in \mathcal{X}$.

Definition B.2 (Observability). A system is observable at time t_0 if for any initial state in the state space $\mathbf{x}(t_0) \in \mathcal{X}$ and a given control sequence $\mathbf{u}(t) \in \mathcal{U}$ defined on the interval $t \in [t_0, t_f]$ the state trajectory $\mathbf{x}(t)$ can be determined for $t \in [t_0, t_f]$.

APPENDIX C

MPC DERIVATIONS

C.1 State Predictor Constants

This section introduces the constants used by the MPC control algorithm.

$$\mathbf{S}_x = \begin{bmatrix} \mathbf{A}_m^d \\ (\mathbf{A}_m^d)^2 \\ \vdots \\ (\mathbf{A}_m^d)^p \end{bmatrix} \in \mathbb{R}^{(p \cdot n_x) \times n_x}$$

$$\mathbf{S}_u = \begin{bmatrix} \mathbf{B}_{m,r}^d & \mathbf{0} & \cdots & \mathbf{0} \\ \mathbf{A}_m^d \mathbf{B}_{m,r}^d & \mathbf{B}_{m,r}^d & \cdots & \mathbf{0} \\ \vdots & \vdots & \ddots & \vdots \\ (\mathbf{A}_m^d)^{p-1} \mathbf{B}_{m,r}^d & (\mathbf{A}_m^d)^{p-2} \mathbf{B}_{m,r}^d & \cdots & \mathbf{B}_{m,r}^d \end{bmatrix} \in \mathbb{R}^{(p \cdot n_x) \times (p \cdot n_r)}$$

$$\mathbf{H}_{vx} = \begin{bmatrix} \mathbf{B}_{m,v}^d & \mathbf{0} & \cdots & \mathbf{0} \\ (\mathbf{A}_m^d) \mathbf{B}_{m,v}^d & \mathbf{B}_{m,v}^d & \cdots & \mathbf{0} \\ \vdots & \vdots & \ddots & \mathbf{0} \\ (\mathbf{A}_m^d)^{p-1} \mathbf{B}_{m,v}^d & (\mathbf{A}_m^d)^{p-2} \mathbf{B}_{m,v}^d & \cdots & \mathbf{B}_{m,v}^d \end{bmatrix} \in \mathbb{R}^{(p \cdot n_x) \times (p \cdot n_v)}$$

$$\mathbf{R}_p = \begin{bmatrix} \mathbf{R} & \mathbf{0} & \cdots & \mathbf{0} \\ \mathbf{0} & \mathbf{R} & \cdots & \mathbf{0} \\ \vdots & \vdots & \ddots & \vdots \\ \mathbf{0} & \mathbf{0} & \cdots & \mathbf{R} \end{bmatrix} \in \mathbb{R}^{(p \cdot n_x) \times (p \cdot n_x)}$$

$$\mathbf{Q}_p = \begin{bmatrix} \mathbf{Q} & \mathbf{0} & \cdots & \mathbf{0} \\ \mathbf{0} & \mathbf{Q} & \cdots & \mathbf{0} \\ \vdots & \vdots & \ddots & \vdots \\ \mathbf{0} & \mathbf{0} & \cdots & \mathbf{Q} \end{bmatrix} \in \mathbb{R}^{(p \cdot n_r) \times (p \cdot n_r)} \quad (\text{C.1})$$

$$\mathbf{A}_{\delta u} = \begin{bmatrix} \mathbf{I}_{n_r} & \mathbf{0} & \cdots & \mathbf{0} & \mathbf{0} \\ -\mathbf{I}_{n_r} & \mathbf{I}_{n_r} & \cdots & \mathbf{0} & \mathbf{0} \\ \vdots & \vdots & \ddots & \vdots & \vdots \\ \mathbf{0} & \mathbf{0} & \cdots & \mathbf{I}_{n_r} & \mathbf{0} \\ \mathbf{0} & \mathbf{0} & \cdots & -\mathbf{I}_{n_r} & \mathbf{I}_{n_r} \end{bmatrix} \in \mathbb{R}^{(p \cdot n_r) \times (p \cdot n_r)} \quad (\text{C.2})$$

$$\mathbf{b}_{\delta u(ub)}[k] = \left[(\Delta \mathbf{u}^d[k-1|k-1] + \boldsymbol{\delta}_{\max})^\top \quad \boldsymbol{\delta}_{\max}^\top \quad \cdots \quad \boldsymbol{\delta}_{\max}^\top \right]^\top \in \mathbb{R}^{p \cdot n_r} \quad (\text{C.3})$$

$$\mathbf{b}_{\delta u(lb)}[k] = \left[(\Delta \mathbf{u}^d[k-1|k-1] + \boldsymbol{\delta}_{\min})^\top \quad \boldsymbol{\delta}_{\min}^\top \quad \cdots \quad \boldsymbol{\delta}_{\min}^\top \right]^\top \in \mathbb{R}^{p \cdot n_r} \quad (\text{C.4})$$

C.2 Weight Matrices

Consider the estimator \mathbf{x}_p from (6.3) written in the following compact form,

$$\mathbf{x}_p[k] = \mathbf{k}_x[k] + \mathbf{S}_u \Delta \mathbf{u}_p[k] \quad (\text{C.5})$$

where $\mathbf{k}_x \in \mathbb{R}^{p \cdot n_x}$ is defined as,

$$\mathbf{k}_x[k] = \mathbf{S}_x \mathbf{x}_{m0}^d[k] + \mathbf{S}_u \mathbf{r}_p[k] + \mathbf{H}_{vx} \mathbf{v}_p[k]. \quad (\text{C.6})$$

By replacing \mathbf{x}_p in (6.6) with the expression given in (C.5), the quadratic terms can be written explicitly in terms of $\Delta \mathbf{u}_p$,

$$J(k, \Delta \mathbf{u}[k]) = \frac{1}{2} \Delta \mathbf{u}_p^T[k] \cdot \underbrace{2(\rho[k] \mathbf{S}_u^T \mathbf{Q}_p \mathbf{S}_u + \mathbf{R}_p)}_{\mathbf{H}[k]} \Delta \mathbf{u}_p[k] + \dots$$

$$\underbrace{2\rho[k] \mathbf{k}_x^T \mathbf{Q}_p \mathbf{S}_u}_{\mathbf{b}[k]} \cdot \Delta \mathbf{u}_p^T[k] + \underbrace{\mathbf{k}_x^T[k] \cdot \mathbf{Q}_p \mathbf{k}_x[k]}_{f[k]} \quad (\text{C.7})$$

where f_0 is a collection of the remaining constant terms. Comparing this with (6.7) expressions for the weights $\mathbf{H}_0 \in \mathbb{R}^{(p \cdot n_r) \times (p \cdot n_r)}$, $\mathbf{b}_0 \in \mathbb{R}^{p \cdot n_r}$ and $f_0 \in \mathbb{R}$ are found,

$$\begin{cases} \mathbf{H}_0[k] &= 2(\rho[k] \mathbf{S}_u^T \mathbf{Q}_p \mathbf{S}_u + \mathbf{R}_p) \\ \mathbf{b}_0[k] &= 2\rho[k] \cdot \mathbf{k}_x^T[k] \mathbf{Q}_p \mathbf{S}_u \\ f_0[k] &= \mathbf{k}_x^T[k] \cdot \mathbf{Q}_p \mathbf{k}_x[k] \end{cases} \quad (\text{C.8})$$

C.3 Inequality Constraints

Two types of constraints are examined, box constraints and inequality constraints.

C.3.1 Box Constraints

Box constraints are used to enforce uniform upper and lower-boundaries on the optimization variable,

$$\begin{cases} \text{concat} \{ \mathbf{u}_{\min}, p \} & \leq \mathbf{u}_p[k] \leq \text{concat} \{ \mathbf{u}_{\max}, p \}, \\ \text{concat} \{ \Delta \mathbf{u}_{\max}, p \} & \leq \Delta \mathbf{u}_p[k] \leq \text{concat} \{ \Delta \mathbf{u}_{\max}, p \}, \end{cases} \quad (\text{C.9})$$

where $\mathbf{u}_p = \mathbf{r}_p + \Delta \mathbf{u}_p$. These box constraints can be rewritten explicitly in terms of $\Delta \mathbf{u}_p$ as,

$$\mathbf{b}_{\text{box}(lb)}[k] \leq \Delta \mathbf{u}_p[k] \leq \mathbf{b}_{\text{box}(ub)}[k], \quad (\text{C.10})$$

where,

$$\mathbf{b}_{\text{box}(lb)}[k] = \max \begin{pmatrix} \text{concat} \{ \mathbf{u}_{\min}, p \} - \mathbf{r}_p, \\ \text{concat} \{ \Delta \mathbf{u}_{\min}, p \} \end{pmatrix} \quad (\text{C.11})$$

$$\mathbf{b}_{\text{box}(ub)}[k] = \min \begin{pmatrix} \text{concat} \{ \mathbf{u}_{\max}, p \} - \mathbf{r}_p, \\ \text{concat} \{ \Delta \mathbf{u}_{\max}, p \} \end{pmatrix} \quad (\text{C.12})$$

C.3.2 Rate of Set-Point Adjustment

The amount the set-point adjustment, $\Delta \mathbf{u}_p$, can change between time-instants, k , can be enforced by applying the following inequality constraint,

$$\mathbf{b}_{\delta u}(lb) \leq \mathbf{A}_{\delta u} \Delta \mathbf{u}_p[k] \leq \mathbf{b}_{\delta u}(ub). \quad (\text{C.13})$$

where $\mathbf{A}_{\delta u}$, $\mathbf{b}_{\delta u}(lb)$ and $\mathbf{b}_{\delta u}(ub)$ were defined at the beginning of this appendix.

C.3.3 Constraint Concatenation

The two sets of constraints given earlier can be combined into the following inequality constraint,

$$\mathbf{M}\Delta\mathbf{u}_p[k] \leq \mathbf{c}[k], \quad (\text{C.14})$$

where,

$$\mathbf{M} = \begin{bmatrix} \mathbf{A}_{\delta u} \\ -\mathbf{A}_{\delta u} \\ \mathbf{I}_{n_r} \\ -\mathbf{I}_{n_r} \end{bmatrix} \in \mathbb{R}^{(p \cdot n_r) \times 4(p \cdot n_r)} \quad \text{and} \quad \mathbf{c}[k] = \begin{bmatrix} \mathbf{b}_{\delta u(ub)}[k] \\ -\mathbf{b}_{\delta u(lb)}[k] \\ \mathbf{b}_{\text{box}(ub)}[k] \\ -\mathbf{b}_{\text{box}(lb)}[k] \end{bmatrix} \in \mathbb{R}^{4(p \cdot n_r)}. \quad (\text{C.15})$$

Note: This differs from box constraints in that each element of $\Delta\mathbf{u}_p$ is dependent on the previous element leading to non-uniform boundaries.

C.4 Kuhn Tucker Conditions

Recall from (6.7) the corresponding cost function to be minimized,

$$J(k, \Delta \mathbf{u}[k]) = \min_{\Delta \mathbf{u} \in \mathcal{U}_\delta} \left[\frac{1}{2} \Delta \mathbf{u}_p^\top [k] \cdot \mathbf{H}_0 [k] \cdot \Delta \mathbf{u}_p [k] + \mathbf{b}_0^\top [k] \cdot \Delta \mathbf{u}_p [k] + f_0 [k] \right]. \quad (\text{C.16})$$

Define an inequality functional mapping $\mathbf{h} : \mathbb{R}^{p \cdot n_r} \mapsto \mathbb{R}^{4p \cdot n_r}$,

$$\mathbf{h}(\Delta \mathbf{u}_p [k]) = \mathbf{M} \Delta \mathbf{u}_p [k] - \mathbf{c} [k]. \quad (\text{C.17})$$

Next, define the LaGrangian, $L : \mathbb{R}^{p \cdot n_r} \mapsto \mathbb{R}$,

$$L(\Delta \mathbf{u}_p [k]) = \frac{1}{2} \Delta \mathbf{u}_p^\top [k] \cdot \mathbf{H}_0 [k] \cdot \Delta \mathbf{u}_p [k] + \mathbf{b}_0^\top [k] \cdot \Delta \mathbf{u}_p [k] + f_0 [k]. \quad (\text{C.18})$$

The constraints on the system dynamics can be adjoined to the LaGrangian, L , by introducing the time-varying LaGrange multiplier vector $\boldsymbol{\lambda}_p$ with \mathbf{h} . The result is the Hamiltonian function, H_λ ,

$$H_\lambda(\Delta \mathbf{u}_p [k]) = \frac{1}{2} \Delta \mathbf{u}_p^\top [k] \cdot \mathbf{H}_0 [k] \cdot \Delta \mathbf{u}_p [k] + \mathbf{b}_0^\top [k] \cdot \Delta \mathbf{u}_p + \dots \\ f_0 [k] + \boldsymbol{\lambda}_p^\top [k] \cdot (\mathbf{M} \Delta \mathbf{u}_p [k] - \mathbf{c} [k]), \quad (\text{C.19})$$

where,

$$\boldsymbol{\lambda}_p [k] = \left[\lambda_0 [k] \quad \lambda_1 [k] \quad \dots \quad \lambda_{4p-1} [k] \right]^\top. \quad (\text{C.20})$$

By taking the partial derivative of H_λ with respect to $\Delta \mathbf{u}_p$,

$$\frac{\partial H_\lambda [k]}{\partial \Delta \mathbf{u}_p [k]} = \mathbf{b}_0^\top [k] + \Delta \mathbf{u}_p^\top [k] \cdot \mathbf{H}_0 [k] + \boldsymbol{\lambda}_p^\top [k] \cdot \mathbf{M}. \quad (\text{C.21})$$

Finally, by setting (C.21) identically equal to zero, the optimal solution, $\Delta \mathbf{u}_p^*$ can be expressed as,

$$\Delta \mathbf{u}_p^* [k] = - (\mathbf{H}_0 [k])^{-1} (\mathbf{b}_0 [k] - \mathbf{M}^\top \boldsymbol{\lambda}_p^* [k]) \quad (\text{C.22})$$

where $\boldsymbol{\lambda}_p^*$ satisfies the Kuhn-Tucker conditions,

$$\left\{ \begin{array}{l} \mathbf{M} \cdot \Delta \mathbf{u}_p - \mathbf{c} [k] \leq \mathbf{0}_{4p \cdot n_r}, \\ \mathbf{b}_0^\top [k] + 2\Delta \mathbf{u}_p^\top [k] \cdot \mathbf{H}_0 [k] + (\boldsymbol{\lambda}_p^* [k])^\top \mathbf{M} = \mathbf{0}_{p \cdot n_r}^\top, \\ \boldsymbol{\lambda}_p^* [k] \cdot (\mathbf{M} \cdot \Delta \mathbf{u}_p [k] - \mathbf{c} [k]) = 0, \\ \boldsymbol{\lambda}_p^* [k] \geq \mathbf{0}_{p \cdot n_r}. \end{array} \right. \quad (\text{C.23})$$

APPENDIX D

LINEAR ACTUATOR MODEL

The electro-mechanical actuator (EMA) example discussed in the body of this dissertation is defined in this appendix.

D.1 Linear State Space Model

The EMA model used in this body of work is a fifth-order SISO model with a disturbance input. The five states consists of motor current, i_m , motor speed, ω_m , motor position, θ_m , actuator speed, ω_ℓ and the actor position, θ_ℓ . The inputs to the model are the reference position, θ_{ref} and the load torque, T_{load} , modeled as a disturbance. The output of the model is the actuator position, θ_ℓ . The system is represented by the state-space representation in (5.2) where $\mathbf{x}_m = [i_m \ \theta_m \ \omega_m \ \theta_\ell \ \omega_\ell]^\top$, $\mathbf{r} = \theta_{\text{ref}}$ and $\mathbf{v} = T_{\text{load}}$. Additionally, the matrices \mathbf{A}_m , $\mathbf{B}_{m,r}$, $\mathbf{B}_{m,v}$, \mathbf{C}_m and $\mathbf{D}_{m,v}$ are defined as,

$$\left\{ \begin{array}{l} \mathbf{A}_m = \begin{bmatrix} a_{11} & a_{12} & a_{13} & 0 & 0 \\ 0 & 0 & 1 & 0 & 0 \\ a_{31} & a_{32} & a_{33} & a_{34} & 0 \\ 0 & 0 & 0 & 0 & 1 \\ 0 & a_{52} & 0 & a_{54} & a_{55} \end{bmatrix}, \\ \mathbf{B}_{m,r} = \begin{bmatrix} b_{r1} \\ 0 \\ 0 \\ 0 \\ 0 \end{bmatrix}, \quad \mathbf{B}_{m,v} = \begin{bmatrix} 0 \\ 0 \\ 0 \\ 0 \\ b_{v5} \end{bmatrix}, \quad \mathbf{C}_m = \mathbf{I}_5 \text{ and } \mathbf{D}_{m,v} = d_{v1}, \end{array} \right. \quad (\text{D.1})$$

where the coefficients are given as,

$$\left\{ \begin{array}{lll} a_{11} = -(R_{tt} + k_1 k_2) L_{tt}^{-1}, & a_{12} = -k_1 k_3 k_4 L_{tt}^{-1}, & a_{13} = -(k_e + k_1 k_3) L_{tt}^{-1}, \\ a_{31} = k_t J_m^{-1}, & a_{32} = -k_{cs} N_{cm}^{-2} J_m^{-1}, & a_{33} = -b_m J_m^{-1}, \\ a_{34} = k_{cs} N_{cl} N_{cm}^{-1} J_m^{-1}, & a_{52} = k_{cs} N_{cl} N_{cm}^{-1} J_\ell^{-1}, & a_{54} = -(k_\ell + k_{cs} N_{cl}^2) J_\ell^{-1}, \\ a_{55} = -b_\ell J_\ell^{-1}, & b_{r1} = k_1 k_3 k_4 k_5 L_{tt}^{-1}, & b_{v5} = -J_\ell^{-1}, \\ d_{v1} = 0. \end{array} \right. \quad (\text{D.2})$$

A block diagram of the linear actuator model is given in Figure D.1. Values for the modeling parameters are provided in the next section.

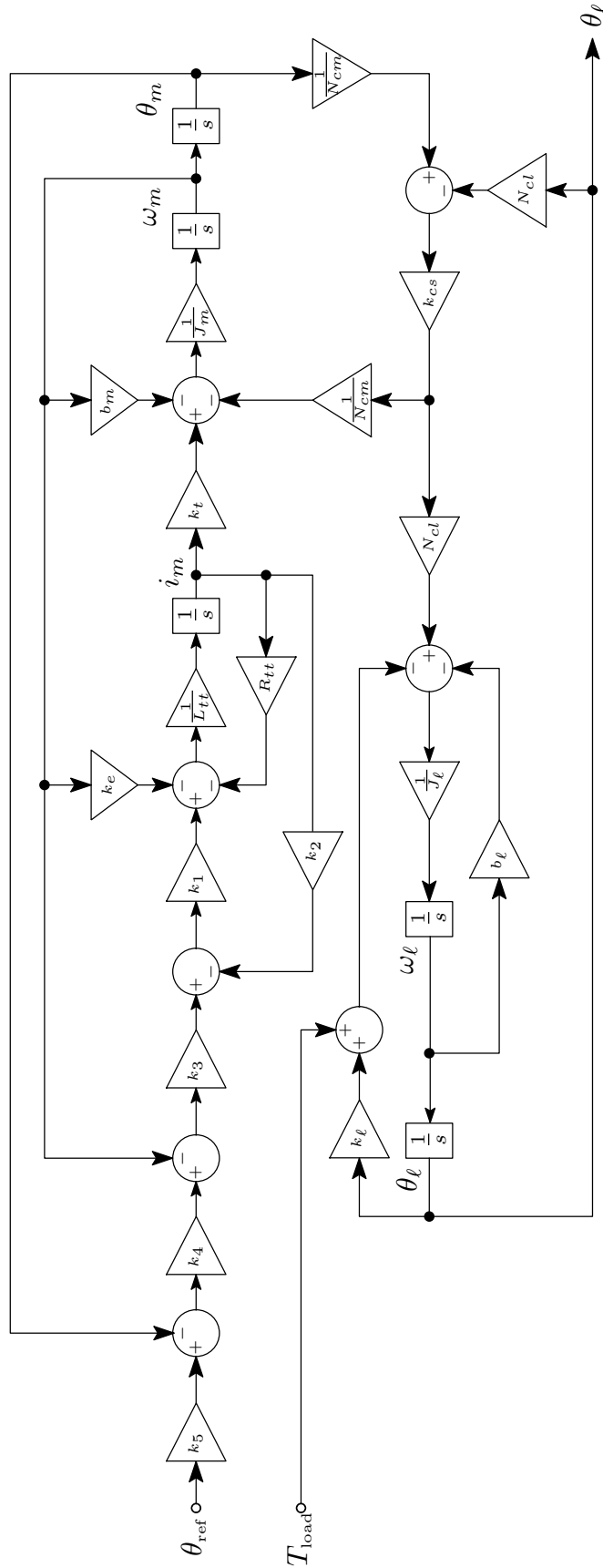


Figure D.1: Block diagram of the fifth-order actuator model.

D.2 Modeling Parameters

A list of the modeling parameters used in the actuator model are provided in Table D.1. Provided for each modeling parameter is a description, corresponding units, value and uncertainty (where applicable).

Table D.1: List of actuator modeling parameters with values and corresponding uncertainty.

Sym	Units	Value	Uncertainty (95%)	Description
b_ℓ	in · lbf / (rad/s)	1.00	±10%	Load damping
b_m	in · lbf / (rad/s)	4.60×10^{-2}	±10%	Motor damping
k_{cs}	rad/rad	4.00×10^5	–	Coupling stiffness
k_e	V / (rad/s)	1.25×10^{-1}	±5%	Back-emf coef.
k_ℓ	in · lbf/rad	0.00	–	Load stiffness
k_1	V/V	1.23×10^3	–	Controller gain 1
k_2	V/A	7.54×10^{-2}	–	Controller gain 2
k_3	V / (rad/s)	1.53×10^{-1}	–	Controller gain 3
k_4	s ⁻¹	6.87×10^1	–	Controller gain 4
k_5	rad/rad	8.00	–	Controller gain 5
k_t	in · lbf/A	8.27×10^{-1}	±5%	Motor torque coef.
J_ℓ	in · lbf · s ²	2.00×10^{-2}	±20%	Load inertia
J_m	in · lbf · s ²	1.60×10^{-3}	±20%	Motor inertia
L_{tt}	H	3.97×10^{-4}	±5%	Turn-to-turn inductance
N_{cl}	–	1.00	–	Load coupling
N_{cm}	–	8.00	–	Motor coupling
R_{tt}	Ω	3.78×10^{-1}	±5%	Turn-to-turn resistance

APPENDIX E

ACTUATOR / PROGNOSTIC MODEL

The actuator model from Appendix D is examined further to develop a prognostic model for a selected failure mode.

E.1 Failure Modes and Effects

Results from a failure modes, effects and criticality analysis (FMECA) study of the EMA suggest that the leading modes of failure are associated with the bearings [78, 79, 80], position feedback sensors [81, 82], electronic components [83] and electric motors [84, 81]. In this study, the BLDC motor was identified as the critical component where the primary failure mechanisms is breakdown of insulation between turns of the same winding. According to [85, 86, 87], stator insulation can fail due to several reasons: high stator core or winding temperature; contamination from oil, moisture and dirt; short circuit or starting stresses; electrical discharges; and leaking in the cooling system. For the EMA under investigation, winding temperature was identified as the dominant failure mechanism due to exposure of excessive environmental factors (i.e. temperature, thermal cycling, humidity).

E.2 Physics Based Model

In the case of the brushless DC motor, the winding temperature is related to the power loss in the copper windings, assuming the copper losses are the primary source of power loss. A first order thermo-electrical model, shown in Figure E.1, can be used to describe the relationship between power loss in the copper windings with respect to the winding-to-ambient temperature [51, 88], represented as T_{wa} and defined as,

$$T_{wa}(t) \triangleq T_w(t) - T_a(t) \quad (\text{E.1})$$

where the symbols T_w and T_a correspond to the winding temperature and ambient temperature respectively. The symbols R_0 , C_{wa} and R_{wa} refer to the winding resistance, thermal capacitance and thermal resistance of the windings, accordingly. The equivalent state space representation for Figure E.1 can be written as,

$$\dot{T}_{wa}(t) = \left[-\frac{1}{R_{wa}C_{wa}} \right] T_{wa}(t) + \left[\frac{R_0}{C_{wa}} \right] i_m^2(t) \quad (\text{E.2})$$

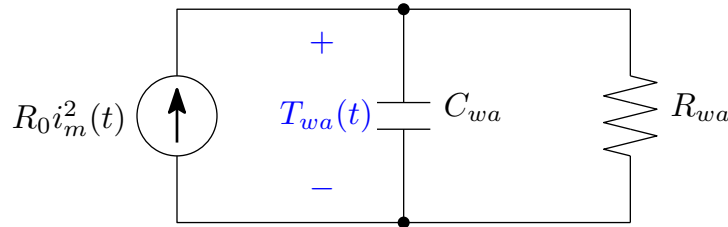


Figure E.1: Schematic of the first-order thermal model.

E.3 Fault Growth Model

Motor winding insulation degrades at a rate related to the winding temperature, T_w . Let the RUL be represented as, t_{RUL} . The RUL at time t can be related to T_w using Arrhenius' law [51],

$$t_{\text{RUL}}(t) = c_0 \exp\left(\frac{E_a}{k_B T_w(t)}\right), \quad (\text{E.3})$$

where the symbols E_a , k_B and c_0 are constants representing activation energy, Boltzmann's constant and an empirical model fit, respectively. Next, let the fault dimension, L , be defined as the accumulated RUL consumed,

$$L(t) = L_0 + \int_{t_0}^t \frac{1}{t_{\text{RUL}}(\tau)} d\tau. \quad (\text{E.4})$$

where L_0 is the initial fault dimension. Substituting (E.3) into (E.4) gives,

$$L(t) = L_0 + \int_{t_0}^t c_0^{-1} \exp\left(-\frac{E_a}{k_B T_w(\tau)}\right) d\tau. \quad (\text{E.5})$$

By differentiating both sides with respect to time and applying the second fundamental theorem of integral calculus to the right-hand side, an expression for \dot{L} can be found,

$$\dot{L}(t) = c_0^{-1} \exp\left(-\frac{E_a}{k_B T_w(t)}\right), \quad (\text{E.6})$$

By applying (E.1) to (E.6) \dot{L} can be re-written in terms of T_{wa} ,

$$\dot{L}(t) = c_0^{-1} \exp\left\{-\frac{E_a}{k_B [T_{wa}(t) + T_a(t)]}\right\} \quad (\text{E.7})$$

A block diagram for the deterministic fault-growth model is provided in Figure E.2.

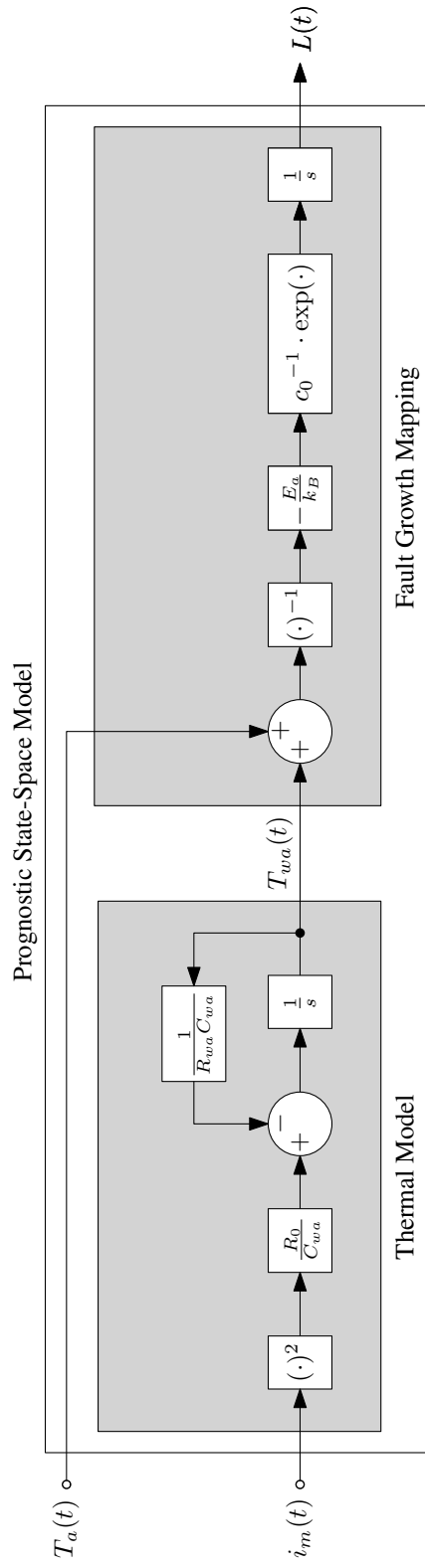


Figure E.2: Block diagram equivalent fault-growth state-space model.

E.4 Prognostic Model

The feature used in the prognostic model, f_p , is the difference between the winding and ambient temperature,

$$f_p(t) = T_w(t) - T_a(t) \quad (\text{E.8})$$

The complete prognostic model can be written as,

$$\begin{cases} \dot{T}_{wa}(t) &= -(R_{wa}C_{wa})^{-1} T_{wa}(t) + (R_0C_{wa}^{-1}) i_m^2(t) \\ \dot{L}(t) &= c_0^{-1} \exp\left\{-\frac{E_a}{k_B} (T_{wa}(t) + T_a(t))^{-1}\right\} \\ f_p(t) &= T_{wa}(t) \end{cases} \quad (\text{E.9})$$

where T_a and i_m are inputs and f_p is a measured output. By applying the ZOH discretization approximation from (A.6), and substituting the parameter values from Table E.1, the final expression for the prognostic model can be given,

$$\begin{cases} T_{wa}[k+1] &= [1 - T_s (R_{wa}C_{wa})^{-1}] T_{wa}[k] + [T_s R_0 C_{wa}^{-1}] i_m^2[k] + n_{1,1}[k] \\ L[k+1] &= T_s c_0^{-1} \exp\left\{-\frac{E_a}{k_B} (T_{wa}[k] + T_a[k])^{-1}\right\} + L[k] + n_{1,2}[k] \\ f_p[k] &= T_{wa}[k] + n_2[k] \end{cases} \quad (\text{E.10})$$

where T_s , $n_{1,1}$, $n_{1,2}$ and n_2 correspond to the discrete sample-time, process noise of the thermal model, fault dimension and feature measurement noise, respectively. Additive zero-mean Gaussian noise is introduced after discretization to avoid problems when discretizing continuous-time stochastic variables.

Table E.1: List of prognosis modeling parameters.

Sym	Units	Value	Description
c_0	hr^{-1}	3.174×10^{-5}	Constant of proportionality
k_T	$\text{eV}/^\circ\text{K}$	8.62×10^{-5}	Boltzmann's constant
C_{wa}	$\text{W}/(^\circ\text{K}/\text{s})$	1.00×10^1	Thermal capacitance
E_a	eV	8.00×10^{-1}	Activation energy
R_0	Ω	1.60×10^{-1}	Winding resistance
R_{wa}	$^\circ\text{K}/\text{W}$	7.50×10^{-1}	Thermal resistance

REFERENCES

- [1] “Aeronautical design standard handbook for condition based maintenance systems for us army aircraft systems,” Handbook ADS-79B-HDBK, Aviation Engineering Directorate, Redstone Arsenal, Alabama, USA, January 16, 2011.
- [2] R. Darby, “Commercial jet hull losses, fatalities rose sharply in 2005,” *Datalink*, pp. 51–53, August 2006.
- [3] M. Wald, “Fatal airplane crashes drop 65%,” *The New York Times*, October 1 2007.
- [4] B. G. Kanki, “Aircraft maintenance research: The nasa program,” in *Proceedings of the Human Factors and Ergonomics Society*, pp. (3)771–774, 2000.
- [5] A. N. Srivastava, R. W. Mah, and C. Meyer, “Integrated vehicle health management – automated detection, diagnosis, prognosis to enable mitigation of adverse events during flight,” Technical Plan Version 2.02, National Aeronautics and Space Administration, December 2008.
- [6] K. Krishnakumar, S. Viken, and N. Nguyen, “Integrated resilient aircraft control - stability, maneuverability, and safe landing in the presence of adverse conditions,” technical plan, National Aeronautics and Space Administration, May 2009.
- [7] D. Korsmeyer, “Intelligent systems devision - prognostics center of excellence.” Online: <http://ti.arc.nasa.gov/groups/pcoe/>, September 7, 2009.
- [8] A. Hess, “Prognostics and health management lead.” Keynote Speaker at the Integrated System Health Engineering and Management Conference, October 7-10, 2005.
- [9] G. Vachtsevanos, L. Tang, G. Drozeski, and L. Gutierrez, “From mission planning to flight control of unmanned aerial vehicles: Strategies and implementation tools,” *Annual Reviews in Control*, vol. 29, pp. 101–115, April 2005.
- [10] G. Vachtsevanos, F. Lewis, M. Roemer, A. Hess, and B. Wu, *Intelligent Fault Diagnosis and Prognosis for Engineering Systems*. Hoboken, NJ, USA: John Wiley & Sons, 2006. ISBN 987-0-0471-72999-0.
- [11] J. Jiang and Q. Zhao, “Should we use parameter estimation or state estimation bated methods for fdi,” in *Proceedings of the international federation of automatic control on SAFEPROCESS*, (Hull, UK), pp. 474–479, August 1997.
- [12] R. J. Patterson, “Fault-tolerant control: the 1997 situation,” in *Proceedings of the International Federation of Automatic Control symposium on SAFEPROCESS*, (Hull, UK), pp. 1033–1055, August 1997.

- [13] N. E. Wu, Y. M. Zhang, and K. Zhou, "Detection, estimation and accommodation of loss of control effectiveness," *International Journal of Adaptive Control and Signal Processing*, vol. 14, no. 7, pp. 948–956, 2000.
- [14] Y. M. Zhang and J. Jiang, "An active fault-tolerant control system against partial actuator failures," in *IEE Proceedings - Control Theory and Applications*, pp. 95–104, 2002.
- [15] M. Orchard, *A Particle Filtering-based Framework for On-line Fault Diagnosis and Failure Prognosis*. PhD thesis, School of Electrical and Computer Engineering, Georgia Institute of Technology, Atlanta, GA 30332 USA, November 2007.
- [16] M. Orchard, G. Kacprzynski, K. Goebel, B. Saha, and G. Vachtsevanos, "Advances in uncertainty representation and management for particle filtering applied to prognostics," in *1st International Conference on Prognostics and Health Management (PHM)*, (Denver, CO, USA), October 6-9, 2008.
- [17] M. Orchard, G. Kacprzynski, K. Goebel, B. Saha, and G. Vachrsevanos, *Advances in Uncertainty Representation and Management for Particle Filtering Applied to Prognosis*, vol. 39. Springer Netherlands, 2009. ISBN 978-90-481-3017-7.
- [18] M. Schwabacher, "A survey of data-driven prognostics," in *Proceedings of the AIAA Infotech@Aerospace Conference*, (Reston, VA, USA), American Institute for Aeronautics and Astronautics, Inc., 2005.
- [19] W. Yu and T. A. Harris, "A new stress-based fatigue life model for ball bearings," *Tribology Transactions*, vol. 44, no. 1, pp. 11–18, 2001.
- [20] P. Paris and F. Erodogan, "A critical analysis of crack propagation laws," *ASME Journal of Basic Engineering Transactions*, vol. 85, pp. 528–534, 1963.
- [21] P. C. Paris, M. P. Gomez, and W. E. Anderson, "A rational analytic theory of fatigue," *The Trend in Engineering*, vol. 13, no. 1, pp. 9–14, 1961.
- [22] Y. Zhang and J. Jiang, "Bibliographical review on reconfigurable fault-tolerant control systems," in *Proceeding of the SAFEPROCESS 2003: 5th Symposium on Detection and Safety for Technical Processes*, (Washington D.C., USA), pp. 265–276, 2003.
- [23] Y. Zhang and J. Jiang, "Bibliographical review on reconfigurable fault-tolerant control systems," *Annual Reviews in Control*, vol. 32, pp. 229–252, March 2008.
- [24] J. S. Eterno, J. L. Weiss, D. O. Looze, and A. S. Willsky, "Design issues for fault-restructurable aircraft control," in *IEEE Conference on Decision and Control*, pp. 900–905, 1985.

- [25] D. Nguyen and D. B. Liu, "Recovery blocks in real-time distributed systems," in *Proceedings of the Annual Reliability and Maintainability Symposium*, pp. 149–154, 1998.
- [26] R. Isermann, "Process fault detection based on modeling and estimation methods - a survey.," *Automatica*, vol. 20, no. 4, pp. 387–404, 1984.
- [27] Zhenyu and D. L. Hicks, "Synthesis of robust restructurable/reconfigurable control," in *9th International conference on control, automation, robotics and vision*, (Singapore), pp. 1–6, December 5-8, 2006.
- [28] J. Stoustrup, M. J. Grimble, and H. Niemann, "Design of integrated systems for the control and detection of actuator/sensor faults," *Sensor Review*, vol. 17, no. 2, pp. 38–149, 1997.
- [29] K. Zhou, J. C. Doyle, and K. Glover, "Robust and optimal control," in *Proceedings of the 35th IEEE Decision and Control*, (Kobe, Japan), December 11-13, 1996.
- [30] D. D. Siljak, "Reliable control using multiple control systems," *International Journal of Control*, vol. 31, no. 2, pp. 303–329, 1980.
- [31] G. H. Yang, S. Y. Zhang, J. Lam, and J. L. Wang, "Reliable control using redundant controllers," *IEEE Transactions on Automatic Control*, vol. 43, no. 11, pp. 1588–1593, 1998.
- [32] R. Rausch, K. Goebel, N. Eklund, and B. Brunell, "Integrated fault detection and accommodation: A model-based study," *Journal of Engineering for Gas Turbines and Power*, vol. 129, pp. 962–969, October 2007.
- [33] F. Filippetti, G. Franceschini, C. Tassoni, and P. Vas, "Recent developments of induction motor drives fault diagnosis using ai techniques," *IEEE Transactions on Industrial Electronics*, vol. 47, pp. 994–1004, October 2000.
- [34] J. D. Kleer and B. C. Williams, "Diagnosing multiple faults," *Artificial Intelligence*, vol. 32, no. 1, pp. 97–130, 1987.
- [35] V. A. Skormin, J. Apone, and J. J. Dunphy, "On-line diagnostics of a self-contained flight actuator," *IEEE Transactions on Aerospace and Electronic Systems*, vol. 30, pp. 186–196, January 1994.
- [36] A. S. Willsky, "A survey of design methods for failure detection in dynamic systems," *Automatica*, vol. 12, no. 6, pp. 601–611, 1976.
- [37] B. Wu, S. Abhinav, T. Khawaja, and S. Panagiotis, "An approach to fault diagnosis of helicopter planetary gears," in *IEEE Autotestcon*, (San Antonio, TX, USA), September 20-23, 2004.
- [38] D. Ye and G.-H. Yang, "Adaptive fault-tolerant tracking control against actuator faults with application to flight control," *IEEE Transactions on Control Systems Technology*, vol. 14, pp. 1088–1096, November 2006.

- [39] A. Saberi, A. A. Stoorvogel, P. Sannuti, and H. Niemann, “Fundamental problems in fault detection and identification,” *International Journal of Robust and Nonlinear Control*, vol. 10, pp. 1209–1236, November 2000.
- [40] J. F. Monaco, W. D.G., and A. J. D. Bateman, “A retrofit architecture for model-based adaptive flight control,” in *AIAA 1st Intelligent Systems Technical Conference*, (Chicago, IL, USA), September 20-22 2004.
- [41] D. G. Ward, J. F. Monaco, R. L. Barron, and R. A. Bird, “System for improved receding-horizon adaptive and reconfigurable control,” March 2001.
- [42] R. Isermann, “Supervision, fault-detection and fault diagnosis methods – an introduction,” *Journal of Control Engineering Practice*, vol. 5, pp. 639–652, May 1997.
- [43] A. H. Levis, “Challenges to control: A collective view,” *IEEE Transactions on Automatic Control*, vol. 32, pp. 275–285, April 1987.
- [44] N. E. Wu, “Robust feedback design with optimized diagnostic performance,” *IEEE Transactions on Automatic Control*, vol. 42, pp. 1264–1268, September 1997.
- [45] J. A. Primbs, *Nonlinear Optimal Control: A Receding Horizon Approach*. PhD thesis, California Institute of Technology, California Institute of Technology, Pasadena, California 91125 USA, January 1999.
- [46] H. Kwakernaak and R. Sivan, *Linear Optimal Control Systems*. Wiley-Interscience, first ed., 1972. ISBN 0-471-51110-2.
- [47] A. Locatelli, *Optimal Control - An Introduction*. Basel, Switzerland: Birkhäuser, 2000. ISBN 3-7643-6408-4.
- [48] J. Saak and P. Benner, “Proceedings of applied mathematics and mechanics,” in *Application of LQR Techniques to the Adaptive Control of Quasilinear Parabolic PDEs*, vol. 7, Wiley InterScience, 2007.
- [49] A. Bensoussan, G. D. P. abd M. Delfour, and S. Mitter, *Representation and Control of Infinite Dimensional Systems*. Boston, MA, USA: Birkhäuser, 2nd ed., 2007.
- [50] A. Bogdanov, S. Chiu, L. Gokdere, and W. Vian, J., “Stochastic optimal control of a servo motor with a lifetime constraint,” in *Proceedings of the 45th IEEE Conference on Decision & Control*, pp. 4182–4187, December 2006.
- [51] L. U. Gokdere, A. Bogdanov, S. L. Chiu, K. J. Keller, and J. Vian, “Adaptive control of actuator lifetime,” in *IEEE Aerospace Conference*, March 2006.
- [52] C. E. García, D. M. Preth, and M. Morari, “Model predictive control: Theory and practice – a survey,” *Automatica*, vol. 25, pp. 335–348, May 1989.

- [53] W. H. Kwon, A. N. Bruckstein, and T. Kailath, “Stabilizing state feedback design via the moving horizon method,” *International Journal of Control*, vol. 37, no. 3, pp. 631–643, 1983.
- [54] W. Kwon and A. Pearson, “A modified quadratic cost problem and feedback stabilization of a linear system,” *IEEE Transactions on Automatic Control*, vol. 22, pp. 838–842, October 1977.
- [55] D. Q. Mayne and H. Michalska, “Receding horizon control of nonlinear systems,” *IEEE Transactions on Automatic Control*, vol. 35, no. 7, pp. 814–824, 1990.
- [56] S. D. Cairano, A. Bemporad, I. Kolmanovskiy, and D. Hrovat, “Model predictive control of magnetically actuated mass spring dampers for automotive applications,” *International Journal of Control*, vol. 80, pp. 1701–1716, November 2007.
- [57] E. F. Camacho and C. Bordons, *Model Predictive Control*. Springer-Verlag, 2nd ed., 2004. ISBN 978-1-85-233694-3.
- [58] J. Maciejowski, *Predictive Control with Constraints*. Harlow, UK: Prentice-Hall, Pearson Education Limited, 2002. ISBN 978-0-20-139823-6.
- [59] S. J. Qin and T. A. Badgwell, “A survey of industrial model predictive control technology,” *Control Engineering Practice*, vol. 11, pp. 733–764, July 2003.
- [60] J. Richalet, “Industrial applications of model based predictive control,” *Automatica*, vol. 29, pp. 1251–1274, 1993.
- [61] J. Richalet, A. Rault, J. L. Testud, and J. Papon, “Model predictive heuristic control: Applications to industrial processes,” *Automatica*, vol. 14, no. 5, pp. 413–428, 1978.
- [62] B. Heck, L. Wills, and G. Vachtsevanos, “Software technology for implementing reusable, distributed control systems,” *IEEE Control Systems Magazine*, vol. 23, pp. 21–35, February 2003. Outstanding Paper Award.
- [63] J. Boskovic and R. Mehra, “Hybrid fault-tolerant control of aerospace vehicles,” in *Proceedings of the 2001 IEEE International Conference on Control Applications*, pp. 441–446, September 2001.
- [64] W. Liu, “An on-line expert system-based fault tolerant control system,” *Expert Systems With Applications*, vol. 11, no. 1, pp. 59–64, 1996.
- [65] M. Guler, S. Clements, L. Wills, B. Heck, and G. Vachtsevanos, “Generic transition management for reconfigurable hybrid control systems,” *IEEE Control Systems Magazine*, vol. 23, pp. 36–49, February 2003.
- [66] L. B. Gutierrez, G. Vachtsevanos, and B. Heck, “A hierarchical/intelligent control architecture for unmanned aerial vehicles,” in *Proceedings of 11th Mediterranean Conference on Control and Automation MED*, (Rhodes, Greece), June 2003.

- [67] E. W. Kamen, G. J. Vachtsevanos, A. Doustmohammadi, and W. Mahmood, "A hybrid analytical/intelligent approach to the modeling and control of dedds," in *Proceedings of the IEEE/IFAC Joint Symposium on Computer-Aided Control System Design*, March 1994.
- [68] N. S. Clements, *Fault Tolerant Control of Complex Dynamical Systems*. PhD thesis, School of Electrical and Computer Engineering, Georgia Institute of Technology, Atlanta, GA 30332 USA, April 2003.
- [69] N. Clements, B. Heck, and G. Vachtsevanos, "Component based modeling and fault tolerant control of complex systems," in *Proceedings of the 19th Digital Avionics Systems Conference*, vol. 2, pp. 6F4/1–6F4/4, October 7-13, 2000.
- [70] G. Drozeski, B. Saha, and G. Vachtsevanos, "A fault detection and reconfigurable control architecture for unmanned aerial vehicles," in *Proceedings of the IEEE Aerospace Conference*, (Big Sky, MT, USA), March 2005.
- [71] G. Drozeski and G. Vachtsevanos, "A fault-tolerant architecture with reconfigurable path planning applied to an unmanned rotorcraft," in *Proceedings of the American Helicopter Society 61st Annual Forum*, June 2005.
- [72] L. Tang, G. J. Kacprzynski, K. Goebel, A. Saxena, B. Saha, and G. Vachtsevanos, "Prognostics-enhanced automated contingency management for advanced autonomous systems," in *1st International Conference on Prognostics and Health Management (PHM)*, (Denver, CO, USA), pp. 1–9, October 6-9, 2008.
- [73] M. Mufti and G. Vachtsevanos, "An intelligent approach to fault detection and identification," in *Proceedings of American Control Conference*, June 1995.
- [74] G. Bajpai, B. C. Chang, and A. Lau, "Reconfiguration of flight control systems for actuator failures," *IEEE Aerospace and Electronic Systems Magazine*, vol. 16, no. 9, pp. 29–33, 2001.
- [75] A. Bemporad, M. Morari, and N. L. Ricker, *Model Predictive Control Toolbox for MATLAB*. The Mathworks, Inc., 2004.
- [76] R. Fletcher, *Practical Methods of Optimization*. New York, NY, USA: John Wiley & Sons Ltd., 2nd ed., May 2000. ISBN 978-0-471-49463-8.
- [77] G. B. Dantzig and M. N. Thapa, *Linear Programming and Extensions*. Princeton: Princeton University Press, 1963. ISBN 0-69-108000-3.
- [78] D. S. Bodden, N. S. Clements, B. Schley, and G. Jenney, "Seeded failure testing and analysis of an electro-mechanical actuator," in *IEEE Aerospace Conference*, (Big Sky, MT, USA), March 3-10, 2007.
- [79] R. Schoen, T. Habetler, F. Kamran, and R. Bartfield, "Motor bearing damage detection using stator current monitoring," *IEEE Transactions on Industry Applications*, vol. 31, pp. 1274–1279, November/December 1995.

- [80] B. Zhang, G. Georgoulas, M. Orchard, A. Saxena, D. Brown, G. Vachtsevanos, and S. Liang, "Rolling element bearing feature extraction and anomaly detection based on vibration monitoring," in *16th Mediterranean Conference on Control and Automation*, (Ajaccio, France), June 25-27, 2008.
- [81] D. W. Brown, D. Edwards, G. Georgoulas, B. Zhang, and G. Vachtsevanos, "Real-time fault detection and accommodation for cots resolver position sensors," in *1st International Conference on Prognostics and Health Management (PHM)*, (Denver, CO, USA), October 6-9, 2008.
- [82] A. Murray, B. Hare, and A. Hirao, "Resolver position sensing system with integrated fault detection for automotive applications," in *Proceedings of IEEE Sensors*, vol. 2, pp. 864–869, 2002.
- [83] M. Baybutt, S. Nanduri, P. W. Kalgren, D. S. Bodden, N. S. Clements, and S. Alipour, "Seeded fault testing and in-situ analysis of critical electronic components in ema power circuitry," in *IEEE Aerospace Conference*, (Big Sky, MT, USA), pp. 1–12, 2008.
- [84] D. Brown, G. Georgoulas, H. Bae, R. Chen, Y. H. Ho, G. Tannenbaum, J. B. Schroeder, and G. Vachtsevanos, "Particle filter based anomaly detection for aircraft actuator systems," in *IEEE Aerospace Conference*, (Big Sky, MT, USA), March 7-14, 2009.
- [85] N. H. Malik, A. A. Al-Arainy, and M. I. Quereshi, *Electrical Insulation in Power Systems*. Marcel Dekker, Inc., New York, NY, 1998.
- [86] S. Nandi and H. A. Toliyat, "Condition monitoring and fault diagnosis of electrical machines - a review," in *Proceedings of the 34th Annual Meeting of the IEEE Industry Applications*, pp. 197–204, 1999.
- [87] P. J. Tavner and J. Penman, *Condition Monitoring of Electrical Machines*. Research Studies Press, 1987. ISBN 978-0-86341-741-2.
- [88] H. Nestler and P. K. Sattler, "On-line estimation of temperatures in electrical machines by an observer," *Electric Power Components and Systems*, vol. 21, pp. 39–50, January 1993.

VITA

Douglas Brown received the B.S. degree in electrical engineering from the Rochester Institute of Technology in 2006 and the M.S degree in electrical engineering from the Georgia Institute of Technology in 2008. He is a recipient of the National Defense Science and Engineering Graduate (NDSEG) Fellowship and is currently a Ph.D. candidate in electrical engineering at the Georgia Institute of Technology specializing in control systems. His research interests include incorporation of Prognostics Health Management (PHM) for fault-tolerant control. Prior to joining Georgia Tech, Mr. Brown was employed as a project engineer at Impact Technologies where he worked on incipient fault detection techniques, electronic component test strategies, and diagnostics/prognostic algorithms for power supplies and RF component applications.